
**SPECTROSCOPIC & THERMODYNAMIC
INVESTIGATIONS OF THE PHYSICAL
BASIS OF ANHYDROBIOSIS IN
CAENORHABDITIS ELEGANS
DAUER LARVAE**

DISSERTATION

zur Erlangung des akademischen Grades

Doctor rerum naturalium
(Dr. rer. nat.)

Vorgelegt

der Fakultät Mathematik und Naturwissenschaften
der Technischen Universität Dresden

von

Sawsan E. Abu Sharkh

geboren am 31. Januar 1985 in Hebron, Palästina

Eingereicht am 12. Dezember 2014

Betreuer:

Prof. Dr. Karim Fahmy
Abteilung Biophysik, Helmholtz-Zentrum Dresden- Rossendorf (HZDR)

Gutachter

Prof. Dr. Stefan Diez
Max-Planck-Institut für Molekulare Zellbiologie und Genetik (MPI-CBG)

Prof. Dr. Andreas Barth
Department of Biochemistry and Biophysics, Stockholm University

PUBLICATIONS

This paper originates from a part of the PhD thesis:

- Sawsan E. Abusharkh, Cihan Erkut, Jana Oertel, Teymuras V. Kurzchalia, and Karim Fahmy. *The role of phospholipid headgroup composition and trehalose in the desiccation tolerance of Caenorhabditis elegans*. Langmuir, 30 (43), (2014), pp 12897–12906.

Papers published prior PhD:

- Saqer M. Darwish , Sawsan E. Abu sharkh , Musa M. Abu Teir , Sami A. Makharza and Mahmoud M. Abu-hadid. *Spectroscopic investigations of pentobarbital interaction with human serum albumin*. Journal of molecular structure, 932 (2010),pp. 122-129.
- Sawsan E. Abu sharkh , Musa M. Abu Teir ,Mahmoud M Abu-hadid, Saqer M. Darwish. *Spectroscopic study of Propofol binding to human serum albumin* Biophysical reviews and letters, 5 (2010), pp. 209–226.
- Sami Makharza; Jihan Auisa; Sawsan Abu Sharkh; Jamal Ghabboun; Maryam Faroun; Hasan Dweik; Wadie Sultan; Mukhles Sowwan. *Structural and thermal analysis of copper-doped poly(N-isopropylacrylamide) films*. International journal of polymer analysis and characterization, 15 (2010), pp. 254-265.

ABSTRACT

Anhydrobiotic organisms have the remarkable ability to lose extensive amounts of body water and survive in an ametabolic, suspended animation state. Distributed to various taxa of life, these organisms have evolved strategies to efficiently protect their cell membranes and proteins against extreme water loss. At the molecular level, a variety of mutually non-exclusive mechanisms have been proposed to account particularly for preserving the integrity of the cell membranes in the desiccated state. Recently, it has been shown that the dauer larva of the nematode *Caenorhabditis elegans* is anhydrobiotic and accumulates high amounts of trehalose during preparation for harsh desiccation (preconditioning), thereby allowing for a reversible desiccation / rehydration cycle.

Here, we have used this genetic model to study the biophysical manifestations of anhydrobiosis and show that, in addition to trehalose accumulation, the dauer larvae exhibit a systemic chemical response upon preconditioning by dramatically reducing their phosphatidylcholine (PC) content. The *C. elegans* strain *daf-2* was chosen for these studies, because it forms a constitutive dauer state under appropriate growth conditions. Using complementary approaches such as chemical analysis, time-resolved FTIR-spectroscopy, Langmuir-Blodgett monolayers, and fluorescence spectroscopy, it is shown that this chemical adaptation of the phospholipid (PL) composition has key consequences for their interaction with trehalose. Infrared-spectroscopic experiments were designed and automated to particularly address structural changes during fast hydration transients. Importantly, the coupling of headgroup hydration to acyl chain order at low humidity was found to be altered on the environmentally relevant time scale of seconds. PLs from preconditioned larvae with reduced PC content exhibit a higher trehalose affinity, a stronger hydration-induced gain in acyl chain free volume, and a wider spread of structural relaxation rates during lyotropic transitions and sub-headgroup H-bond interactions as compared to PLs from non-preconditioned larvae. The effects are related to the intrinsically different hydration properties of PC and phosphatidylethanolamine (PE) headgroups, and lead to a larger hydration-dependent

rearrangement of trehalose-mediated H-bond network in PLs from preconditioned larvae. This results in a lipid compressibility modulus of ~ 0.5 mN/m and 1.2 mN/m for PLs derived from preconditioned and non-preconditioned larvae, respectively.

The ensemble of these changes evidences a genetically controlled chemical tuning of the native lipid composition of a true anhydrobiote to functionally interact with a ubiquitous protective disaccharide. The biological relevance of this adaptation is the preservation of plasma membrane integrity by relieving mechanical strain from desiccated trehalose-containing cells during fast rehydration. Finally, the thermo-tropic lipid phase behavior was studied by temperature-dependent ATR-FTIR and fluorescence spectroscopy of LAURDAN-labeled PLs. The results show that the adaptation to drought, which is accomplished to a significant part by the reduction of the PC content, relies on reducing thermo-tropic and enhancing lyotropic phase transitions. The data are interpreted on a molecular level emphasizing the influence of trehalose on the lipid phase transition under biologically relevant conditions by a detailed analysis of the lipid C=O H-bond environment.

The salient feature of the deduced model is a dynamic interaction of trehalose at the PL headgroup region. It is proposed here that the location of trehalose is changed from a more peripheral to a more sub-headgroup-associated position. This appears to be particularly pronounced in PLs from preconditioned worms. The sugar slides deeper into the inter-headgroup space during hydration and thereby supports a quick lateral expansion such that membranes can more readily adapt to the volume changes in the swelling biological material at reduced humidity. The data show that the nature of the headgroup is crucial for its interaction with trehalose and there is no general mechanism by which the sugar affects lipidic phase transitions. The intercalation into a phosphatidylethanolamine-rich membrane appears to be unique. In this case, neither the phase transition temperature nor its width is affected by the protective sugar, whereas strong effects on these parameters were observed with other model lipids. With respect to membrane preservation, desiccation tolerance may be largely dependent on reducing phosphatidylcholine and increasing the phosphatidylethanolamine content in order to optimize trehalose headgroup interactions. As a consequence, fast mechanical adaptation of cell membranes to hydration-induced strain can be realized.

*Dedicated to my parents, my husband and my
lovely daughter Rawand*

For their endless love, support and encouragement

ACKNOWLEDGMENT

First and foremost, all praises to Allah (God) for providing me the blessings and the strengths to accomplish this thesis.

The thesis dissertation marks the end of a long and eventful journey for which there are many people that I would like to acknowledge for their support along the way.

First, I would like to express my deeper gratitude to my supervisor Prof. Karim Fahmy for giving me the opportunity to work in such an inspiring research topic. His efforts of stimulating scientific discussions, his confidence, and the support he gave me also in times, where the work did not proceed with ease are invaluable. I am also grateful to him for patiently going through the chapters of my thesis and for his critical comments. I will be forever grateful for his endless encouragement and support.

I thank respectfully the thesis reviewers, who take trouble to read and give their advice to complete this research work. Also, I would like to extend my gratitude to my thesis advisory committee members Prof. Stefan Diez and Prof. Teymuras Kurzchalia for their support, advisement and enthusiastic discussions during the TAC meetings.

I would like to offer my sincere thanks to our collaborator, Prof. Teymuras Kurzchalia and his group members, especially Dr. Cihan Erkut, for their contributions, encouragement and for allowing me the opportunity to work in their lab. I also would like to show a special gratitude to my former supervisors, Prof. Saqer Darwish and Dr. Musa Abu Teir, for motivating and encouraging me to go further in graduate studies.

Thanks are also extended to Dr. Andrea Cherkouk for endless encouragement and friendship. Special thanks to Jenny Philipp for helping me to put all my ideas into practice. I also grateful to all members of our group, Prof. Satoru Tsushima, Dr. Jana Oertel, Ahmed Sayed, Lisa Fishermeier, Muhammad Obeid and Gisela Gabernet for the convenient atmosphere to do science and helpful discussions.

I am much indebted to my husband Sami Makharza and my lovely daughter Rawand, who made the most impossible steps seem as the most simple, easy and natural thing to do during my study.

There are no words enough to thank my affectionate and adorable parents, my brothers, my sisters, my brothers in law and my dear friends Alaa Shaheen, Mai Yasin, Rana Bastati and Asma Afeefy for their continued love, support and interest.

Finally, I extend my appreciation to the Dresden International PhD program- International Max Planck Research School for Cell, Developmental and Systems Biology for providing me productive learning environments, instructive courses as well as the

financial support given throughout this study.

CONTENTS

Abstract	
Dedication	
Acknowledgment	

1 Literature Review: The Studied System	1
1.1 Significance of the Work	2
1.2 Anhydrobiosis-Theoretical Background	5
1.2.1 A Brief History	5
1.2.2 Common Molecular Mechanisms involved in Desiccation Tolerance	6
1.3 <i>Caenorhabditis elegans</i> , A Model Organism for Biophysical Studies of Desiccation Tolerance	9
1.3.1 Life Cycle of <i>C. elegans</i>	9
1.3.2 The Dauer Larva	11
1.4 Biological Membranes	11
1.4.1 Lipid Bilayers: Fluidity	12
1.4.2 Thermodynamics of Membranes: Phase Transition of Lipids . .	14
1.5 Objectives of the Study	16
2 Methods: Biophysical Techniques for Studying Lipid Membranes	19
2.1 Fourier Transform Infrared Spectroscopy (FTIR)	20
2.1.1 Fundamentals of IR Spectroscopy	20
2.1.2 Physical Basis of IR Spectroscopy	22
2.1.3 Fourier Transform Infrared Spectrometer	23
2.1.4 Principles of Attenuated Total Reflection (ATR)-FTIR Spectroscopy	26
2.1.5 ATR-FTIR difference Spectroscopy	28
2.1.6 Time-Resolved FTIR Spectroscopy	28
2.2 Langmuir-Blodgett System	29
2.2.1 Langmuir Film Balance	29
2.2.2 Surface Pressure-Area Isotherm	30
2.3 Fluorescence Spectroscopy	31
2.3.1 Basic Fluorescence Theory	31
2.3.2 Fluorescence Measurements	33
2.3.3 Fluorophores	34
2.4 Differential Scanning Calorimetry (DSC)	35
2.4.1 DSC Working Principle	35
2.4.2 Basic DSC Theory	37
3 Materials & Data Acquisition	39
3.1 Organisms & Culture Conditions	40
3.1.1 Nematode & Bacteria Culture Conditions	40
3.2 Desiccation & Preconditioning Assay	41
3.2.1 Controlled Humidity Environments	41
3.2.2 Dauer Larvae Preconditioning Assay	41

3.3	Biochemical Analysis of <i>C. elegans</i> Dauer PLs	42
3.3.1	Organic Extraction & Column Separation	42
3.3.2	Thin Layer Chromatography (TLC) Analysis	43
3.4	Materials	44
3.5	Time-Resolved FTIR Spectroscopy Studies	44
3.5.1	Hydration-Perturbation Measurements	44
3.5.2	Time-Resolved Spectra Acquisition	46
3.5.3	Spectral Processing	49
3.6	Thermo-tropic Measurements by ATR-FTIR Spectroscopy	51
3.6.1	Temperature-Induced Phase Transition Determination of <i>C. elegans</i> Dauer Larvae Membrane PLs	51
3.7	Langmuir-Blodgett Monolayer Studies	53
3.7.1	Formation of PLs Monolayer	53
3.7.2	Surface Pressure-Area Isotherm Measurements	53
3.8	Thermo-tropic Measurements by Fluorescence Spectroscopy	55
3.9	Differential Scanning Calorimetry (DSC) Studies	56
3.9.1	DSC Measurements	56
4	Dynamics of Headgroup Hydration & Acyl Chain Disorder in <i>C. elegans</i> PLs	57
4.1	Hydration-Induced Lyotropic Structural Transitions in <i>C. elegans</i> Derived PLs	58
4.2	Desiccation Stress Depletes Phosphatidylcholine in Cell Membranes & Enhances their Interaction with Trehalose	65
4.3	Interaction of Trehalose with PLs & Residual Water in Response to Membrane Hydration	70
4.4	Hydration-Induced Volume Changes & Lipid Expansion Coefficient in <i>C. elegans</i> PL Films (Swelling Behavior)	73
4.5	Discussion	75
4.6	Conclusions	81
5	Thermo-tropic Phase Behavior & Headgroup Interactions of <i>C. elegans</i> PLs in the Dehydrated State	83
5.1	Temperature-Induced Phase Transitions in PLs from Dauer Larvae in the Absence of Trehalose	85
5.2	Temperature-Induced Phase Transitions in PLs from Dauer Larvae in the Presence of Trehalose	88
5.3	Thermally Induced Changes of H-Bonding in the Sub-Headgroup Region of <i>C. elegans</i> PLs in the Absence of Trehalose	90
5.4	Thermally Induced Changes of H-Bonding in the Sub-Headgroup Region of <i>C. elegans</i> PLs in the Presence of Trehalose	95
5.5	Discussion	99

5.6	Conclusions	99
6	Fluorescence Spectroscopy Studies of the Gel-to Liquid Transition in PLs from <i>C. elegans</i> Dauer Larvae	101
6.1	Use of LAURDAN Fluorescence Intensity to Monitor the Effect of Preconditioning on Membrane Fluidity & PLs Order	102
6.2	LAURDAN reveals Different Fluidity & Hydration in the Presence of Trehalose in the Gel & Liquid Phase of PLs Bilayer	106
6.3	Temperature Dependence of the Generalized Polarization Measured by LAURDAN-loaded PL Vesicles in Response to Preconditioning & Trehalose Binding	109
6.4	Discussion	111
6.5	Conclusions	112
7	Outlook	115
	Bibliography	117
	Declaration	

LIST OF FIGURES

1.1	The chemical structure of trehalose. Trehalose is a natural disaccharide formed by an α,α -1,1-glucosidic bond between two α -glucose units.	6
1.2	A simple model of the protective action of trehalose on membranes during desiccation and rehydration. ²¹ In the fully hydrated state (top figure), PL headgroups interact with water. This interaction maintains the membrane in the liquid crystalline phase. Upon desiccation in the presence of trehalose, the hydration effect of water is compensated by the presence of the sugar (middle left figure), thus preserving the lipid order. Therefore, the membrane stays intact upon rehydration (bottom left figure). However, in the absence of trehalose, desiccation leads to PL packing heterogeneity and reduced acyl chain density (middle right figure), thereby destabilizing the membrane and resulting in damage to the membrane upon influx of water (bottom right figure).	8
1.3	Life cycle and timing of developmental stages of <i>C. elegans</i> grown at 25 °C (A). Adapted from Altun and Hall (2009) ⁵³ and modified by C. Erkut (2012). ⁵⁶ Worm are drawn approximately to scale. (B) Micrographs of laid eggs, larval stages and adults adapted from Fielenbach and Antebi (2008). ⁵⁵ Under favorable conditions <i>C. elegans</i> goes through four larval stages before molting to an adult. When conditions are unfavorable (limited food or overcrowding) <i>C. elegans</i> undergoes an the alternate dauer developmental stage, which can live several months. Upon return to favourable conditions, dauer larvae recover and mature to adulthood.	10

1.4	Schematic illustration of the fluid mosaic model. The plasma membrane structure is described as a fluid combination of phospholipids, cholesterol, proteins, and carbohydrates (A). The PLs are arranged in a bilayer with the polar hydrophilic head regions are in contact to the aqueous phases while the hydrophobic hydrocarbon tails are sandwiched between the hydrophilic heads (B). Space-filling model of a PL molecule structure (C). ⁶⁰	14
1.5	Scheme of PL phase transitions from gel states (solid ordered), to fluid states (liquid disordered) at a well-defined melting transition temperature (T_m).	16
2.1	Localized vibrations of the methylene group highlighting the symmetric (A) and asymmetric (B) stretches, and the bending: scissoring (C), rocking (D), wagging (E) and twisting (F) vibrations.	23
2.2	Michelson Interferometer: The beam of a global light source is split and recombined with a tunable optical path length difference generating polychromatic interference.	24
2.3	Schematic representation of ATR Principle: multiple internal reflection of the IR beam in the ATR crystal induces an evanescent field penetrating the first μm of the sample which can remain open at the upper side and can be studied under physiological conditions, i. e., in presence of solution.	27
2.4	Jablonski diagram: S_0 : ground state, S_1 : singlet state, V_s : excited vibrational state, T_1 and T_2 : triplet states, A: absorption of a photon, IC: internal conversion, F: Fluorescence emission, ISC: inter-system crossing, P: phosphorescence.	33
2.5	A schematic diagram of LAURDAN , a fluorescent dye commonly used in fluorescence spectroscopy of lipidic phases.	35
2.6	Principle scheme of a differential scanning calorimeter.	36

3.1	Schematic representation of a controlled humidity chamber. The NaOH solution at the bottom of the chamber creates a 98% RH over the sample, under which the sample dries until reaching an equilibrium with the air. The Thermo-hygrometer constantly displays current temperature and RH information. Grease is spread between the lid and the main body to improve isolation from the outside.	42
3.2	Schematic representation of large unilamellar vesicles (LUVs) preparation from multilamellar vesicles (MLVs) using the extrusion through a 100-nm polycarbonate filter.	45
3.3	Schematic diagram of the time-resolved FTIR hydration perturbation setup. A PL film (sample) is deposited on the ATR crystal, separated by a gas phase and a dialysis membrane (distance < 1mm) from a saturated NaCL salt solution to maintain 75% RH above the PL film. After recording an IR reference absorption spectrum of the PL film, a TTL signal initiates a heating current (4 s) in the salt solution, leading to a transient increase of the RH by 5-7% RH.	46
3.4	(A) schematic diagram showing time sequence of spectra acquisition for one pulse. By rapid scan FTIR spectroscopy, the relaxation of the PL film to its initial hydration state is monitored in ten time intervals (rectangular trigger levels). (B) Flowchart showing the structure for a macro written in OPUS macro software (BRUKER, Karlsruhe) that controls data acquisition, experiment synchronization, and spectra calculations.	48
3.5	Raw data of hydration-induced difference spectra. The plot shows the overlay of ten difference spectra, each induced in NPLs by an independent hydration pulse (water background subtracted from 3000 to 800 cm^{-1}). Each difference spectrum has been recorded 19 s after the hydration pulse, corresponding to the midpoint of the time traces shown in Figs. 4.2 and 4.8 in the next chapter. The spectra are reproduced within the noise level, evidencing the high degree of reproducibility and the full relaxation of the sample after each hydration pulse.	50

3.6	Schematic representation of pressure-area isotherm measurement steps using Langmuir-Blodgett technique.	54
4.1	Hydration pulse-induced rapid scan FTIR-difference spectra of a PL films. By rapid scan FTIR spectroscopy, the relaxation of the PL film to its initial hydration is monitored. A) Overview of the time-dependent evolution of difference spectra in response to a single hydration pulse. In an automated fashion, 10 hydration pulses were applied and difference spectra co-added for each time slice to improve the signal to noise ratio. Inset: i) The first difference spectrum at $t=0$ calculated from the first data acquisition interval and the reference spectrum. The increased absorption between 4000 and 3000 cm^{-1} is caused by water uptake by the PL film. Absorption changes of the PL acyl chains (3000 - 2800 cm^{-1} , water background subtracted for clarity) and headgroups (1800 - 1000 cm^{-1}) are smaller and exhibit negative and positive lobes due to hydration-induced shifts of their vibrational frequencies. ii) initial PL absorption (reference spectrum).	60
4.2	Time-resolved hydration-pulse-induced IR absorption changes of PL extracts in the absence of trehalose. A) Representative selection of hydration-induced difference spectra of NPLs recorded at the indicated times after the hydration pulse. The hydration-induced down shift of the $\nu(\text{C=O})$ and $\nu_{as}(\text{PO}_2^-)$ causes the difference bands at $1741/1713$ and $1242/1204\text{ cm}^{-1}$ due to increased H-bonding to the ester carbonyl and phosphates, respectively. Increase of acyl chain free volume is monitored by the up-shift of the $\nu_s(\text{CH}_2)$ and $\nu_{as}(\text{CH}_2)$ frequencies from 2849 to 2859 and from 2917 to 2949 cm^{-1} , respectively. Spectra are normalized to the amplitude of the $\nu(\text{C=O})$ difference band. B) As in (A) obtained with PPLs. C) Relaxation of absorption changes in A. IR frequencies are assigned to chemical groups as indicated. The loss of water to the gas phase (reduction of $\nu(\text{OH})$ amplitude) is shown for comparison (blue). D) As (C) obtained with PPLs. Spectral noise is $< 0.1\text{ mAU}$ (see Fig. 3.5) Color code: NPLs black, PPLs green, water: blue.	62

4.3	Correlation of PL headgroup composition and hydration responses. A) TLC radiogram of ^{14}C -labeled PLs. Among the major PL classes, only PC displays a dramatic decrease in the preconditioned sample. PE: Phosphatidylethanolamine, PC: Phosphatidylcholine, PI: Phosphatidylinositol, PS: Phosphatidylserine, S: Starting point. Dimensions are indicated with arrows. Solvent 1: $\text{CHCl}_3:\text{CH}_3\text{OH}:32\% \text{NH}_3$ (65:35:5, v:v:v); solvent 2: $\text{CHCl}_3:\text{CH}_3\text{OH}:(\text{CH}_3)_2\text{CO}:\text{CH}_3\text{COOH}:\text{H}_2\text{O}$ (50:10:20:12.5:5, v:v:v:v:v)). B) Time-resolved hydration-pulse-induced IR absorption changes of an NPLs film (black) and a PPLs film (green) which was supplemented with bovine PC (PPLs:PC= 2:1), thereby PC addition to the PPLs film restores the $\nu(\text{CH}_2) / \nu(\text{C=O})$ amplitude ratio of NPLs.	66
4.4	Time-resolved hydration-pulse-induced IR absorption changes. Representative selection of hydration-induced difference spectra recorded at the indicated times (Fig. 4.2 (A-B)) after the hydration pulse of (A) PPLs, (B) PPLs which was supplemented with bovine PC (PPLs:PC= 2:1) and (C) NPLs.	67
4.5	Interaction of trehalose with PL monolayers. Expansion of a monolayer of PPLs (A) and NPLs (B) before (1) and after (2) injection of trehalose (TRE) to the subphase at a final concentration of 125 mM. Broken arrows exemplify the area increase induced by trehalose at constant pressure. C) The molecular area A_t occupied by TRE in the monolayers is derived from the slope of the linear regressions of the RT. $\ln(\Delta A_L/A_L)$ plots over a range of pressures. The free enthalpy difference of binding of TRE to PPLs vs. NPLs is reduced by $1.6 \text{ kJ} < \Delta\Delta G_0 < 5 \text{ kJ}$ (determined from the offsets of the linear regressions and allowing an uncertainty of the minimal area per lipid of $45\text{-}65 \text{ \AA}^2$).	68

- 4.6 **The expansion isotherms of DMPA monolayer** on phosphate buffer 10 mM (pH 7.4) as subphase (A). Left branch (1): subphase without trehalose. Right branch(2): after addition of 125 mM trehalose which increases surface pressure (π). B) The molecular area A_t occupied by TRE in the lipidic film is derived from the slope of the linear regressions of the RT and is equal to 44 \AA^2 . $\ln(\Delta A_L/A_L)$ plots over a range of pressures. The free enthalpy of binding of TRE to DMPA lipid film is $-9.1 \text{ kJ} < \Delta G_0 < -7.4 \text{ kJ}$ 69
- 4.7 **Molecular modeling of α,α -trehalose single molecule.** The predicted projection surface of trehalose has a long and short axis of 10.9 and 6.5 \AA .¹²⁶ 70
- 4.8 **Time-resolved hydration-pulse-induced IR absorption changes of PL extracts in the presence of trehalose.** A) Representative selection of hydration-induced difference spectra of NPLs recorded at the indicated times after the hydration pulse. The hydration-induced down shift of the $\nu(\text{C=O})$ and $\nu_{as}(\text{PO}_2^-)$ causes the difference bands at $1741/1700 \text{ cm}^{-1}$ due to increased H-bonding to the ester carbonyl. Little changes are observed for the phosphates at $1249\text{-}1200 \text{ cm}^{-1}$. The increase of acyl chain free volume is monitored by the up-shift of the $\nu_s(\text{CH}_2)$ and $\nu_{as}(\text{CH}_2)$ frequencies ($2849/2859$ and $2917/2949 \text{ cm}^{-1}$, respectively). B) As in (A) but obtained with PPLs. C) Relaxation of absorption changes of NPLs. D) as in (C) but for PPLs. Infrared frequencies are assigned to chemical groups as indicated. The loss of water to the gas phase (reduction of $\nu(\text{OH})$ amplitude) is shown for comparison (blue) as well as the change in H-bonding to trehalose. 72

- 4.9 **Time-resolved volume and H-bond changes.** Relative expansion of PL films in the absence (A) and presence (B) of trehalose. The evaluation is based on the time-dependent data shown in Figs. 2 and 8, respectively. The sequence of swelling / shrinking is indicated by the selected time points, the slopes α are relative expansion coefficients ($\alpha = \Delta(\Delta V/V) \cdot \Delta \Gamma^{-1}$, standard error $< 10^{-2}$ %). C) $\nu(\text{OH})$ contour of water adsorbed during the hydration pulse in the absence (blue) and presence (red) of trehalose. D) Hydration-induced absorption changes of trehalose in PLs. Color code: black, NPLs; green, PPLs. 75
- 4.10 **Absorption change ΔA of the symmetric CH_2 stretching mode as a function of the chemical potential of water.** The time-dependent amplitude of the $2849/2859 \text{ cm}^{-1}$ difference bands (in per cent of the total absorption at 2850 cm^{-1}) is plotted versus the chemical potential of water in the absence (A) and presence of trehalose (B). From the slopes, compressibility modules are derived (see chapter 3.5.3). . . . 78
- 4.11 **Dynamic interaction of trehalose with lipid headgroups during transient hydration at reduced humidity.** Hydration of the trehalose-containing PLs leads to the insertion of the disaccharide into the headgroup/sub-headgroup interface (vertical arrows), allowing direct and water-mediated H-bonding to the ester carbonyls. The stronger water headgroup interaction in PC restricts this motion in NPLs (A), whereas efficient intercalation of the sugar occurs in the PE-dominated PPLs (B). The higher water-induced acyl chain disorder in PPLs further allows a larger gain of molecular area (horizontal arrows) upon fast hydration, leading to a “softer” (lower lateral tension) response of PPLs. 80
- 5.1 **Temperature-dependent ATR-FTIR spectral changes.** The main characteristic stretching absorption bands are: OH ($3800\text{-}3000 \text{ cm}^{-1}$), CH_2 ($2970\text{-}2820 \text{ cm}^{-1}$), C=O ($1800\text{-}1660 \text{ cm}^{-1}$) and PO_2^- ($1250\text{-}1050 \text{ cm}^{-1}$). Panels A-C: NPLs; panels D-F: PPLs. Spectra were acquired at the indicated temperatures at 75% relative humidity. 86

- 5.2 **Lipid melting curves.** The increase in the $\nu_s(\text{CH}_2)$ peak vibrational frequency of PPLs (green circles) and NPLs (black squares) is plotted as a function of temperature (2-80 °C) (A). For comparison the left and the right scale is the same in panel A. The first derivatives of the presented curves on (B). The peak maxima (vertical dotted lines) indicate the phase transition temperatures of both NPLs and PPLs. The first derivative plot shows the phase transitions as the regions of greatest slope. 87
- 5.3 **Temperature-dependent ATR-FTIR spectral changes induced by trehalose.** The main characteristic stretching absorption bands: OH (3800-3000 cm^{-1}), CH_2 (2970-2820 cm^{-1}), C=O (1800-1660 cm^{-1}) and PO_2^- (1250-1050 cm^{-1}). Panels A-C: NPLs; panels D-F: PPLs. Spectra were acquired at the indicated temperatures at 75% relative humidity. . 88
- 5.4 **Lipid melting curves in the presence of trehalose.** The increase in the $\nu_s(\text{CH}_2)$ peak vibrational frequency of PPLs (green circles) and NPLs (black squares) is plotted as a function of temperature (2-80 °C) (A). For comparison the left and the right scale is the same in panel A. The first derivatives of the presented curves on (B). The peak maxima (vertical dotted lines) indicate the phase transition temperatures of both NPLs and PPLs. The first derivative plot shows the phase transitions as the regions of greatest slope. 90

- 5.5 Infrared absorption spectra of carbonyl (C=O) stretching modes of NPLs.** Panel A: 6 °C (gel phase); Panel B: 10 °C (at the T_m); Panel C: 70 °C (fluid phase). The original bands (black circles) are fitted with 2 Gaussians (blue line, green line), representing two distinct states of hydration: $\nu\text{C=O}_{Free}$ (higher wavenumber, dehydrated) and $\nu\text{C=O}_{H-bonded}$ (lower wavenumber, hydrated), respectively. The summation of the fit components is shown in red. The relative area (area under the fitted peak) of the C=O band components are given as percentages underneath the respective fitting curve. The correlation coefficients (R^2) for the fitted curves were always 0.999. The vertical dotted lines indicate the positions of the fit components of pure NPLs. All analyzed bands originate from the heating scan. 93
- 5.6 Infrared absorption spectra of carbonyl (C=O) stretching modes of PPLs.** Panel A: 6 °C (gel phase); Panel B: 10 °C (at the T_m); Panel C: 70 °C (fluid phase). The original bands (black circles) are fitted with 2 Gaussians (blue line, green line), representing two distinct states of hydration: $\nu\text{C=O}_{Free}$ (higher wavenumber, dehydrated) and $\nu\text{C=O}_{H-bonded}$ (lower wavenumber, hydrated), respectively. The summation of the fit components is shown in red. The relative area (area under the fitted peak) of the C=O band components are given as percentages underneath the respective fitting curve. The correlation coefficients (R^2) for the fitted curves were always 0.999. The vertical dotted lines indicate the positions of the fit components of pure PPLs. All analyzed bands originate from the heating scan. 94

- 5.7 Infrared absorption spectra of Carbonyl (C=O) stretching vibrational bands of NPLs in the presence of trehalose (TRE).**
 Panel A: 6 °C (gel phase); Panel B: 10 °C (at the T_m); Panel C: 70 °C (fluid phase). The original bands (black circles) are fitted with 2 Gaussians (blue line, green line), representing two distinct states of hydration: $\nu\text{C=O}_{Free}$ (higher wavenumber, dehydrated) and $\nu\text{C=O}_{H-bonded}$ (lower wavenumber, hydrated), respectively. The summation of the fit components is shown in red. The relative area (area under the fitted peak) of the C=O band components are given as percentages underneath the respective fitting curve. The correlation coefficients (R^2) for the fitted curves were always 0.999. The vertical dotted lines indicate the positions of the fit components of NPLs containing trehalose. All analyzed bands originate from the heating scan. 97
- 5.8 Infrared absorption spectra of Carbonyl (C=O) stretching vibrational bands of PPLs in the presence of trehalose (TRE).**
 Panel A: 6 °C (gel phase); Panel B: 10 °C (at the T_m); Panel C: 70 °C (fluid phase). The original bands (black circles) are fitted with 2 Gaussians (blue line, green line), representing two distinct states of hydration: $\nu\text{C=O}_{Free}$ (higher wavenumber, dehydrated) and $\nu\text{C=O}_{H-bonded}$ (lower wavenumber, hydrated), respectively. The summation of the fit components is shown in red. The relative area (area under the fitted peak) of the C=O band components are given as percentages underneath the respective fitting curve. The correlation coefficients (R^2) for the fitted curves were always 0.999. The vertical dotted lines indicate the positions of the fit components of PPLs containing trehalose. All analyzed bands originate from the heating scan. 98

- 6.1 **Temperature effect on the fluorescence excitation and emission spectra of LAURDAN** in LUVs composed of NPLs (black) and PPLs (green) prepared in phosphate buffer (10 mM, pH 7.4). The measurements were performed at 2 °C (panel A & B), 25 °C (panel C & D) and 65 °C (panel E & F). The total lipid concentration was 0.3 mM with the ratio of LAURDAN probe to lipid (1:1000). Fluorescence spectra were normalized to their maximum. The excitation spectra were measured at an emission wavelength of 440 nm, and the emission spectra were measured with an excitation wavelength of 340 nm. 105
- 6.2 **Temperature effect on the fluorescence excitation and emission spectra of LAURDAN** in LUVs composed of NPLs (black) and PPLs (green) in the presence of trehalose, which was prepared in phosphate buffer (10 mM, pH 7.4). The measurements were performed at 2 °C (panel A & B), 25 °C (panel C & D) and 65 °C (panel E & F). The total lipid concentration was 0.3 mM with the ratio of trehalose to lipid (20:1). Fluorescence spectra were normalized to their maximum. The excitation spectra were measured at an emission wavelength of 440 nm, and the emission spectra were measured with an excitation wavelength of 340 nm. 108
- 6.3 **Temperature dependence of LAURDAN GP values** of NPLS (black) and PPLs (green) in different phases, at the indicated temperatures in Fig. 6.1. The GP values were calculated by $GP = (F_{440} - F_{490}) / (F_{440} + F_{490})$, using emission wavelengths at 440 and 490 nm as explained in chapter 3.8. 110
- 6.4 **Temperature dependence of LAURDAN GP Values in the presence of trehalose** of NPLS (black) and PPLs (green) in different phases, at the indicated temperatures in Fig. 6.2. The GP values were calculated by $GP = (F_{440} - F_{490}) / (F_{440} + F_{490})$, using emission wavelengths at 440 and 490 nm as explained in chapter 3.8. 111

- 6.5 **Schematic representation of LAURDAN Fluorescent Probe (naphthalene moiety: violet, lauric acid tail: blue) location in the PLs bilayer.** LAURDAN detects the polarity of its environment and thus water penetration into the hydrophobic-hydrophilic interfacial region in the bilayer. Its orientation and water content varies in gel phase (ordered, panel A) and liquid phase (disordered, panel B) of PLs bilayer. In the gel phase, lipids have a more restricted motion (so few water molecules sensed by LAURDAN probe). But, in the liquid phase, increased of water accessibility is observed and accordingly increasing of membrane fluidity. 113
- 7.1 **(A) DSC heating scans of DMPA, DMPC, DMPE and DMPG vesicles (1mg/ml) in the absence and presence of trehalose (~20 mg/ml)** are revealing the main gel to liquid-crystalline phase transition temperature (T_m). The results show that the trehalose lipid interaction is highly dependent on the headgroup. (B) The chemical structure of these model lipids with different headgroups (PA, PC, PE and PG). . . 116

LIST OF TABLES

4.1	Normalized amplitudes of absorption changes of selected group frequencies of PLs. The tabulated values are the peak to peak intensities of the absorption differences in the first difference spectrum after the hydration pulse in per cent of the intensity of the negative depletion signal at 1740 cm^{-1} (ester carbonyl $\nu(\text{C=O})$ of the initial state). The wavenumber ranges of the spectral changes are given for each mode. The second to last column shows the relative expansion of the PL films (volume change per water added per phosphate). The last column shows the area of trehalose occupied in the respective PL monolayer and the free energy of trehalose binding to the monolayer. See Materials and Data Acquisition for details. TRE: trehalose.	64
5.1	The relative areas (AC=O_{Free} and $\text{AC=O}_{H-bonded}$) of H-bonded and free C=O groups of the the two component fitted peaks of the carbonyl (C=O) stretching band shown in NPLs and PPLs in the absence and in the presence of trehalose (TRE). The data are acquired at $6\text{ }^{\circ}\text{C}$ (gel phase), $10\text{ }^{\circ}\text{C}$ (T_m) and $70\text{ }^{\circ}\text{C}$ (fluid phase). The relative area (A) is significance indicator proportional to the number of free and H-bonded C=O groups.	96

ACRONYMS

C. elegans	Caenorhabditis elegans
Daf	Dauer-constitutive
TRE	Trehalase
L1	First larval stage
L2	Second larval stage
L2d	Pre-dauer stage
L3	Third larval stage
L4	Fourth larval stage
MLVs	Multilamellar vesicles
LUVs	Large Unilamellar Vesicles
PL	Phospholipid
PLs	Phospholipids
PPLs	Phospholipids extracted from preconditioned larvae
NPLs	Phospholipids extracted from non-preconditioned larvae
PC	Phosphatidylcholine
PE	Phosphatidylethanolamine
PS	Phosphatidylserine
PI	Phosphatidylinositol
PG	Phosphatidylglycerol
DMPA	1,2-dimyristol-sn-glycero-3-phosphate
DMPC	1,2-dimyristoyl-sn-glycero-3-phospho-choline
DMPE	1,2-dimyristoyl-sn-glycero-3-phosphoethanolamine
DMPG	1,2-dimyristoyl-sn-glycero-3-phospho-(1'-racglycerol)
Bovine PC	L- α -phosphatidylcholine (Bovine PC)
IR	Infrared
FTIR	Fourier Transform Infrared Spectroscopy
ATR	Attenuated Total Reflection
ATR-FTIR	Attenuated Total Reflection-Fourier-Transform Infrared Spectroscopy
LAURDAN	6-Dodecanoyl-2-Dimethylaminonaphthalene
ν	Wavenumber

ν_{as}	Anti-symmetric stretching wavenumber
ν_s	Symmetric stretching wavenumber
λ	Wavelength
λ_{ex}	Excitation Wavelength
λ_{em}	Emission Wavelength
DS	Difference Spectrum
S_0	Gel phase
L_o	Liquid-ordered phase
P_β	Ripple phase
L_d	Fluid phase
T_m	Main melting transition temperature
DSC	Differential Scanning Calorimetry
TLC	Thin Layer Chromotography
GP	Generalized Polarization
RH	Relative Humidity
π	Surface Pressure

LITERATURE REVIEW: THE STUDIED SYSTEM

Contents

1.1	Significance of the Work	2
1.2	Anhydrobiosis-Theoretical Background	5
1.2.1	A Brief History	5
1.2.2	Common Molecular Mechanisms involved in Desiccation Tolerance	6
1.3	<i>Caenorhabditis elegans</i>, A Model Organism for Biophysical Studies of Desiccation Tolerance	9
1.3.1	Life Cycle of <i>C. elegans</i>	9
1.3.2	The Dauer Larva	11
1.4	Biological Membranes	11
1.4.1	Lipid Bilayers: Fluidity	12
1.4.2	Thermodynamics of Membranes: Phase Transition of Lipids . . .	14
1.5	Objectives of the Study	16

1.1 Significance of the Work

Anhydrobiotic organisms are distinguished by their remarkable ability to survive extreme desiccation. Prominent examples are bacteria,¹ yeast,^{2,3} tardigrades,⁴ brine shrimps,⁵ plants,⁶ rotifers⁷ certain insect larvae⁸ as well as various nematode species.^{9–11} At the molecular level, these organisms have evolved mechanisms that preserve the structure of their biological membranes and proteins at extremely diminished water content.^{12,13} Many of them synthesize disaccharides such as trehalose as desiccation-protectants. Although its functional mechanism is not fully understood, trehalose can confer desiccation tolerance not only to many anhydrobiotes in the nature but also to mammalian cells^{14,15} and organelles¹⁶ where it is not naturally produced. Nematodes such as *Aphelelenchus avenae* have been studied for their capability of surviving desiccation¹⁷ and changing their carbohydrate and lipid composition in preparation for anhydrobiosis.¹⁸ However, nematode species exhibit varying degrees of desiccation tolerance and differ in stress-related signaling pathways in response to reduced humidity.¹⁹ Recently, it has been shown that *Caenorhabditis elegans* (*C. elegans*), one of the best-characterized nematodes, is an anhydrobiote. Its metabolically depressed dauer larvae can tolerate extreme water loss after an initial mild desiccation treatment, so-called preconditioning.²⁰ The *C. elegans* genome is fully sequenced and well annotated. Due to the applicability of powerful genetic and biochemical methods, the worm serves as one of the best genetic models in biological research. Therefore, it is also a prime candidate to study the phenomenon of anhydrobiosis at the molecular level by correlating physical, chemical, and spectroscopic data with specific genotypes. A temperature-sensitive mutant of *C. elegans*, *daf-2(e1370)* arrests in the dauer stage when grown at 25 °C regardless of the environmental conditions. Its desiccation tolerance depends on many factors, among which is the ability to synthesize trehalose. This sugar is accumulated upon preconditioning and trehalose-deficient mutants are extremely sensitive to harsh desiccation.²¹

Electron microscopy revealed that preconditioned dauer larvae exhibit an intact morphology after a desiccation / rehydration cycle whereas non-preconditioned or trehalose-deficient worms showed massive rupture of cell membranes and membranous

organelles. In the same study, infrared spectroscopy of living preconditioned larvae revealed reversible hydration-dependent changes of absorption bands in the methylene stretching frequency range indicative of structural transitions of acyl chains. Remarkably, non-preconditioned larvae showed irreversible desiccation-dependent IR-absorption changes. In concert with the electron micrographs, the data supported the *in vivo* role of trehalose for maintaining cell membrane structure²¹ in agreement with studies on phase transitions in model lipids.^{22–24} The protective effect of the sugar is typically ascribed to its vitrification and/or water replacing properties.²⁵

Rehydration of dry dauer larvae in their natural environment is a fast process and happens almost instantaneously when rainwater penetrates the habitat after a period of drought. Under these conditions, cell membranes become exposed to sudden and steep gradients of hydration, which cause different swelling rates of the diverse biological tissues and materials in adjacent compartments. The mechanical response of membranes to this effect is governed by the hydration-induced (i.e. lyotropic) phase transitions of its lipids. The coordination of these processes appears to be the critical factor to preserve membrane integrity during the exit from the dry state. Experimental data show that sugar–headgroup interactions are crucial in mediating the protective effect of trehalose. These interactions result particularly in the dramatic lowering of the phase transition temperature in the dry state²⁶ and in preservation of phase separation in lipid mixtures.^{22,23} Structural models from molecular dynamics calculations confirm the intercalative action of trehalose at the headgroup region in general²⁷ but without a clear preference for vitrification, water replacement or hydration force mechanisms.²⁸ Therefore, these three hypotheses have never been assumed to be mutually exclusive.

In contrast to these studies on model compounds at thermodynamic equilibrium, the dynamic hydration behavior of natural lipid–carbohydrate mixtures from anhydrobiotes has not been investigated. Particularly, lyotropic transitions on the time scale of seconds, during which membrane damage may occur under natural conditions, has never been explored. We have surmised that protective mechanisms should particularly be effective during this sudden deviation from equilibrium and may not be fully understood by static experiments or simulations, which have been performed in bulk water phase. Therefore, we have established time-dependent IR-absorption experiments to monitor the structural

response of *C. elegans* phospholipids (PLs) to transient hydration changes within a few seconds at reduced humidity to study lipid dynamics on the natural time scale of seconds. The use of IR-spectroscopy, among other techniques, for the quantitative evaluation of hydration-dependent states of lipids has been comprehensively reviewed.²⁹ This method offers the advantage of a label-free detection of structural changes with chemical group-specific resolution.

We were particularly interested in identifying and understanding on a molecular level the physical differences in fast lyotropic transitions in PLs extracted from preconditioned vs. non-preconditioned dauer larvae. Our data show that already in the absence of trehalose, PLs extracted from preconditioned larvae (PPLs) respond to hydration transients with a larger increase of acyl chain free volume as compared to PLs of non-preconditioned larvae (NPLs). This property correlates with an altered PL headgroup composition, namely a decrease of the PC:PE ratio upon preconditioning. In fact, preconditioning changes the chemical composition of the *C. elegans* lipids such that in the presence of trehalose, a smaller lateral compressibility modulus of stacked bilayers can be maintained at reduced humidity, thereby, less force is generated within the PL bilayer when it expands during the rehydration-induced swelling of the neighboring biomaterials. The underlying trehalose-mediated H-bond network is more excessively rebuilt during hydration transients in PPLs allowing acyl chain packing and sub-headgroup H-bonding changes to relax at faster rates than the water exchange with the gas phase. Thus, the lipid chemistry is tailored during preconditioning such that lyotropic transitions link water-mediated H-bond networks in the headgroup and sub-headgroup region more efficiently to acyl chain disorder, resulting in the softening of the PL bilayers. These chemical and physical changes appear to represent an essential molecular adaptation to anhydrobiosis as they reduce mechanical strain that builds up upon hydration transients of cell membranes. Additionally, the thermo-tropic phase behavior of NPLs and PPLs dauer larvae and its dependence on trehalose has been addressed for the first time by temperature-dependent FTIR and fluorescent LAURDAN labeling measurements.

1.2 Anhydrobiosis-Theoretical Background

1.2.1 A Brief History

The term Anhydrobiosis is derived from Greek and indicates state of dormancy evoked by dehydration. In 1702, Anton Van Leeuwenhoek, the inventor of the microscope, described elegantly how dry rotifers that he collected from dry roof gutters revive with a few drops of water under the microscope.³⁰ Nearly 250 years later David Keilin was the first person who described anhydrobiosis as: ‘a particular state of an organism when it shows no visible sign of life and when its metabolic activity becomes hardly measurable’,³¹ which he called ‘cryptobiosis’. He also coined the term cryobiosis, anoxybiosis and osmobiosis for cryptobiotic states in extreme cold, oxygen deficiency and osmotic stress, respectively.³¹ However, the term anhydrobiosis that is perhaps the most common form of cryptobiosis applies when cryptobiosis is simply triggered by environmental desiccation. Anhydrobiosis may confer an extreme stress tolerance in which an organism loses almost all of its entire cellular water but retain the ability to revive after rehydration.³² This ability to survive almost complete desiccation is a characteristic property of many organisms. The first anhydrobiotic nematode identified was *Anguina tritici*. Some others are *Acrobeloides nanus*,³³ *Anguina agrostis*,³⁴ *Aphelenchus avenae*,³⁵ *Ditylenchus dispaci*,³⁶ *Panagrellus silusiae*,³⁷ several *Panagrolaimus* species¹⁰ and *Tylenchus polyhyphnus*,³⁸ which currently hold the record of the longest dormancy (39 years) among nematodes. Recently, it has been shown for the first time that the *C. elegans* dauer is an anhydrobiote.^{20,21} This finding opens a new perspective since *C. elegans* is already one of the best studied model organisms, which allows investigating the molecular mechanisms underlying anhydrobiosis in a genetically characterized system. Entering anhydrobiosis needs a coordinated series of events to protect the native structure of biomolecules and to prevent oxidative damage.³⁹ Importantly, the elucidation of the mechanisms, which allow some organisms to survive desiccation, may lead to the development of new methods for protecting biological materials that do not normally support drying.

1.2.2**Common Molecular Mechanisms involved in Desiccation Tolerance**

The anhydrobiotic organisms, in order to survive desiccation, have to successfully tolerate two different stresses. First is the potential damage that occurs to the organism during the desiccation phase and the second is the stress that occurs upon rehydration. Therefore, it is important to preserve the biological structure and molecules in the dry state and also during subsequent rehydration.⁴⁰ Most of the desiccation-tolerant organisms use common mechanisms to control and to tolerate as well as to stabilize their cellular structures during severe desiccation. These mechanisms include accumulation of non-reducing disaccharides during drying such as trehalose (formed by an α,α -1,1-glucosidic bond between two α -glucose units, see Fig. 1.1), e.g. in bacteria, fungi, lower plants and animals or sucrose, e.g. in higher plants.³² Furthermore, accumulation of heat shock and late embryogenesis abundant (LEA) proteins occur concurrently to stabilize the cells and tissues in the dehydrated state.^{41,42} The following section briefly describes the three hypotheses that have previously been proposed for the roles of sugars in desiccation states and membrane protection.

Water Replacement, Water Entrapment and Vitrification Hypothesis

The water replacement hypothesis first expressed by James Clegg⁴³ in 1967 and since then has been extended significantly. It states that sugars replace water molecules that interact with polar headgroups of lipids, suggesting that the hydroxyl groups of sugars can substitute for the H-bonding of water to polar residues of lipids.

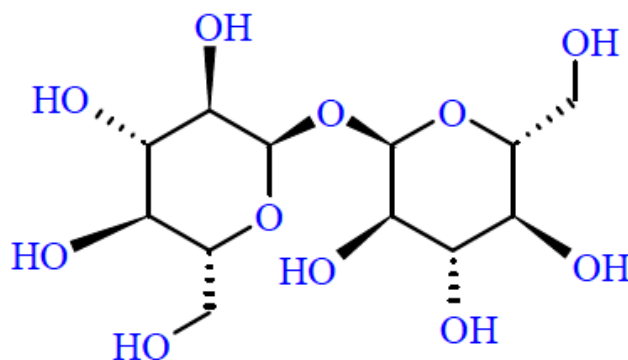


Figure 1.1: The chemical structure of trehalose. Trehalose is a natural disaccharide formed by an α,α -1,1-glucosidic bond between two α -glucose units.

This is important as it preserves the lipid order by maintaining sufficient spacing between lipids to keep the acyl chains in a liquid-crystalline state. Therefore, the membrane stays intact upon rehydration as schematically shown in Fig. 1.2.²¹ In the absence of sugar, removal of water around the cellular membrane during desiccation allows the PL molecules to pack more closely together. This eventually results in packing heterogeneity and reduced acyl chain density, thereby destabilizing the membrane and resulting in irreversible membrane damage when water is added during rehydration. In summary, the hydration effect of water can be imitated by sugars, suggesting that trehalose can preserve the physiological organization of PL membranes in the desiccated state. Interestingly, recent investigations have shown that the α,α -1-glucosidic linkage appears to be of prime importance to confer the stabilizing function to the disaccharide.⁴⁴

The water entrapment hypothesis, in contrast, proposes that sugars entrap residual water molecules near the surfaces of macromolecules, thereby maintaining their hydration and native properties in low water environments.⁴⁵ Despite this hypothesis was first proposed to explain protein stabilization, it can be generalized as well to membranes.

Finally, the process of vitrification suggests that sugars can form biological glasses or a ‘glassy state’ within the cells upon dehydration. This glassy structure, i.e., an amorphous highly viscous state, protects the subcellular structures by dramatically reducing the chemical reactions rates as well as the molecular diffusion rate.⁴⁶ Despite these different mechanisms, it appears that the three hypothesis are not mutually exclusive, in other words all mechanisms may operate at the same time. All these theories briefly mentioned above are indeed promising to explain the molecular details of anhydrobiosis and desiccation tolerance. However, it remains a large challenge to actually prove the occurrence of any of these processes in the natural lipids of an anhydrobiote.

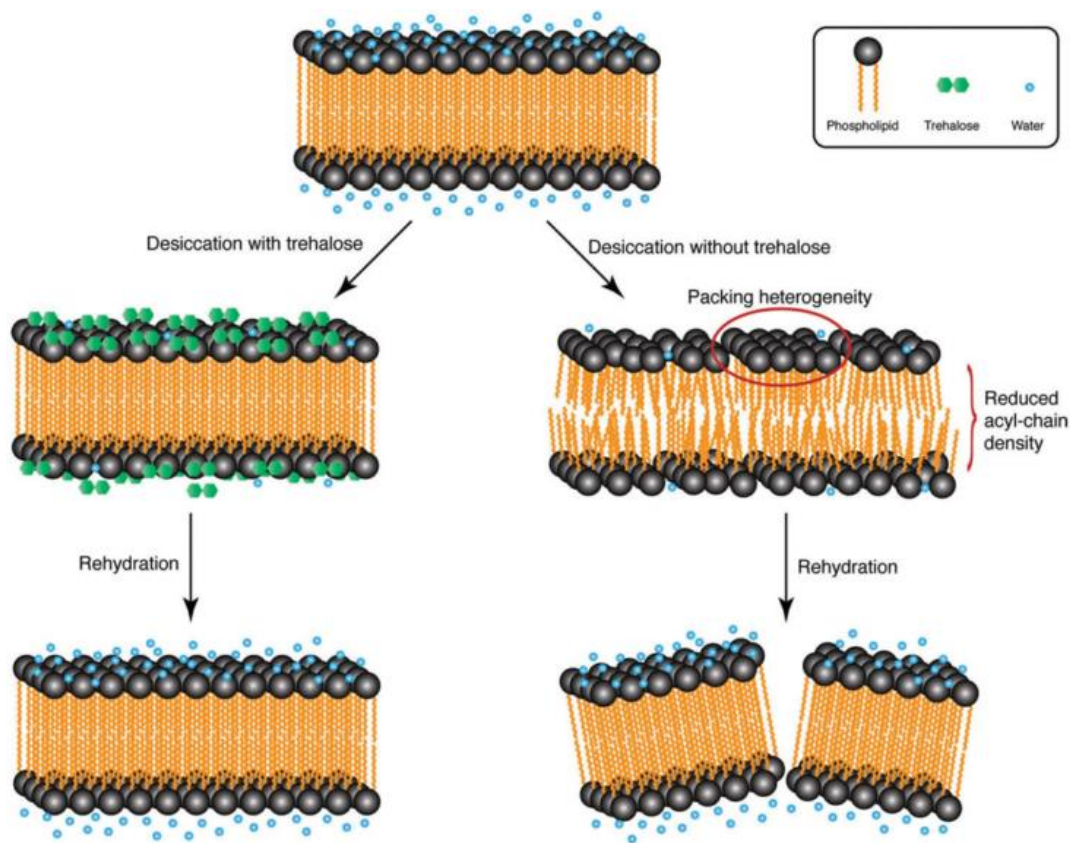


Figure 1.2: A simple model of the protective action of trehalose on membranes during desiccation and rehydration.²¹ In the fully hydrated state (top figure), PL headgroups interact with water. This interaction maintains the membrane in the liquid crystalline phase. Upon desiccation in the presence of trehalose, the hydration effect of water is compensated by the presence of the sugar (middle left figure), thus preserving the lipid order. Therefore, the membrane stays intact upon rehydration (bottom left figure). However, in the absence of trehalose, desiccation leads to PL packing heterogeneity and reduced acyl chain density (middle right figure), thereby destabilizing the membrane and resulting in damage to the membrane upon influx of water (bottom right figure).

It will be shown that the generality stated by each of these hypotheses is not fully applicable. Instead, the lipid headgroup composition very much influences how trehalose affects the phase transitions and other lipidic properties. The salient concept of this work is the direct comparison of native *C. elegans* lipids that have been derived either from desiccation-sensitive or a desiccation tolerant larval state of the nematode. Such a comparison is crucial to identify the protective mechanisms that are actually selected by evolution to confer desiccation tolerance to the organism. Here, the use of a *C. elegans* strain that forms a constitutive dauer state was of particular advantage to reach at this comparison.

Caenorhabditis elegans, A Model Organism for Biophysical Studies of Desiccation Toler-

1.3 ance

Nematodes are a diverse group of invertebrates that exist as parasites in other animals or parasites of plants, or as free-living forms in soil, freshwater, and marine environments. The life cycle of some nematodes includes specialized stages for resisting environmental stresses, such as a protective cyst or dauer.⁴⁷ *Caenorhabditis elegans* (Caeno, recent; rhabditis, rod; elegans, nice) is a free-living, non-parasitic soil nematode.⁴⁸ It was first described and named by Émile Maupas in 1900.⁴⁹ It has been successfully used as a model organism since the early 1970's when Sidney Brenner (Nobel Prize 2002) had introduced the nematode as an experimental model in Developmental Biology and Genetics. Several attractive features of *C. elegans* biology have contributed to its choice as a model experimental organism that possesses simplicity in various research fields. *C. elegans* is small (about 1.3 mm in length and 80 microns in diameter), transparent, easy to culture in the laboratory by growing quickly on bacterial lawn, such as *Escherichia coli* (*E.coli*) on agar plates.⁵⁰ In 1998, *C. elegans* became the first multicellular organism for which a complete genome sequence was obtained.⁵¹

1.3.1 Life Cycle of *C. elegans*

C. elegans has a short life cycle, going from egg to an adult in 3 days at 25 °C⁵² (see Fig. 1.3A, modified from⁵³). Its life span is short around 2 to 3 weeks under favourable living condition, which is important to reduce the experimental cycle and facilitate the biological studies.⁵⁰ Importantly, the period of *C. elegans* growth can be easily regulated by temperature. When the growth temperature is lowered to 15 °C, the development takes about twice as long.⁵⁴ The life cycle of *C. elegans*, similar to other nematodes, is comprised of the embryonic stage, four larval stages (L1-L4) and adulthood.⁵² It varies depending on certain environmental conditions. Under favourable conditions, *C. elegans* undergoes reproductive development and progresses rapidly from embryo to the

first larval state (L1) and molts into the second (L2), third (L3) and the fourth (L4) larval stages, and finally into the young adult stage as seen in Fig. 1.3B.⁵⁵ The young adults eventually restart the process by laying and (self)-fertilizing eggs.

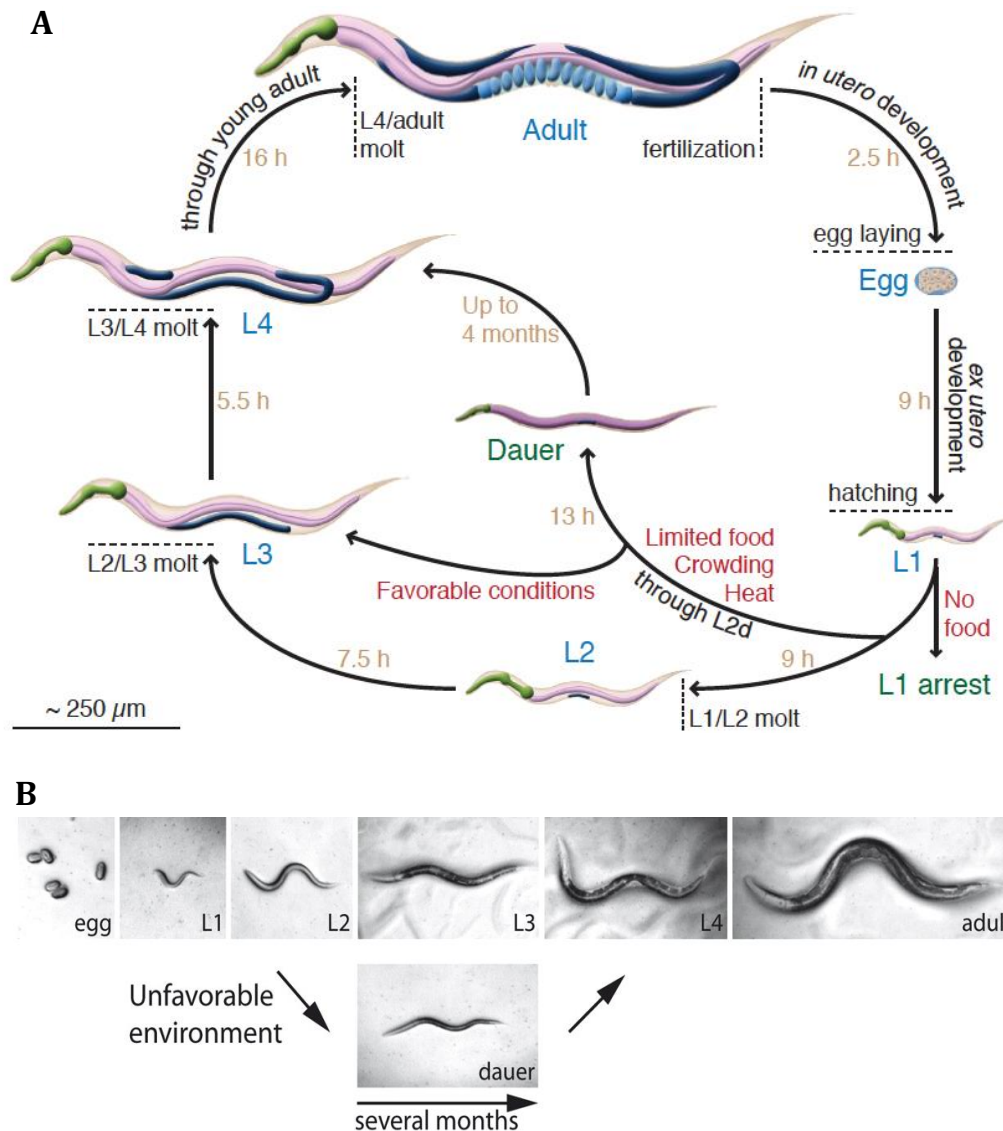


Figure 1.3: Life cycle and timing of developmental stages of *C. elegans* grown at 25 °C (A). Adapted from Altun and Hall (2009)⁵³ and modified by C. Erkut (2012).⁵⁶ Worms are drawn approximately to scale. (B) Micrographs of laid eggs, larval stages and adults adapted from Fienbach and Antebi (2008).⁵⁵ Under favorable conditions *C. elegans* goes through four larval stages before molting to an adult. When conditions are unfavorable (limited food or overcrowding) *C. elegans* undergoes an alternate dauer developmental stage, which can live several months. Upon return to favourable conditions, dauer larvae recover and mature to adulthood.

1.3.2 The Dauer Larva

The L1 stage is considered as a decision point, where the animal monitors three basic environmental conditions such as the amount of food, population density, temperature. When the egg hatches into an environment without food, it stops developing further and stays as an arrested L1. In the L1 stage, upon unfavorable conditions, such as overcrowding, or scarcity of food, or high temperature, the worm undergoes development to an alternative second larval stage known as the pre-dauer stage (L2d). As a response to these persistent conditions, L2d worms develop into a special stage known as the dauer (enduring) larva.⁵⁷ This is a survival strategy to overcome unfavorable conditions that would otherwise lead to a certain death.

Dauers are indeed special, as they can remain viable for up to four months without feeding, while they roam slowly and spend significantly low energy. Upon return to favorable environments, dauers molt directly into L4 (Fig. 1.3B), bypassing L3 and then develop into fertile adults.⁵⁸ Irrespective of the environmental parameters, large, pure dauer populations can easily be obtained in the liquid culture of the temperature-sensitive dauer constitutive mutant strain *daf-2(e1370)*. At 15 °C, these worms remain in the reproductive cycle, while at 25 °C, they stop developing further and they are arrested in the dauer stage. This is due to a temperature-sensitive mutation in the *daf-2* gene that encodes for an insulin-like growth factor (IGF-1). The dauer stage has many distinguishing properties characterized by a linear body morphology, as well as entry into a reduced state of metabolism (quiescence) and enhancement stress resistance for surviving unfavourable environmental conditions.⁵⁹

1.4 Biological Membranes

Biological membranes have long been and still are at the focus of much current research in biophysics and biochemistry, principally because of the important role they play in both the structure and function of all cells. Lipids, proteins, and carbohydrates are the main components of real biological membranes. One hypothesis for the structure of the cell membrane is the Fluid Mosaic Model proposed by Singer & Nicholson, which is still

the textbook picture of membrane organization (Fig. 1.4A⁶⁰). This model proposed that the membrane lipids form a two-dimensional bilayer that has to be in a fluid-like, liquid-crystalline state (Fig. 1.4B) in order to fulfil its biological tasks.⁶¹ This fluidity is modulated by the motional dynamics of the lipid molecules and especially their hydrophobic fatty acid chains. Hence, the regulation in the fluidity strongly influenced the permeability and mechanical properties of the membrane.⁶²

Lipids, the main components of biological membranes, are a class of relatively water-insoluble organic molecules. Lipids consist of a polar hydrophilic head and one to three nonpolar hydrophobic carbon chains. They are commonly categorized among three major classes: phospholipids, glycolipids, and cholesterol.⁶³ One of the main lipid components of most biological membranes is phospholipid (PL), which is amphiphilic (or amphipathic) in nature, that is, it has a hydrophilic and a hydrophobic part (Fig. 1.4C). A phospholipid is composed of two fatty acids, a glycerol unit, a phosphate group and a polar molecule. The length of the hydrocarbon fatty acid chains lies in the range from 12 to 24 carbon atoms. Usually, one chain is unsaturated carrying one or more *cis*-double bonds that introduce “kinks” in the carbon chain which favours the fluid nature of lipid membranes.^{64,65} The polar headgroups of PLs can be choline, ethanolamine, serine, inositol and glycerol. Accordingly, PLs are classified on the basis of their headgroup, thus the five major classes of PLs are phosphatidylcholine (PC), phosphatidylethanolamine (PE), Phosphatidylserine (PS), phosphatidylinositol (PI), and phosphatidylglycerol (PG).⁶⁶ In *C. elegans*, the distribution of PL headgroups is 55% ethanolamine, 32% Choline, 8% sphingomyelin, and 5% other PL classes, and this distribution changes in response to temperature.^{67,68} It will be shown in this work that it also changes in dauer larvae during acquiring desiccation tolerance.

1.4.1 Lipid Bilayers: Fluidity

The amphiphilic nature of lipid molecules defines their ability to form different types of structures in aqueous environment, among which a lipid bilayer is the most relevant structure formed in biological membranes. PLs submerged in an aqueous solution spontaneously associate to form bilayers, with their hydrophobic tails sandwiched between

the hydrophilic heads (Fig. 1.4B). This structure excludes the water molecules from the hydrophobic tails while keeping the hydrophilic head in contact with the aqueous solution. The fluidity of a lipid bilayer is highly affected by fatty acid composition and temperature. Clearly, the ability of PL molecules to pack against one another is influenced by the differences in the length and saturation of the fatty acid tails. If the lipid fatty acyl chains are short or have double bonds the bilayer is more fluid. This is because the short chains will interact less with one another than long chains. Moreover, the double bonds introduce kinks in the hydrocarbon tails, which generates steric hindrance for the PLs to pack tightly, thus the bilayer fluidity is increased. In addition, bilayer fluidity depends on temperature: at low temperatures, the fatty acyl chains of bilayer lipids can pack closely together to form an ordered arrangement. When the temperature is increased, the lipid molecules adopt a large number of thermally activated less regular structures of higher entropy, causing the bilayer to melt into a more disordered arrangement.⁶⁵ A central part of the work presented here is the observation of such structural transitions in real time and as a function of humidity using infrared spectroscopy (see chapter 3.5).

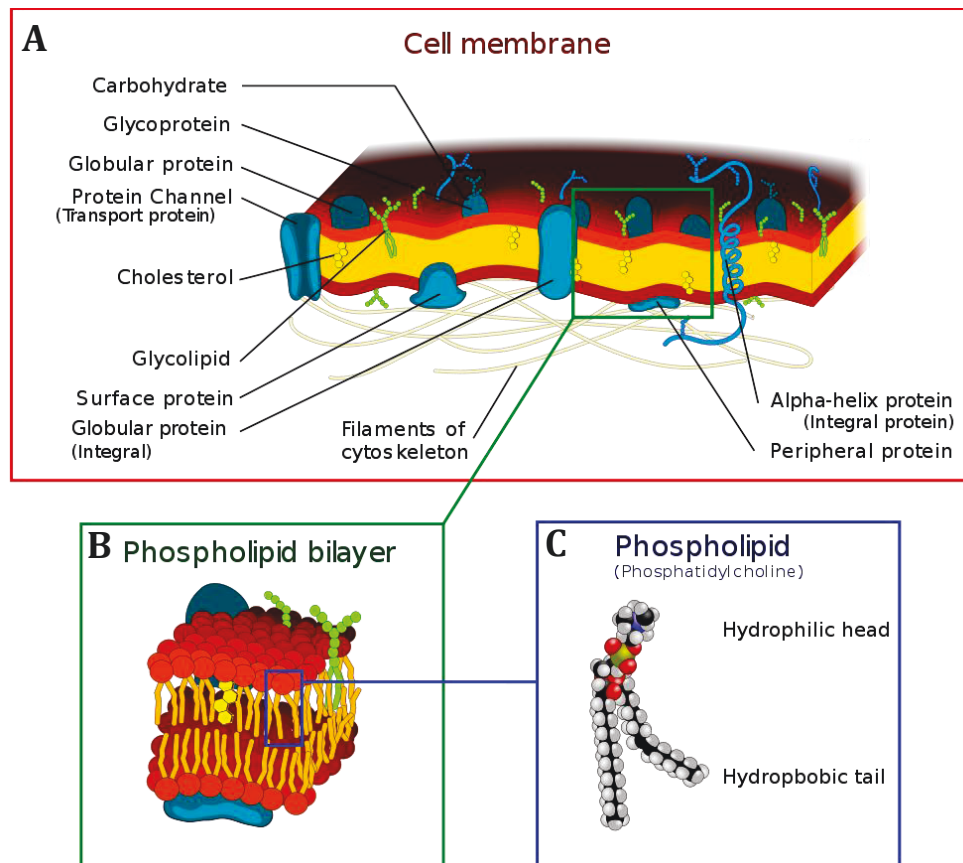


Figure 1.4: Schematic illustration of the fluid mosaic model. The plasma membrane structure is described as a fluid combination of phospholipids, cholesterol, proteins, and carbohydrates (A). The PLs are arranged in a bilayer with the polar hydrophilic head regions are in contact to the aqueous phases while the hydrophobic hydrocarbon tails are sandwiched between the hydrophilic heads (B). Space-filling model of a PL molecule structure (C).⁶⁰

1.4.2 Thermodynamics of Membranes: Phase Transition of Lipids

This section will briefly introduce the basic theory of phase transitions in the lipid bilayers and the significance of transitions for biological membranes. In fact, lipid structures can exist in different phases, depending on a very narrow range of chemical and physical parameters such as temperature, pressure, degree of hydration and the chemical composition of the PL itself, that are close to the physiological conditions.⁶⁹ In the bio-membrane literature, there are four temperature dependent phases as the following:⁷⁰

- Gel phase (S_0): It is a crystalline state where the lipids are highly ordered, and

with the chains in ‘all-trans’ conformation ordered and tilted. Commonly, it is also called the solid-ordered phase. This phase is favoured at low temperatures due to its low entropy.

- Liquid-ordered phase (L_0): In this phase all the lipid chains are ordered, while the lateral order of the lipids is random (liquid). It is normally observed only in membranes containing sterols.⁷¹
- Ripple phase (P_β): In this phase the system is partially gel and partially fluid. The occurrence of this phase is dependent on the lipid headgroup, chain length, hydration, etc., and it is easily abolished by addition of various biomolecules.⁷²
- Fluid phase (L_d): In this phase all the lipid chains are disordered and the lipid headgroups move freely within the bilayer. It is also called the liquid-disordered phase. This phase is favoured at high temperatures due to its high entropy.

In accordance with the above mentioned, three phase transitions may appear in the PL: the subtransition, the pretransition and the main melting transition (T_m). The transition between these phases occurs at well-defined temperatures and the main melting transition takes place from gel to fluid phase, if the temperature is raised across the melting temperature of the membrane. Figure 1.5 illustrates the bilayer melting transition in the biologically relevant gel and fluid phases. For most biological membranes this is in the range of 10–40 °C depending on a number of factors, such as the chain length, chain saturation, headgroup size and charge, co-addition of cholesterol, binding of molecules to the surface, etc.

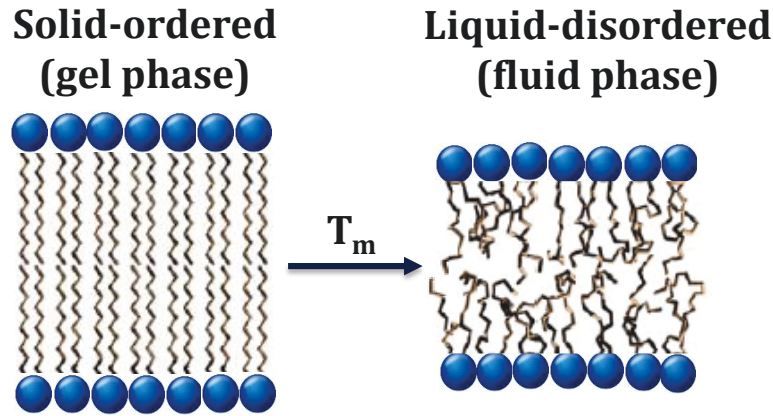


Figure 1.5: Scheme of PL phase transitions from gel states (solid ordered), to fluid states (liquid disordered) at a well-defined melting transition temperature (T_m).

1.5 Objectives of the Study

The molecular mechanisms underlying desiccation tolerance in *C. elegans* dauer larvae are not completely understood. Therefore, finding a biophysical approach to render cells resistant to desiccation has been an area of major interest. In this study, a well-established strain of *C. elegans* (*daf-2(e1370)* mutant) can be switched between a desiccation-sensitive and a desiccation-tolerant state (see below). The latter differ in their ability to synthesize trehalose and exhibit physiological as well as morphological manifestations of the different degrees of desiccation tolerance are used. The objectives of this study are summarized as the following:

Aim 1: Provide a novel experimental approach to study structural transitions in PLs from dauer larvae on a molecular level and with a time-resolution of seconds.

Aim 2: Compare structural transitions induced by hydration (lyotropic transitions) or temperature (thermo-tropic transitions) in PLs from desiccation-sensitive and desiccation-tolerant dauer larvae.

Aim 3: Understand at molecular detail how trehalose preserves the membrane structure and integrity during dehydration / rehydration and how it affects the lyotropic and thermo-tropic phase transition of *C. elegans* PLs at reduced humidity.

For these purposes, we have specifically developed hydration pulse-induced time-resolved Fourier-transform infrared (FTIR) difference spectroscopy (aim 1) to address the dynamics of hydration-dependent lipid structural changes within seconds as a function of basal hydration and trehalose in PLs derived from *C. elegans* dauer larvae. Additionally, Langmuir-Blodgett isotherms data have been recorded at the air/water interface to reveal how trehalose interacts with native PLs from dauer larva. These experiments allow deriving both the surface coverage of trehalose and its lipid binding energy. The dependence of trehalose insertion and surface coverage on lipid head groups is of particular interest to provide a molecular model of its biological function that will be compared with the IR data. Finally, the temperature-induced phase transitions of *C. elegans* PLs dauer larva have been observed in vitro using temperature-dependent FTIR and fluorescent LAURDAN labeling measurements. The fundamental concept of the study is the comparison of the results from all of these experiments for PLs derived from either the desiccation-sensitive (non-preconditioned) or the desiccation-tolerant (preconditioned) dauer state of *C. elegans* larvae.

METHODS: BIOPHYSICAL TECHNIQUES FOR STUDYING LIPID MEMBRANES

Contents

2.1	Fourier Transform Infrared Spectroscopy (FTIR)	20
2.1.1	Fundamentals of IR Spectroscopy	20
2.1.2	Physical Basis of IR Spectroscopy	22
2.1.3	Fourier Transform Infrared Spectrometer	23
2.1.4	Principles of Attenuated Total Reflection (ATR)-FTIR Spectroscopy	26
2.1.5	ATR-FTIR difference Spectroscopy	28
2.1.6	Time-Resolved FTIR Spectroscopy	28
2.2	Langmuir-Blodgett System	29
2.2.1	Langmuir Film Balance	29
2.2.2	Surface Pressure-Area Isotherm	30
2.3	Fluorescence Spectroscopy	31
2.3.1	Basic Fluorescence Theory	31
2.3.2	Fluorescence Measurements	33
2.3.3	Fluorophores	34
2.4	Differential Scanning Calorimetry (DSC)	35
2.4.1	DSC Working Principle	35
2.4.2	Basic DSC Theory	37

The real-time observation of the structure, dynamics and differences at the molecular level of membrane lipids requires structure-sensitive methods that allow observing subtle conformational changes in model and native PLs under conditions, as close to native conditions as possible such as solutions, vesicles, hydrated films etc. FTIR and especially time-resolved FTIR spectroscopy is the method of choice to observe the hydration sensitive transitions of native membrane PLs. We have specifically developed hydration pulse-induced time-resolved FTIR difference spectroscopy to address dynamic hydration-dependent lipid structural changes within seconds as a function of basal hydration, and trehalose in living *C. elegans* dauer larvae as well as in extracted lipids. Additionally, DSC and Langmuir-Blodgett isotherms data have been recorded to reveal how trehalose can energetically and structurally affect the lipid phase behavior to support a native lipid structure upon water loss. Fluorescence Spectroscopy was used to determine the H-bonding state of water that penetrates into the lipid layer below the headgroups between acyl chains and the glycerol backbone independence of hydration.

Fourier Transform Infrared Spectroscopy

2.1 (FTIR)

2.1.1 Fundamentals of IR Spectroscopy

Infrared spectroscopy (IR), which is used in a wide variety of scientific fields, is one of the most important absorbance techniques available. It is a non-destructive tool that measures the frequencies of molecular vibrations which gives information about the structure of a material by investigating its interaction with the electrical component of the IR radiation. An IR spectrum is obtained by passing radiation through a sample and determining what fraction of the incident radiation is absorbed at a certain energy. The IR spectrum is usually divided into three regions: near-IR (0.8-2.5 μm wavelength), mid-IR (2.5-25 μm wavelength) and far-IR (25-1000 μm wavelength) regimes. The mid-IR is often used to study fundamental vibrations and associated rotational-vibrational structure.

The IR spectrum is a graph of wavenumber (ν) vs. absorbance as a measure of band intensity, where (ν) is number of waves in a length of one centimeter and the unit used is cm^{-1} . The wavenumber has an important advantage of being linear with energy. It is given by the following relationship:⁷³

$$\vartheta = \frac{1}{\lambda} = \frac{\nu}{c} \quad (2.1)$$

Where λ is the wavelength, ϑ is the frequency and c is the velocity of light.

Commonly, IR spectra are measured in transmission-absorption mode with gas, liquid, or solid phase samples. During the measurement, radiation propagates directly through the sample and is absorbed at frequencies where resonant energy transfer occurs. The absorbance (A) at a given wavelength is directly proportional to the concentration of a sample according to the Beer's-Lambert Law, which is given as the following:

$$A = \log_{10} \left(\frac{I_0}{I} \right) = \varepsilon dc \quad (2.2)$$

Where I_0 is the intensity of the incident light, I is the transmitted intensity, ε is the extinction coefficient that reflects the transition probability, c is the concentration of the sample, and d is the thickness through which radiation is traveling.⁷⁴

The resulting IR spectra of most materials consist of a large number of absorption bands. These bands originate in the interaction between light and nuclear motions (vibrational and rotational modes) of the molecules, which are excited by the absorption of IR radiation. Since the constituents of a typical biological sample are present in a condensed phase (solids, liquids or solutions), only vibrational modes are observed. Consequently, IR spectra of biological samples are only vibrational spectra.⁷⁵ The large number of vibrational modes (i.e., $3N-6$, with N the number of atoms) in polyatomic molecules is a potential problem in interpreting IR spectra. Interpretation is however facilitated when the complexity of their chemical structure is restricted. For example all methylene stretching modes in a lipid are very similar and evaluated as a whole independently of their assignment to a specific acyl chain or segment. The most important reduction of information, however, is the use of difference spectroscopy. Here, only absorption changes in response to a specific perturbation, rather than the total

absorption of a sample is measured and evaluated as shown below (chapter 2.1.5).

2.1.2 Physical Basis of IR Spectroscopy

A molecule can be looked upon as a system of masses joined by bonds with spring-like properties. The atoms in a molecule can undergo different kinds of motion, including vibration and rotation about a bond. In general, a molecule can only absorb radiation when the incoming IR radiation is of the same frequency as one of the fundamental modes of vibration of the molecule. However, overtones and combination modes of vibration also occur. For linear diatomic molecules consisting of “a” and “b” atoms, there is only one mode of vibration, i.e., stretching of the bond and the vibrational frequency, w_{vib} is given by the equation:

$$w_{vib} = \frac{1}{2\pi} \sqrt{\frac{k}{\mu}} \quad (2.3)$$

Where k is the force constant of the bond and μ is the reduced mass of the molecule possessing this bond, which is represented by the following equation:

$$\frac{1}{\mu} = \frac{1}{m_a} + \frac{1}{m_b} \quad (2.4)$$

The equation of vibrational frequency can be modified to give the wavenumber values.

$$\nu = \frac{1}{2\pi c} \sqrt{\frac{k}{\mu}} \quad (2.5)$$

The Polyatomic molecules containing many N atoms will have $3N$ degrees of freedom (because of x , y , z coordinates for each atoms). For the co-linear molecules, because of two possible rotational degrees, there are $3N-5$ degrees of freedom of vibration.⁷⁶ Different Descriptive names are often given to vibrational modes that give rise to absorption. Vibrations can be subdivided into two classes, depending on whether the bond length or bond angle is changing as shown in figure 2.1: 1. Stretching (symmetric and asymmetric): is associated with a motion of atoms causing elongation and shortening of the chemical bond. The symmetric vibrations are generally weaker

than asymmetric vibrations since the former typically leads to a smaller change in dipole moment.

2. Bending (in plane vibrations: scissoring and rocking, and out-of plane vibrations: wagging and twisting):

- Scissoring mode is an in plane movement of atoms during which the angle between the bonds changes.
- Rocking mode, which involves atoms swinging back and forth in phase the symmetry plane of the molecule.
- Wagging mode is an in-phase, out-of-plane movement of atoms, while other atoms of the molecule are in the plane.
- Twisting mode is the movement of the atoms where the plane is twisted.

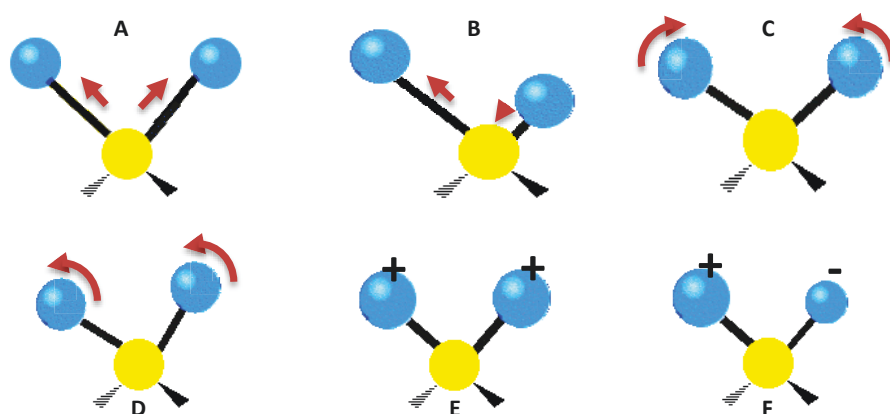


Figure 2.1: Localized vibrations of the methylene group highlighting the symmetric (A) and asymmetric (B) stretches, and the bending: scissoring (C), rocking (D), wagging (E) and twisting (F) vibrations.

2.1.3 Fourier Transform Infrared Spectrometer

Fourier transform infrared spectroscopy (FTIR), a common laboratory technique, has become a very valuable tool to study biomolecules in biological and medical areas. The FTIR method is based on the interference of radiation between two beams. The schematic diagram, figure 2.2, represents the Michelson Interferometer. Radiation from

a global light source (black-body radiation) strikes the beamsplitter. Some of the light is transmitted to a movable mirror and some of the light is reflected to a stationary mirror before both beams are recombined again on the detector where they interfere with each other. The moving mirror modulates the interference of each frequency of light with a corresponding modulation frequency. In general, the paths of light returning from the stationary mirror and the moving mirror are not in phase. Thus, they interfere constructively and destructively to produce a pattern called an interferogram. The most important feature of the interferogram is that every individual data point of this signal contains information over the entire IR region. In essence, the detector is always observing all frequencies at the same time. The interferogram is a plot of intensity versus time (where each sampled time interval corresponds to a defined optical path difference). By performing a Fourier Transform, the interferogram can be decomposed into its component wavelengths to produce a plot of intensity versus wavenumber, i.e. an IR spectrum.⁷⁷

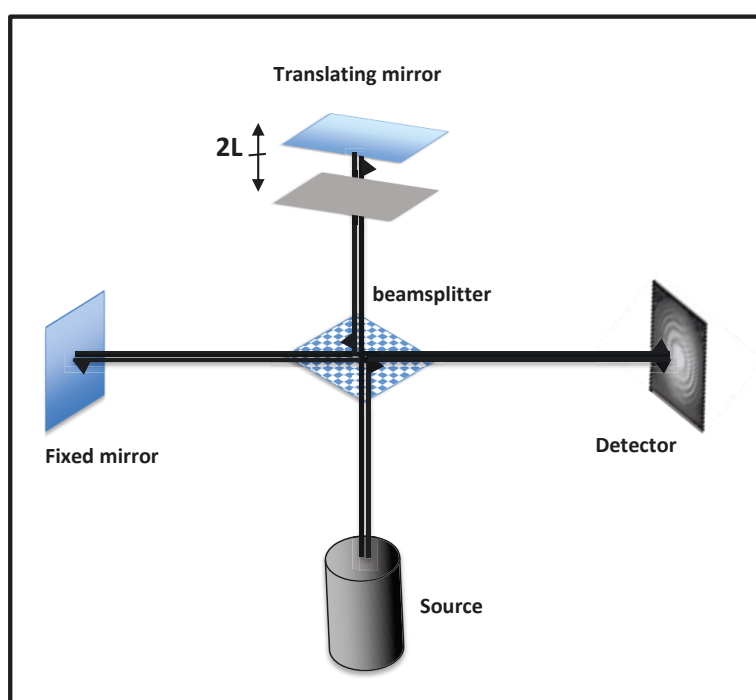


Figure 2.2: Michelson Interferometer: The beam of a global light source is split and recombined with a tunable optical path length difference generating polychromatic interference.

Fourier-Transformation: The essential equations for a Fourier-transformation relating the intensity falling on the detector, $I(\delta)$, to the spectral power density at a particular

wavenumber, ν , given by $B(\nu)$, are as follows:⁷⁸

$$I(\delta) = \int_0^{+\infty} B(\nu) \cos(2\pi\nu\delta) d\nu \quad (2.6)$$

which is one half of cosine Fourier-transform pair, with the other being:

$$B(\nu) = \int_{-\infty}^{+\infty} I(\delta) \cos(2\pi\nu\delta) d\delta \quad (2.7)$$

Equation 2.6 shows the variation in power density as a function of the difference in pathlength, which is an interference pattern. Equation 2.7 describes the variation in intensity as a function of wavenumber for an idealized, totally symmetric, interferogram that is fully described by cosine terms only.

Advantages: Some of the major advantages of FT-IR over the dispersive technique include:⁷⁸

1. Multiplex advantage (Fellgett): Improvement in the signal to noise ratio (SNR), proportional to the square root of the number of resolution elements.
2. Throughput advantage (Jacquinot): The total source output can be passed through the sample continuously, resulting in a substantial gain in energy at the detector, translating to higher signals and improved SNRs.
3. High scan rate: The mirror has the ability to move short distances rapidly to acquire spectra on a millisecond timescale.
4. Laser Referencing (Connes Advantage): By using a He-Ne laser as a reference, the mirror position is known with high precision.
5. Negligible stray light: The detector responds only to modulated light by AC coupling.
6. Powerful computers: Advances in computers and new algorithms have allowed for fast Fourier-transformation.

Principles of Attenuated Total Reflection (ATR)-FTIR

2.1.4 Spectroscopy

Several additional combined research techniques have been derived from FTIR, such as ATR-FTIR spectroscopy. Over the past few years, attenuated total reflection (ATR) has become one of the most powerful and versatile improvements in infrared absorption spectroscopy. ATR spectroscopy operates by measuring the changes that occur in a totally internally reflected IR beam when the beam comes in contact with a sample, and was independently pioneered by Fahrenfort⁷⁹ and Harrick⁸⁰ in the early 1960's.

It is essential to understand the basic principles that govern the absorption of the IR light at the reflecting interface of an internal reflection element (IRE). These principles have a profound impact on: (1) the spectrum intensity, (2) the band shape, (3) the intensity ratio between bands located at different wavelengths, (4) the ratio between the contributions of the bulk of the solvent and the sample, (5) the quantitative evaluation of surface concentrations, and (6) the impact of the polymer (or metallic layers) on the signal to noise ratio.

The principle of ATR is schematically shown in figure 2.3. When the light beam propagates from an optically denser medium (refractive index n_1) toward an optically rarer medium (refractive index n_2 , $n_1 > n_2$), the light beam is completely reflected at the interface of the two media if the angle of incidence (θ) exceeds the critical angle (θ_c) and multiple internal total reflections occur within the IRE until the beam exists the material. The critical angle can be defined as a function of the refractive indices of two media:

$$\theta_c = \sin^{-1} \left(\frac{n_2}{n_1} \right) \quad (2.8)$$

At each reflection, an evanescent field extends into the adjacent optically rarer medium. This evanescent field may be described as a standing electromagnetic wave normal to the interface of the two media. It results from the superposition of the electric fields of the incident and reflected waves. The amplitude of this evanescent wave (E) decays

exponentially with distance from the interface as following:⁸⁰

$$E = E_0 e^{-\left(\frac{z}{d_p}\right)} \quad (2.9)$$

Where E_0 is the time averaged electric field intensity at the interface ($z=0$), z is the distance from the interface of the rarer medium, and d_p is the penetration depth of the evanescent field. The penetration depth (d_p) is defined as the distance where the amplitude of the electric field is $1/e$ of E_0 , which is a function of refractive indices n_1 and n_2 , the incidence angle θ , and the wavelength of the radiation λ :⁸⁰

$$d_p = \frac{\lambda}{2\pi \sqrt{n_1^2 \sin^2 \theta - n_2^2}} \quad (2.10)$$

Using eq.2.9 for ATR diamond crystal, then the penetration depth of the evanescent wave is 0.15λ for water and 0.12λ for air. If the optically rarer medium – or constituents therein - is absorbing IR radiation, attenuated total reflection (ATR) is resulting at characteristic wavelengths corresponding to the vibrational resonant frequency. One of the main advantages of ATR spectroscopy is the ability to study samples under physiological conditions avoiding problems resulting from strong water absorbance in the interesting IR regions. Moreover samples can remain open at the upper side enabling manipulations (i.e., stimuli) and further simultaneous studies.

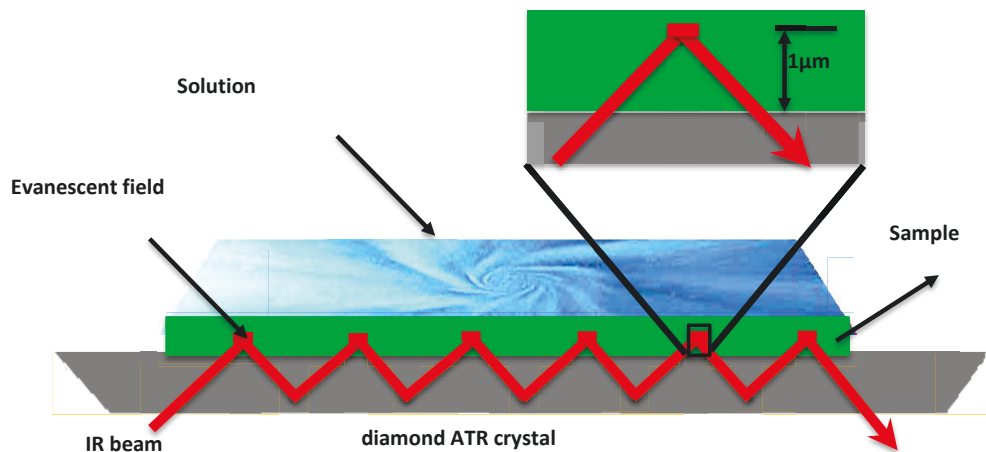


Figure 2.3: Schematic representation of ATR Principle: multiple internal reflection of the IR beam in the ATR crystal induces an evanescent field penetrating the first μm of the sample which can remain open at the upper side and can be studied under physiological conditions, i. e., in presence of solution.

2.1.5 ATR-FTIR difference Spectroscopy

To monitor conformational changes upon a stimulus by FTIR (e. g. light, change in pH, water network disturbance) it is inefficient to look at absolute spectra due to their extremely large number of overlapping bands. To overcome this problem, FTIR difference spectroscopy is performed, i.e. for an FTIR difference spectrum induced by a reaction from A to B, one calculates the absorbance spectrum of B minus the absorbance spectrum of A. Thus, the vibrations from groups that are not changed during the reaction cancel each other, and only the changes during the reaction are seen allowing the resolution of individual absorptions.⁸¹ ATR-FTIR difference spectroscopy hence provides an excellent tool for label-free characterization of conformational changes in proteins (secondary structure and side chain changes) and lipids. Additionally, this technique provides information that is complementary to X-ray structure analysis, including information on H-bonding, the protonation state, the charge distribution, and time dependence of reactions.

2.1.6 Time-Resolved FTIR Spectroscopy

Today's commercially available FTIR spectrometers are equipped with instrumentation that allows the measurements to be performed in a time-dependent fashion.⁸² Fast data acquisition using the FTIR technique enables time-resolved measurements in different modes: step-scan and rapid-scan FTIR. For step-scan FTIR a periodic process is monitored by stepwise alteration of the position of the moving mirror in the Michelson interferometer. At each position a complete process is recorded with a constant path length difference of the mirrors. Post-processing of the data includes sorting of data points to merge interferograms for each time point and after Fourier transformation spectra are obtained for each time point. The advantage of step-scan FTIR is that time-resolution is no longer limited by the maximum speed of the moving mirror but by the much faster electronic processing (detector electronics, analogue-to-digital converter etc.), however only relatively fast and strictly reproducible processes can be studied.

In this study, rapid-scan FTIR mode has been used, where after taking a reference spectrum of the sample in its ground state, one induces a reaction in the sample (e.g. by laser flash) and records interferograms in shorter times than the half-lives of the reactions using a high mirror speed. For one complete forward and backward movement of the mirror, up to 4 spectra can be obtained which results in a maximum time resolution of about 10 ms at 12 cm^{-1} optical resolution. A single experiment can yield a full series of time-resolved spectra used here to observe hydration-induced lipid structural changes.

2.2 Langmuir-Blodgett System

Among the various techniques used to deposit an ultrathin organic film on a solid substrate, the Langmuir-Blodgett technique is the most favorable since it allows (i) control over the monolayer thickness, (ii) uniform monolayer deposition over large areas and (iii) production of multilayer structures that can have altering layer composition. Another advantage of Langmuir-Blodgett technique is that it allows deposition of monolayers on almost all types of solid substrates.⁸³ This has been used here to study the interaction of trehalose with lipidic films.

2.2.1 Langmuir Film Balance

Irving Langmuir was the first person to conduct systematic studies on monolayers floating on water and was awarded the Nobel Prize for his work. In the early 1920's Langmuir also reported the transfer of monolayers of fatty acid from the surfaces of water onto solid substrates. But a more elaborate definition of such monolayer transfer (sequential monolayer transfer) was given later by Katherine Blodgett. Hence, these monolayer assemblies are called Langmuir-Blodgett (LB) films and the floating monolayers are referred to as Langmuir films.

Langmuir-Blodgett Technique enables precise control of the monolayer thickness and a homogeneous deposition of the monolayer over large areas, so it can be used in studying the properties of the natural biological membranes and in building of biosensors with a high stability and good response.⁸⁴

The Langmuir film balance consists of a rectangular trough (here, a Kibron Micro Trough S) that holds the subphase and prevents its leakage over the edges with Teflon barriers, two of which are movable, a small diameter (0.5 mm) special alloy wire connected to a microbalance, a temperature sensor and a temperature control plate, which is placed directly under the trough. In this thesis, Langmuir-Blodgett films were formed from lipid molecules as a model for cell membranes. These lipids are amphiphilic molecules, which consist of a hydrophilic and a hydrophobic part, which form insoluble monolayers at an air-water interface. In this work, Langmuir trough experiments of model lipids and *C. elegans*-derived membrane lipids at the air/water interface were conducted. The data concern the organization and molecular interactions within the films and allow deriving both the molar area of trehalose in the monolayers and its lipid binding energy.

2.2.2 Surface Pressure-Area Isotherm

A surface pressure isotherm, is a plot of the surface pressure versus area per molecule. It offers valuable information regarding the size and the shape of the molecules from the monolayer, as well as interactions that appear between those molecules.⁸⁵ To prepare an insoluble Langmuir film, the substance studied must be soluble in an organic volatile solvent (such as benzene, hexane, chloroform), then it will be spread at the interface. A time for solvent evaporation is needed. After that the experiment commences by compressing the film with the help of the movable barriers and the values of the surface pressure are automatically registered.⁸⁶ With increasing concentration of the molecules, the monolayer is passing from a very diluted two-dimensional gas-like state (the molecules have great distances from one another, the surface pressure is low) to a “liquid” state. Generally, there are two types of liquid state: a liquid expanded state and a liquid condensed state, depending on the orientation of the molecules. The next state is the solid one, where the molecules are closely packed and the surface pressure is higher. In this study, emphasis was put on retrieving the molar area of trehalose in the monolayer when it diffuses from the subphase into the lipidic phase.

2.3 Fluorescence Spectroscopy

2.3.1 Basic Fluorescence Theory

Fluorescence spectroscopy deals with the excitation and emission of the biomolecules under study. Any molecule can go into an electronically excited state when exposed to light of a wavelength (energy level) equal to the energy gap between the ground state and excited state. This is known as absorbance of light. The amount of light absorbed depends on the concentration of the absorbing molecule and its absorption cross-section. This connection is described in Lambert-Beers law. Measurement of the absorbance of a sample over a wavelength range results in an absorbance spectrum.⁸⁷

Luminescence is the emission of light from any substance and involves the relaxation from an excited to the ground state after absorption of a photon. It is formally divided into two categories: fluorescence and phosphorescence, depending upon the electronic configuration of the excited state and the emission pathway. In excited singlet states, the electron in the excited orbital is paired (by opposite spin) to the second electron in the ground state orbital. Consequently, return to the ground state is spin allowed and occurs rapidly by emission of a photon, the process is formally known as Fluorescence. The emission rates of fluorescence are typically 10^8 s^{-1} , so that a typical fluorescence lifetime is near 10 ns. Phosphorescence is emission of light from excited triplet states, in which the electron in the excited orbital has the same spin orientation as the ground-state electron. Transitions to the ground-state are forbidden and the emission rates are correspondingly slow.

The mechanisms of the excitation/emission processes in the molecule are conveniently illustrated by a Jablonski diagram (Figure 2.4), named after the polish scientist Alexander Jablonski. The various energy levels of the molecule are depicted by a stack of horizontal lines. Dependent on the energy of the light, the molecule is excited to different electronic singlet states S_1 , S_2 , etc. Relaxation through emission of light will in principle always occur from the lowest energy excited electronic state of a molecule (S_1) (Kashas rule),⁸⁸ thus when excited to a higher energy electronic singlet state (S_2 or S_3),

the molecule will undergo internal conversion prior to emission. Emission almost always occurs at a specific energy level (wavelength), independent of the energy (wavelength) of the excitation light. There is a loss of energy through radiationless processes (internal conversion), and the emitted light is always red shifted (towards longer wavelength) relative to the excitation light.^{89,90} The difference between excitation and emission wavelength is called the Stokes shift, which is directly related to the energy loss.

An emission spectrum is measured as the light emitted (fluorescence) across a broad wavelength range upon excitation at a fixed wavelength. Similarly, an excitation spectrum can be measured by measuring the emission at one fixed wavelength while exciting the molecule over a wavelength range. As stated above, excitation to different singlet states and to their different vibrational levels occurs at specific excitation wavelengths. This is reflected in the excitation spectrum by “spikes” or “fingers” on top the overall absorbance spectrum, reflecting the transitions to the different singlet states (e.g. $S_0 \rightarrow S_1$, $S_0 \rightarrow S_2$) and to different vibrational levels of the singlet states, depicted by 0, 1, 2, etc. Theoretically, when measuring a single fluorescing molecule, the excitation and absorption spectrum will be identical. Emission almost always takes place from the lowest singlet state S_1 to the ground state i.e. $S_1 \rightarrow S_0$ transition, and the emission spectrum therefore will most often have only a single peak (Gaussian or Lorentzian) shape. If there are “spikes” or “fingers” in the emission spectrum, it is due to transition to a higher vibrational level of S_0 . Eq. 2.11 and Eq.2.12 describe the transitions between ground state and excited state.



The $h\nu$ in Eq. 2.11 is the absorbed photon to excite the electron from S_0 to S_1 state, and the $h\nu_1$ in Eq. 2.12 corresponds to the emitted photon when the electron relaxes to the ground state.

The shape of excitation and emission spectra is often described in the mirror image rule, which says that the emission spectra, the $S_1 \rightarrow S_0$ transition, is a mirror image of the excitation/absorbance spectrum of the $S_0 \rightarrow S_1$ transition.^{89,90} As a consequence

of the above-described properties, the emission spectrum from a given fluorophore measured upon different excitation wavelengths will only vary in intensity but not in shape, and the shape of the emission spectrum is thus independent of the excitation wavelength. The opposite is also true; the excitation spectrum is independent of the emission wavelength. The fact that the fluorescence spectrum is measured as a function of two factors; excitation and emission wavelength, makes fluorescence spectroscopy a versatile method to correlate spectral features to specific structural properties and solvent interactions of chemical compounds.

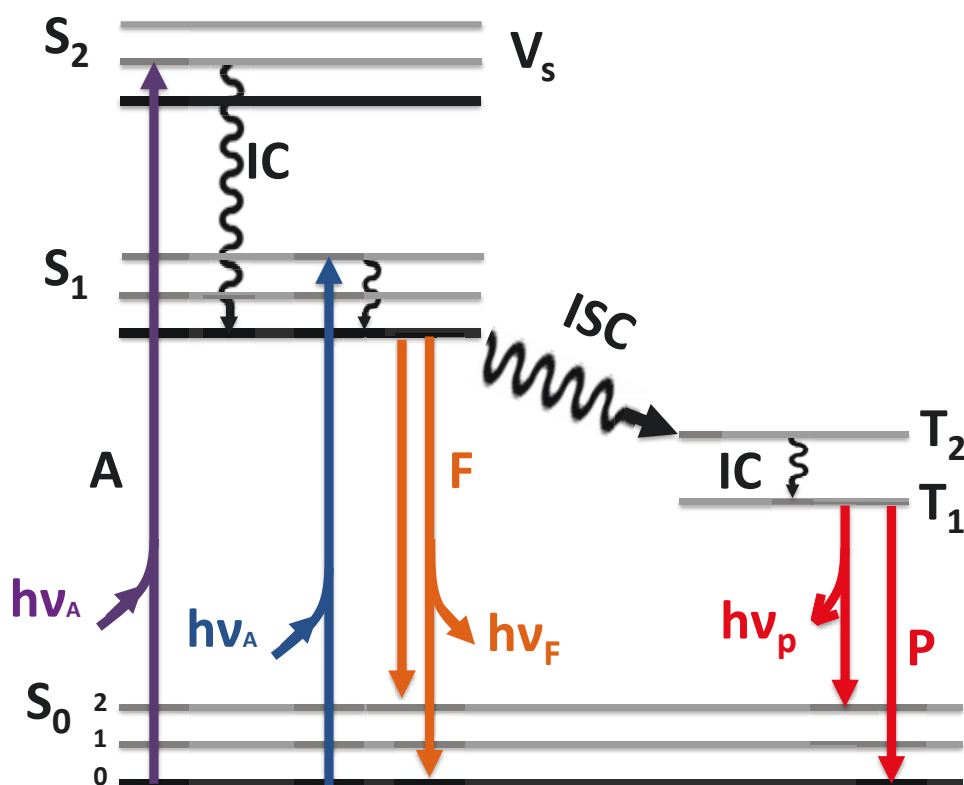


Figure 2.4: Jablonski diagram: S_0 : ground state, S_1 : singlet state, V_s : excited vibrational state, T_1 and T_2 : triplet states, A: absorption of a photon, IC: internal conversion, F: Fluorescence emission, ISC: inter-system crossing, P: phosphorescence.

2.3.2 Fluorescence Measurements

Fluorescence measurements are classified into two main types: 1) steady state measurements, where the sample is excited with continuous beam of light and emission intensity is measured 2) time-resolved measurements of fluorescence intensity decay when the sample is excited by a pulsed laser. In this work, measurements were performed in the

steady state i.e. under constant illumination and observation of emission. A sample reaches its steady state immediately after the illumination and in its simplest form the decay of the fluorescent intensity following a short excitation pulse, $I(t)$, is a single exponential process.

$$I(t) = I_0 e^{\frac{-t}{\tau}} \quad (2.13)$$

Here, I_0 is the fluorescence intensity at time $t = 0$, and τ is the fluorescence lifetime.

2.3.3 Fluorophores

Fluorophores are typically compounds with aromatic rings having a conjugated π -electron system. Fluorophores in biological applications can be broadly divided into two main categories: intrinsic and extrinsic. Intrinsic fluorophores are those that occur naturally and include aromatic amino acids, flavins and derivatives of pyridoxal and chlorophyll. Extrinsic fluorophores are those added to a sample that does not display the desired spectral properties.

Typically, the membranes do not show intrinsic fluorescence; therefore, it is common to label the membranes with fluorescent probes that spontaneously partition into the membranes hydrophobic side chain region. Other lipid probes include fluorophores attached to lipid or fatty acid chains. The local environment surrounding a fluorophore can affect the fluorescence signal. Factors such as pH, temperature, concentration and polarity can in one way or another affect the emission from a given fluorophore. The polarity of the solvent is an especially important factor as it causes a shift in the emission. When the molecule is excited, the dipole moment is higher than in the ground state. In a highly polar environment a “solvent” relaxation will occur, making the dipole moment between ground state and excited state smaller, and thus a lower energy difference between the two states. This will lead to a longer emission wavelength (a red shift) compared to the same molecule in a non-polar environment. Among several different fluorophores, the fluorescent probe 2-dimethylamino-6-lauroylnaphthalene (LAURDAN) has widely used and presented several advantages for the membrane studies. This probe shows spectral sensitivity to the polarity of its environment, with a 50-nm red shift of its emission maximum in polar versus nonpolar environments, so that simple

fluorescence intensity measurements provide information on the membrane polarity. Several studies have shown that LAURDAN spectroscopic properties reflect local water content in the membrane,⁹¹ and hence is the subject of our study. A schematic diagram of the LAURDAN structure is shown in Fig. 2.5.

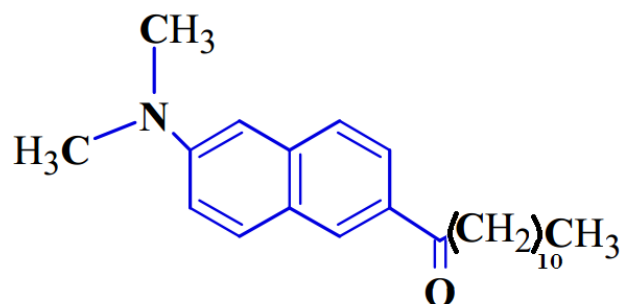


Figure 2.5: A schematic diagram of LAURDAN, a fluorescent dye commonly used in fluorescence spectroscopy of lipidic phases.

2.4 Differential Scanning Calorimetry (DSC)

DSC is a method to measure the thermal behavior of lipid bilayers. This technique is of primary importance in study of phase transitions in lipid/water systems.^{92,93} It is used to monitor and characterize changes in the physical state in polymorphic lipids and also to characterize the perturbations on pure lipids by the interactions with other materials, such as other lipids, proteins, sugars, ions, or small hydrophobic molecules. The thermal behavior of a vesicle is particularly sensitive to perturbing species, which can result in a shifted transition temperature (T_m) or a change in transition enthalpy.^{94–97} This technique complements well the other methods previously described, as it can determine the membrane lipid phase transition and its dependence on "perturbing" compounds such as carbohydrates as shown below.

2.4.1 DSC Working Principle

Briefly, one measures the difference in the amount of heat required to increase the temperature of a sample and a reference as a function of temperature. Depending on the nature of the process (exothermic or endothermic), more or less heat must flow

to the sample. For instance, as a gel state lipid membrane melts (an endothermic phase transition) it will require more heat flowing to the sample in order to increase its temperature at the same rate as the reference.

The basic principle of DSC instrument is shown in figure 2.6. It consists of two cells that are enclosed by an adiabatic shield to prevent uncontrolled heat leakage. One cell is filled with sample (e.g. a lipid/buffer solution) and the other with a reference solution (usually a buffer). The temperature of the cells is then increased linearly as a function of time while keeping the temperature difference between the two cells at zero. The parameters reported from this technique for lipid systems are:

- Transition midpoint temperature, T_m : where the transition is 50 per cent complete.
- Transition enthalpy, ΔH : the actual heat required for the entire transition normalized per mole or per unit weight.
- Heat capacity, C_p : the amount of heat (per gram or per mole) required to raise the temperature of the sample by a given temperature increment.

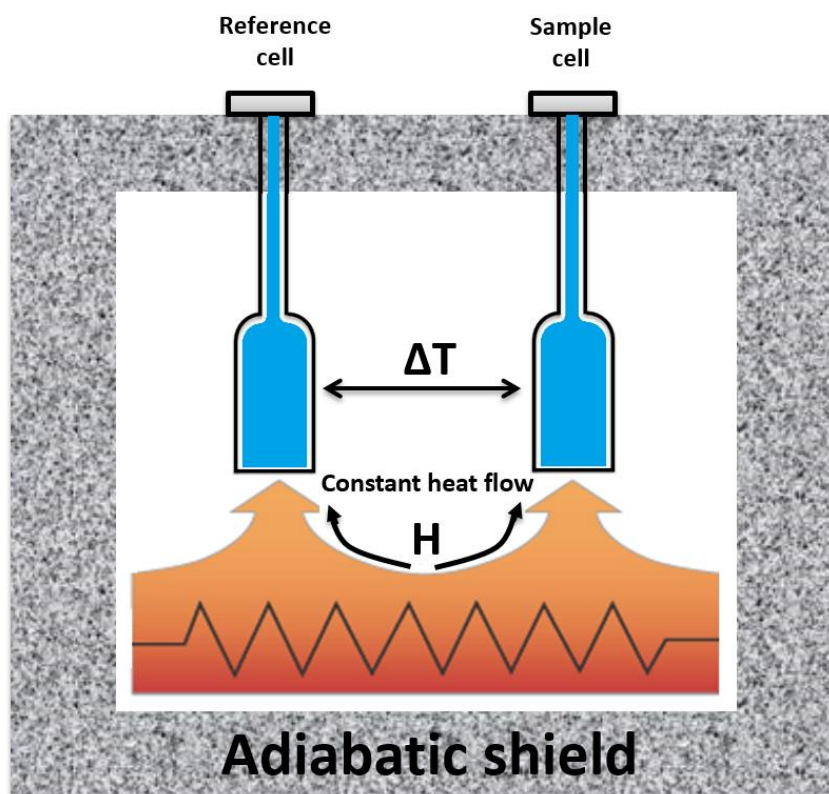


Figure 2.6: Principle scheme of a differential scanning calorimeter.

2.4.2 Basic DSC Theory

If an exothermic or endothermic process takes place within the sample, there will be a significant deviation in the difference between the two heat flows ($\Delta P = P_{sample} - P_{reference} \neq 0$), and a peak will show up in the DSC curve. By integrating the excess power, ΔP , with respect to time, the excess heat flow to the sample is consequently

$$\Delta Q = \int_t^{t+\Delta t} \Delta P(t') dt' \simeq \Delta P \cdot \Delta t \quad (2.14)$$

The heat capacity is given by the energy needed, ΔQ , to heat the system ΔT at constant pressure, i.e.

$$\Delta c_p = \left(\frac{\Delta Q}{\Delta T} \right)_p = \frac{\Delta P}{\Delta T / \Delta t} \quad (2.15)$$

Where $\Delta T / \Delta t$ is known as the scan rate. So by simply monitoring the power difference of the two cells one has a direct measure of the excess heat capacity of the sample substance, from which one can easily derive the transition enthalpy and entropy. Specifically, one can obtain the melting enthalpy and entropy of the lipids from the heat capacity profile of one-component lipid system: the enthalpy change of the transition is obtained by integrating over the heat capacity in the relevant temperature interval, i.e.

$$c_p = \frac{dH}{dT_p} \Rightarrow \Delta H = \int_T^{T+\Delta T} c_p \cdot dT \quad (2.16)$$

The entropy change can then easily be determined, because the transition midpoint, T_m , can be read off the heat capacity profile directly. For a narrow transition, $\Delta S = \Delta H / T_m$.

The DSC enables the precise determination of the temperature and the enthalpy change of the lipid transition from the ordered phase to the fluid phase. Moreover, the shape of the DSC peak carries information about the nature of the transition. In the following, the cooperative phase transition theory of the main (or chain melting) transition of lipid bilayers is introduced, which establishes the quantitative interpretation of DSC curves of PL samples.⁹⁸ The basis of the theory is the assumption that the lipid molecules can be in three different states, namely they can be in the ordered, fluid

and in the interfacial phase. The free energy of the molecules in these states comes from the rotational isomerism of the lipid chains, the electrostatic and van der Waals forces between the molecules and the configurational disorder of the lipid chains. The cooperativity of a transition from the ordered phase to the fluid phase originates in the fact, that the interfacial molecules have an extra free energy contribution from the packing mismatch of the hydrocarbon chains. This tends to reduce the number of the molecules in the interfacial region and causes narrow DSC curves as the melting occurs in a small temperature interval. Here, DSC studies were performed with model lipids to study the role of their headgroup structure for interacting with trehalose.

MATERIALS & DATA ACQUISITION

Contents

3.1	Organisms & Culture Conditions	40
3.1.1	Nematode & Bacteria Culture Conditions	40
3.2	Desiccation & Preconditioning Assay	41
3.2.1	Controlled Humidity Environments	41
3.2.2	Dauer Larvae Preconditioning Assay	41
3.3	Biochemical Analysis of <i>C. elegans</i> Dauer PLs	42
3.3.1	Organic Extraction & Column Separation	42
3.3.2	Thin Layer Chromatography (TLC) Analysis	43
3.4	Materials	44
3.5	Time-Resolved FTIR Spectroscopy Studies	44
3.5.1	Hydration-Perturbation Measurements	44
3.5.2	Time-Resolved Spectra Acquisition	46
3.5.3	Spectral Processing	49
3.6	Thermo-tropic Measurements by ATR-FTIR Spectroscopy .	51
3.6.1	Temperature-Induced Phase Transition Determination of <i>C. elegans</i> Dauer Larvae Membrane PLs	51
3.7	Langmuir-Blodgett Monolayer Studies	53
3.7.1	Formation of PLs Monolayer	53
3.7.2	Surface Pressure-Area Isotherm Measurements	53
3.8	Thermo-tropic Measurements by Fluorescence Spectroscopy	55
3.9	Differential Scanning Calorimetry (DSC) Studies	56
3.9.1	DSC Measurements	56

This chapter describes the materials preparative and experimental methods used throughout this thesis. It first describes the *C. elegans* culture conditions and their native lipid extraction. The implementation of a novel FTIR hydration-perturbation method is described in particular detail because it is not generally applied and was adapted here specifically for the study of fast lyotropic transitions. Then, how Langmuir-Blodgett isotherms were recorded as a function of trehalose PL interactions is also explained in larger detail because the data collection was performed in a continuous pressure-dependent manner rather than measuring sugar-induced area increase of PL films at selected constant pressure values. Additionally, Fluorescence Spectroscopy and DSC measurements are described.

3.1 Organisms & Culture Conditions

3.1.1 Nematode & Bacteria Culture Conditions

The temperature-sensitive dauer-constitutive *daf-2(e1370)* strain of *Caenorhabditis elegans* was obtained from the Caenorhabditis Genetics Center (Minneapolis, MN). This strain of *C. elegans* is a conditional mutant which at 15 °C undergoes a reproductive life cycle similar to the wild type and can thus be propagated. However, eggs grown at 25 °C exclusively develop into dauer larvae. We used the latter regime to obtain large populations of pure dauer larvae whose phenotype can be changed from desiccation-sensitive to-tolerant depending on preconditioning (see chapter 3.2). Worms were maintained at 15 °C on nematode growth medium (NGM) agar plates (1.7% (w/v) agar, 0.25% (w/v) peptone, 50 mM NaCl, 18.5 mM K₂HPO₄, 6.5 mM KH₂PO₄, 1 mM CaCl₂, 1 mM MgSO₄, 13 mM cholesterol) seeded with 10X concentrated *Escherichia coli* strain NA22 as the food source.⁹⁹ Worms first were bleached with alkaline hypochlorite solution (0.5 M NaOH, 75 mM NaOCl) to obtain clean eggs.¹⁰⁰ They were then grown at 25 °C in complete S medium (100 mM NaCl, 37 mM K₂HPO₄, 13 mM KH₂PO₄, 8.8 mM tripotassium citrate, 3 mM CaCl₂, 3 mM MgSO₄, 1.2 mM citric acid monohydrate, 50 µM Na₂EDTA, 25 µM FeSO₄, 10 µM MnCl₂, 10 µM ZnSO₄, 1 µM CuSO₄, 13 µM cholesterol, pH 6) until they completely arrested as dauers (usually for 3-5 days).¹⁰¹ E.

coli NA22 bacteria grown in 2X YT medium (1.6% (w/v) tryptone-peptone, 1% (w/v) yeast extract, 5% (w/v) NaCl, pH 7) was used as the food source ad libitum.¹⁰²

3.2 Desiccation & Preconditioning Assay

3.2.1 Controlled Humidity Environments

Controlled humidity environments were created in sealed chambers that contained defined concentration of NaOH solution at the bottom of the lower compartment as shown in figure 3.1. These desiccation chambers were modified Rotilabo-desiccators (2.15 or 4.35 L; Carl Roth, Germany). Into the lower compartment, 100 ml of NaOH solution was added. The concentration of NaOH was adjusted until 98% RH was reached, based on the empirical data published by Stokes and Robinson.¹⁰³ For better sealing, grease was spread between the lid and the main body of the desiccator. The desiccation Chambers were always kept in a temperature-controlled room at 24 ± 0.5 °C. The temperature and RH within each chamber were continuously measured by a thermo-hygrometer mounted on the lid of the chamber from the inside.

3.2.2 Dauer Larvae Preconditioning Assay

Dauer larvae from liquid cultures or radioactive labeling plates were collected into 15 ml conical tubes (Corning) and washed 2–3 times by pelleting at 1200g for 1 min at room temperature. The supernatant was removed and tubes were filled with distilled water. Then, worms were pelleted again and this washing was repeated 2–3 times to remove bacteria, salts and debris. Finally, the larvae were re-suspended in 2 ml water. One half of the worms were immediately snap-frozen in liquid nitrogen (non-preconditioned group). The remaining was first filtered on Isopore TETP membranes (8 μ m pore size, Millipore, USA) and then placed on the center of a 35 mm plastic Petri dishes, then the dishes were placed into a controlled humidity chamber (preconditioned group). Preconditioning was performed by keeping the worms at 98% RH for 4 days. In the

preconditioning chamber (98% RH) it takes several hours for the water droplet to evaporate. Therefore, dauers were put on petri dishes late in the evening and the preconditioning time was started from the next morning when the excess water had already evaporated. After 4 days of preconditioning, they were collected in 1 ml distilled water and snap-frozen in liquid nitrogen.

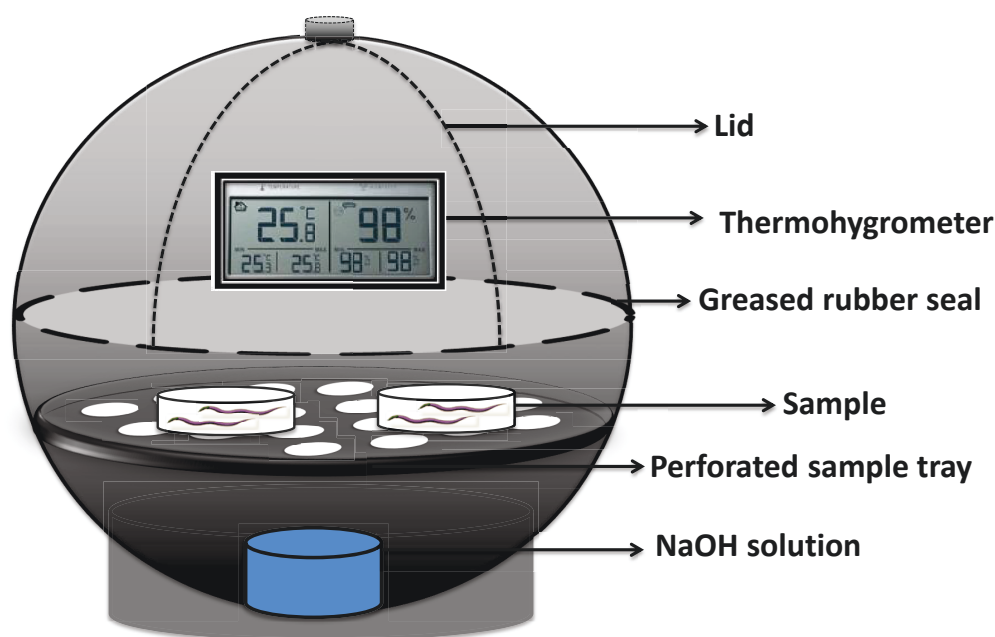


Figure 3.1: Schematic representation of a controlled humidity chamber. The NaOH solution at the bottom of the chamber creates a 98% RH over the sample, under which the sample dries until reaching an equilibrium with the air. The Thermo-hygrometer constantly displays current temperature and RH information. Grease is spread between the lid and the main body to improve isolation from the outside.

3.3 Biochemical Analysis of *C. elegans* Dauer PLs

3.3.1 Organic Extraction & Column Separation

Native *C. elegans* PLs were extracted from preconditioned and non-preconditioned dauer larvae. Frozen worm suspensions were thawed in an ultrasound water bath for 5 min and frozen again in liquid nitrogen, in total five times for efficient homogenization. Total soluble protein amounts were measured by BCA assay (Thermo Scientific, USA) at this stage when necessary. Subsequently, homogenates were extracted via Bligh and

Dyer's method.¹⁰⁴ In this method, 1 ml of homogenate in water was mixed with 3.75 ml of $\text{CHCl}_3:\text{CH}_3\text{OH}$ (1:2, v:v) for at least 25 min and then centrifuged at 3000 g for 5 min at room temperature to pellet cuticles and non-soluble material. The supernatant was transferred into a fresh tube and 1.25 ml CHCl_3 is added. To induce phase separation, 1.25 ml H_2O was finally added to the mixture. After thorough mixing, phase separation was accelerated by centrifugation at 3000 g for 10 min. This yields an upper aqueous phase that contains hydrophobic molecules (e.g. sugars), a lower lipid-enriched organic phase and a thin interphase that contains mostly proteins and DNA. The lower phase is transferred to a tube, dried under N_2 flow and dissolved in $\text{CHCl}_3:\text{CH}_3\text{OH}$ (2:1, v:v). The total organic phase of extracts were separated into three fractions via solid phase extraction (SPE) by loading it on a CHCl_3 -equilibrated silica gel column and eluting subsequently with CHCl_3 , $(\text{CH}_3)_2\text{CO}:\text{CH}_3\text{OH}$ (9:1, v:v) and CH_3OH . Dry weights of each fraction were measured for normalization. Separation was verified by thin layer chromatography on 10 cm HPTLC plates (Merck, Darmstadt, Germany) using $\text{CHCl}_3:\text{CH}_3\text{OH}:\text{H}_2\text{O}$ (45:18:3, v: v: v) as the mobile phase. Only the CH_3OH fraction, which is enriched in PLs and relatively hydrophilic lipid species, was used in subsequent experiments.

Radioactive Labeling of *C. elegans* Dauer Lipids. To radioactively label dauer lipids, eggs were grown at 25 °C until dauer arrest on NGM agar plates with *E. Coli* NA22 bacteria containing 10 μCi ^{14}C -labeled NaCH_3COO (Hartmann Analytic, Germany) to allow for the incorporation of acetate into all synthesized lipids. They were then processed as explained above. Radioactively labeled lipid fractions were normalized by scintillation counting whereas non-labeled lipid fractions were normalized by dry weight or total soluble protein amount in the original homogenate.

3.3.2 Thin Layer Chromatography (TLC) Analysis

For qualitative chemical analysis of PLs, equivalent amounts of total lipid extracts or methanol fractions of SPE were separated on two-dimensional thin layer chromatography (1st dimension $\text{CHCl}_3:\text{CH}_3\text{OH}:\text{NH}_3$ (32%) (65:35:5, v:v:v); 2nd dimension $\text{CHCl}_3:\text{CH}_3\text{OH}:(\text{CH}_3)_2\text{CO}:\text{CH}_3\text{COOH}:\text{H}_2\text{O}$ (50:10:20:12.5:5, v:v:v:v)). TLC plates

with radioactively labeled lipids were sprayed with scintillation solution and placed in an exposure cassette with an X-ray film (Kodak, Germany) for 2 weeks. Other TLC plates were dried and sprayed with 3% (w/v) $\text{Cu}(\text{CH}_3\text{COOH})_2$ in 8% (v:v) H_3PO_4 and baked 5 min at 180 °C to visualize all lipid species with at least one double bond in the hydrocarbon chain.

3.4 Materials

Native *C. elegans* PLs were extracted from preconditioned and non-preconditioned dauer larvae as described above. Several Experiments have been performed on model PLs with different headgroups. The model lipids have been used were: 1,2-dimyristol-sn-glycero-3-phosphate (DMPA), 1,2-dimyristoyl-sn-glycero-3-phosphocholine (DMPC), 1,2-dimyristoyl-sn-glycero-3-phospho-(1'-rac-glycerol) (DMPG), 1,2-dimyristoyl-sn-glycero-3-phosphoethanolamine (DMPE), and L- α -phosphatidylcholine (liver, Bovine PC), which were purchased from Avanti Polar lipids (Alabaster, Alabama, USA). The lipids were used without purification. Each lipid was dissolved from powder into chloroform (+99.9%) and stored at -20 °C until use. Trehalose dihydrate (α -D-glucopyranosyl- α -D-glucopyranoside) was purchased from AppliChem GmbH (Darmstadt, Germany). LAURDAN (2-dimethylamino-6-lauroylnaphthalene) was purchased from Anaspec Inc. (Fremont, USA). Phosphate buffers were prepared using Na_2HPO_4 and $\text{NaH}_2\text{PO}_4 \cdot \text{H}_2\text{O}$. The appropriate amount of salts were added to a volumetric flask and dissolved in millipore water to obtain 10 mM solutions adjusted to pH 7.4 that determined experimentally using pH-meter.

3.5 Time-Resolved FTIR Spectroscopy Studies

3.5.1 Hydration-Perturbation Measurements

Vesicles preparation: Multilamellar PL vesicles (MLVs) were prepared by removing the organic solvent from the lipid extracts by drying under nitrogen gas, followed by vacuum-drying for at least 2 h and re-suspension in water (1 mg/ml). Vesicles were mixed rigorously every 10 minutes during 2 h incubation at 60 °C followed by 15 cycles

of liquid nitrogen freezing and thawing. As shown in figure 3.2, the uniform larger unilamellar vesicles (LUVs) were obtained by extrusion of the MLVs suspension through a 100-nm polycarbonate filter using a LiposoFast extruder (Avestin, Ontario, Canada).

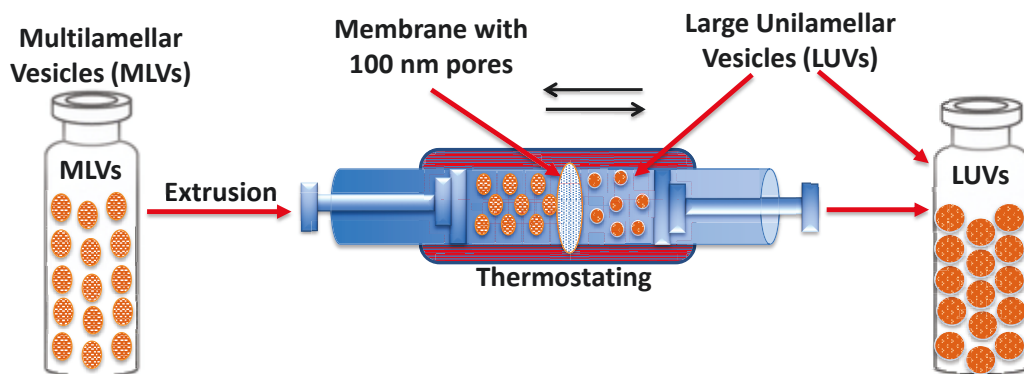


Figure 3.2: Schematic representation of large unilamellar vesicles (LUVs) preparation from multilamellar vesicles (MLVs) using the extrusion through a 100-nm polycarbonate filter.

Experimental Procedures: 20 μL of the vesicles suspension (~ 3 mM lipid) was either supplemented with 2 μL of a 0.15 mM trehalose solution or spread directly on the diamond surface of an attenuated total reflectance ATR-crystal (RESULTEC, Illerkirchberg) and dried under nitrogen gas. The lipid film was equilibrated overnight at a 75% RH using a saturated salt solution in a reservoir. The later was separated from the sample compartment by a dialysis membrane placed 1 mm above the lipid film on the ATR-crystal (see figure 3.3). Hydration pulses were generated by an electrical current (0.7 A) sent for 4 s through a heating wire (0.26 Ohm) immersed in the salt solution. Thereby, the equilibrium with the gas phase below the dialysis membrane is perturbed such that water is transferred from the reservoir, leading to a transient increase of lipid hydration through the gas phase. By calibration of the water (OH) absorption of an individual sample at different RHs, this regime generated at a basal 75% RH an initial water uptake by the PL film that corresponded to a RH change of 5 – 7%.

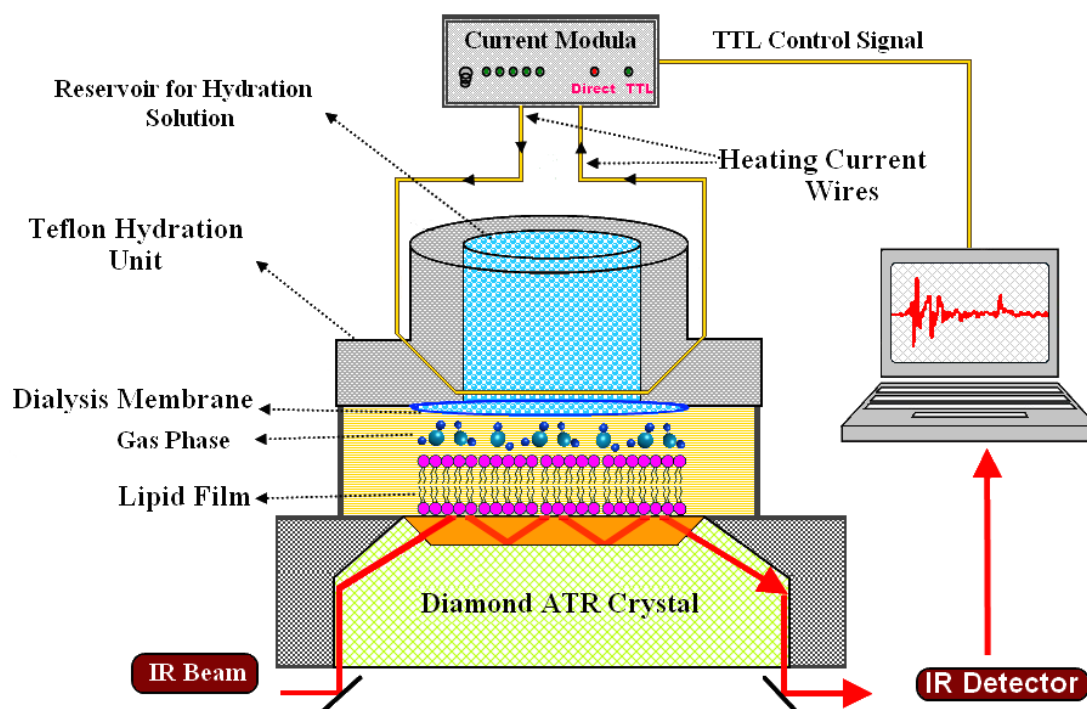


Figure 3.3: Schematic diagram of the time-resolved FTIR hydration perturbation setup. A PL film (sample) is deposited on the ATR crystal, separated by a gas phase and a dialysis membrane (distance < 1mm) from a saturated NaCl salt solution to maintain 75% RH above the PL film. After recording an IR reference absorption spectrum of the PL film, a TTL signal initiates a heating current (4 s) in the salt solution, leading to a transient increase of the RH by 5-7% RH.

3.5.2 Time-Resolved Spectra Acquisition

IR absorption changes were measured during reversion to the initial hydration state over 40-50 s in ten time-slices by rapid scan Fourier Transform Infrared (FTIR) difference spectroscopy using a liquid nitrogen-cooled MCT detector (resolution: 2 cm^{-1} and 3.2 s; using an IFS/66v/S spectrometer, BRUKER Optic GmbH, Karlsruhe, Germany). To monitor the lipid relaxation ten difference spectra were measured after each pulse. Figure 3.4A explains the time sequence of spectra acquisition. There are two times resolution regimes that have been implemented to monitor the IR absorption changes at the lipid film when it loses the extra water molecules gained during the previous hydration pulse. By changing the number of scans for each spectrum, the time resolution of the recorded spectra is controlled and changed. After each current hydration pulse, the FTIR spectrometer recorded 10 single channel spectra which were divided into

two groups of 5 spectra. The first group was measured with a time resolution of 3.185 seconds using 4 scans to record each spectrum. While the second 5 spectra were measured using double number of scans (8 scans), i.e., with a higher signal to noise ratio but with a lower time resolution of 6.37 seconds. Importantly, the lower time resolution for the last 5 spectra in the second group is efficient in the slower process at late times when the sample relaxation induces only small absorption changes. For one hydration pulse, the timing of each spectrum is depicted in Fig. 3.4A.

A total of 100 time-resolved interferograms from 10 hydration pulses were recorded and Fourier-transformed. Using the 10 single channel spectra (S) recorded after the hydration pulse and one common reference single channel spectrum (RS) recorded right before the pulse, one calculates the resulted 10 difference spectra (DS) after each pulse as follows:

$$DS = -\log\left(\frac{S}{RS}\right) \quad (3.1)$$

This results in FTIR-difference spectra, which are calculated relative to the absorption of the equilibrated film immediately before the hydration pulse. Thereby, the difference spectra contain only contributions of those vibrational modes that undergo hydration-induced absorption changes. Static absolute absorbance spectra (reference spectra) were calculated from the single-channel spectra using the spectrum of the pure ATR crystal as reference.

The flowchart in figure 3.4B describes the structure of the measurement macro written using OPUS programming software (BRUKER Optics GmbH, Karlsruhe, Germany) to automise data collection, calculation of difference spectra and averaging of experimental data. In order to increase the signal to noise ratio, the measurement scheme implements an averaging method i.e., repeating the experiment described by Fig 3.4A typically ten times followed by coherently averaging the obtained difference spectra (DS1, DS2,...DS10) resulting from each hydration pulse. PL samples were allowed to fully relax to the initial RH over 8 min before the next hydration pulse was applied (for details see chapter 3.5.3)

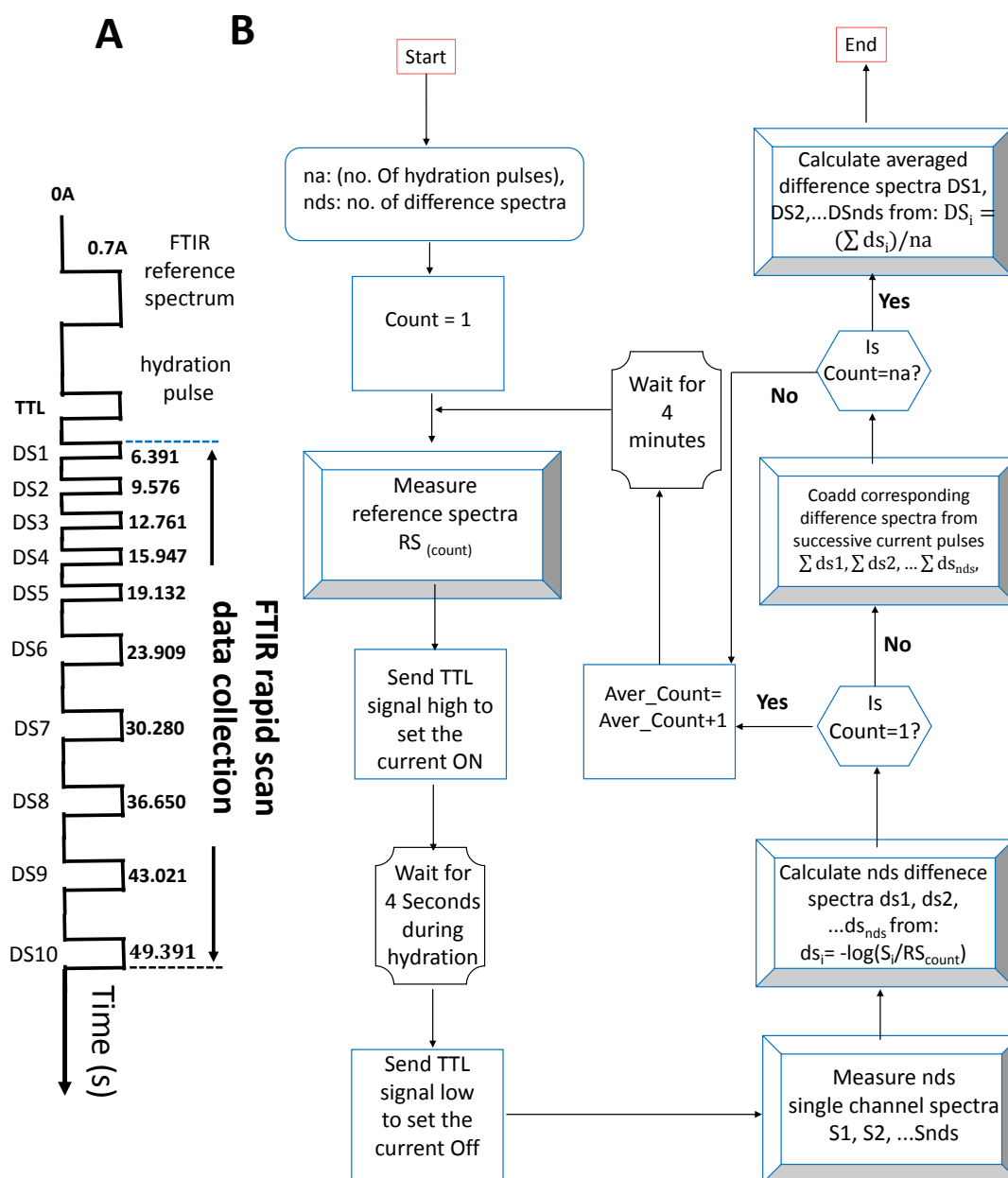


Figure 3.4: (A) schematic diagram showing time sequence of spectra acquisition for one pulse. By rapid scan FTIR spectroscopy, the relaxation of the PL film to its initial hydration state is monitored in ten time intervals (rectangular trigger levels). (B) Flowchart showing the structure for a macro written in OPUS macro software (BRUKER, Karlsruhe) that controls data acquisition, experiment synchronization, and spectra calculations.

3.5.3 Spectral Processing

This section explains in which the time-resolved FTIR spectral processing and how the spectra will be analyzed.

Correction for Swelling of PL Films upon Transient Hydration: The time-resolved absorption spectra monitor the transient water uptake and release via the absorption increase of the water OH stretching $\nu(\text{OH})$ and scissoring bands. They are additionally affected by a general decrease of lipid absorption due to the swelling of the lipidic film upon water uptake in ATR geometry.¹⁰⁵ All spectra were corrected for swelling as described.¹⁰⁶ Briefly, the reference absorption spectrum of the lipidic film was re-scaled for each time-slice to minimize the integral absorption change between 1360 and 800 cm^{-1} . This is equivalent with conservation of total absorption in this spectral range which shows minimal with water absorption. The corresponding weighing factors scale linearly with the volume of the sample at each time-slice in accordance with the use of thin absorbing films.¹⁰⁵ The hydration-induced water OH scissoring band was subtracted from the difference spectra (using a spectrum of liquid water) to better resolve underlying $\nu(\text{C}=\text{O})$ bands. Likewise, the low frequency part of the water $\nu(\text{OH})$ was subtracted to reveal the changes of the symmetric $\nu_s(\text{CH}_2)$ and asymmetric $\nu_{as}(\text{CH}_2)$ methylene stretching modes of the acyl chains. All spectral correction procedures were performed automatically using an Origin 9 script. The relative water content of the samples was determined from the intensity of the water $\nu(\text{OH})$ band relative to the asymmetric PO_2^- absorption as described before¹⁰⁷ and expressed as hydration Γ in (mol H_2O /mol lipid).

Figure 3.5 shows the high reproducibility of the sample responses to ten successive hydration pulses, showing that the variations of the absorption changes are within the spectral noise. The latter is ± 0.3 mAU for the ($\nu(\text{CH}_2)$) in the raw data and it is smaller in all other evaluated spectral regions. After averaging over ten experiments, the noise is further reduced by a factor of ~ 3 . This results in a final uncertainty of the spectral amplitudes of less than 6%. The data also evidence the return to equilibrium before application of another hydration pulse. In fact, this fully reversible spectral

behavior shown in Fig. 3.5 was the criterion for the adjustment of the waiting time (8 min) between hydration pulses.

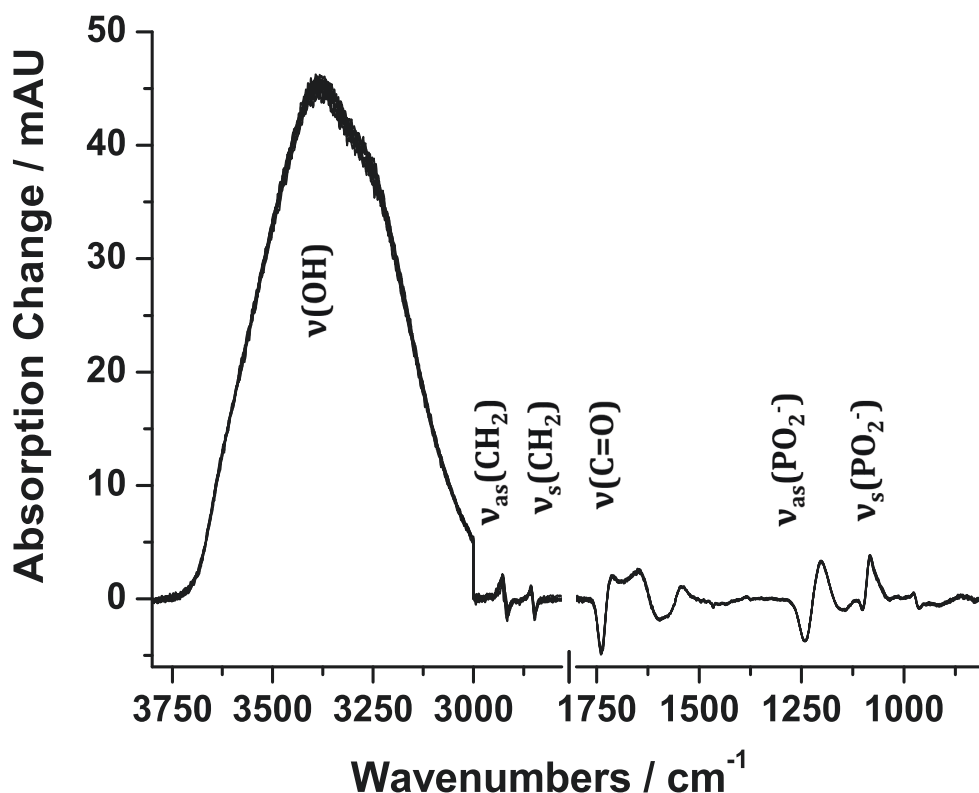


Figure 3.5: Raw data of hydration-induced difference spectra. The plot shows the overlay of ten difference spectra, each induced in NPLs by an independent hydration pulse (water background subtracted from 3000 to 800 cm^{-1}). Each difference spectrum has been recorded 19 s after the hydration pulse, corresponding to the midpoint of the time traces shown in Figs. 4.2 and 4.8 in the next chapter. The spectra are reproduced within the noise level, evidencing the high degree of reproducibility and the full relaxation of the sample after each hydration pulse.

Determination of Hydration-Induced Volume Changes of PL Films: The relation between total absorption and film thickness in ATR geometry¹⁰⁵ allows deriving the relative expansion $\Delta V/V$ of the PL films at each of the time-resolved hydration levels. In fact, these values are the above used scaling factors of the reference spectrum used to correct for the swelling induced absorption decrease. The slope of their plot versus hydration Γ ((mol H_2O)/(mol lipid)) represents the relative molar expansion coefficient $\Delta V \cdot V^{-1} \cdot \Delta \Gamma^{-1}$ per uptake of one water molecule per lipid as shown in Fig. 4.9 (A & B).

Estimation of the Compressibility modulus of PL Films: Using the linear relation between the frequency shift of the symmetric methylene stretch and the area per

lipid:¹⁰⁸ $\Delta\nu_s(\text{CH}_2) = (9.7 \text{ cm}^{-1} / \text{nm}^2) \cdot \Delta A_L$, the spectral data were evaluated to get an estimate of the compressibility module K_c according to the relation:¹⁰⁹

$$\Delta A_L = \frac{2RT \cdot \Delta(\Gamma \ln(a_w))}{K_c} \quad (3.2)$$

The time-dependent activity of water (index i : 1,2,..10 for the ten time-points at which difference spectra were recorded) was linearly approximated by:

$$a_{wi} = \frac{0.75 + \Delta RH \cdot \Delta\Gamma(t_i)}{\Delta\Gamma(t_1)} \quad (3.3)$$

where ΔRH is the initially induced increase of RH after the hydration pulse (here 7%) at time t_1 and $\Delta\Gamma(t_i)$ is the number of excess water molecules per lipid at time t_i relative to the initial hydration $\Gamma(t_0)$. From the amplitudes $\Delta A(\text{CH}_2)$ of the $\nu_s(\text{CH}_2)$ difference band, the underlying frequency shift was divided by the relation $\Delta\nu_s(\text{CH}_2) = 0.35 \times \Delta A(\text{CH}_2) / A(\text{CH}_2)$, where $A(\text{CH}_2)$ is the total absorption of the $\nu_s(\text{CH}_2)$ in the reference spectrum before the hydration pulse. This relation is easily derived for band shifts that are small as compared to the full width at half maximum (FWHM) of a Gaussian band. The experimentally determined FWHM of the $\nu_s(\text{CH}_2)$ at 2850 cm^{-1} is 20 cm^{-1} .

Thermo-tropic Measurements by ATR-FTIR

3.6 Spectroscopy

3.6.1 Temperature-Induced Phase Transition Determination of *C. elegans* Dauer Larvae Membrane PLs

For the temperature-dependent IR measurements, LUVs of NPLs and PPLs were prepared as described above in chapter 3.5. An aliquot of the PLs vesicles ($20 \mu\text{l}$ of $\sim 3 \text{ mM}$) either supplemented with $2 \mu\text{l}$ of a 0.15 mM trehalose or spread directly on a temperature-controlled Bio-crystal ATR unit, dried and equilibrated overnight at a moderate relative humidity 75% using a $400 \mu\text{L}$ saturated salt solution of NaCl. IR absorption Spectra were acquired. Each spectrum was obtained by collecting 256

interferograms with a nominal resolution of 2 cm^{-1} . The equipment was continuously purged with N_2 in order to minimize the contribution peaks of atmospheric water vapor. The temperature dependence of the FTIR Spectra were studied by heating the sample over a temperature range ($2\text{--}80\text{ }^{\circ}\text{C}$) at $2\text{ }^{\circ}\text{C}$ intervals, allowing 4 min equilibration between temperatures. Spectra analysis and display were carried out using OPUS programming software (BRUKER Optics GmbH, Karlsruhe, Germany), MagicPlot Pro software and Origin Pro 9.

The Membrane thermo-tropic phase behavior was monitored by observing the position of the symmetric CH_2 stretching vibration band ($\nu_s(\text{CH}_2)$, around 2850 cm^{-1}) arising from the lipid acyl chains as described previously.¹¹⁰ Band positions were determined by the peak picking routine of the second derivatives of the original absorption IR spectra at different temperature using a 9 points smoothing factor as previously described.^{111–113} The wavenumber of $\nu_s(\text{CH}_2)$ versus temperature plots were constructed. The first derivative of the wavenumber of $\nu_s(\text{CH}_2)$ versus temperature plots was obtained using Origin Pro 9 which clearly show the inflections and are a measure of the cooperativity of the transitions. The gel to liquid-crystalline phase transition temperature (T_m) was determined from the maxima in the first derivatives of the $\nu_s(\text{CH}_2)$ versus temperature plots.

The Thermal-induced conformational changes of *C. elegans* derived NPLs and PPLs were investigated by an analysis of carbonyl stretching band ($\text{C}=\text{O}$) in the absence and presence of trehalose at $T < T_m$, T_m , and $T > T_m$. For examination of the thermal response of $\text{C}=\text{O}$ stretching band at various temperatures, peak deconvolution and curve fitting were performed using the peak-fitting module of MagicPlot Pro software. After the baseline correction of the $\text{C}=\text{O}$ band spectra in the spectral region of $1800\text{--}1660\text{ cm}^{-1}$, we used the minima determined from the second derivative spectra using Origin Pro 9.0 to know the number of the resolved peaks under the broad $\text{C}=\text{O}$ band. All other fitting parameters were optimized by the MagicPlot Pro software through an iterative process to find the best Gaussian curve fit, as it was previously reported but with using different software.¹¹⁴ A combination of Gaussians and Lorentzian did not give better results. The Correlation coefficients (R^2) for all fitted curves were 0.999.

3.7 Langmuir-Blodgett Monolayer Studies

3.7.1 Formation of PLs Monolayer

The lipid monolayers were made by placing dissolved lipid molecules lightly on the subphase surface. Lipid monolayers were formed by spreading 7.5 μL of lipid extracts (1 mg/ml in CHCl_3 : CH_3OH (4:1)) on 20 ml of phosphate buffer (10 mM, $\text{pH} = 7.4$) in a μ -Trough S-LB (Kibron, Helsinki, Finland) using a Hamiltonian micro syringe. The lipid solution was slowly transferred from the syringe to the subphase (buffer) surface, one small drop at a time, with the tip of the syringe placed carefully on the surface. One must try to spread the molecules as much as possible by placing drops at different places of the surface between the two barriers. The Chloroform evaporates quickly and leaves a spread mono molecular and oriented film on the surface as shown in figure 3.6A: The hydrophilic headgroups are oriented towards the subphase, the hydrophobic fatty acid chains towards the air.

3.7.2 Surface Pressure-Area Isotherm Measurements

One hour after spreading, the monolayer was compressed at rate of $0.05 \text{ \AA}^2/\text{chain}/\text{min}$ to a target pressure of 25 mN/m (Fig. 3.6B). Then the monolayer was expanded with the same rate to a pressure of 19 – 20 mN/m (Fig. 3.6C). To study the interaction of the lipids with trehalose, 1 ml of 2.5 M aqueous trehalose solution was injected into the subphase (20 ml) at constant area (Fig. 3.6D). This gives rise to a final trehalose concentration in the aqueous phase of 125 mM and a pressure increase upon trehalose incorporation into the monolayer. After the pressure has stabilized ($\sim 1 \text{ h}$) the film was expanded again to 19 – 20 mN/m as shown in figure 3.6E.

The measured surface pressure π is the difference between the surface pressure of pure subphase and that of the subphase covered with the monolayer. This is considered as the most important indicator of the monolayer properties. These measurements are

performed at a constant temperature. This is known as a surface pressure-area isotherm that is rich in information on the stability of the monolayer.¹¹⁵

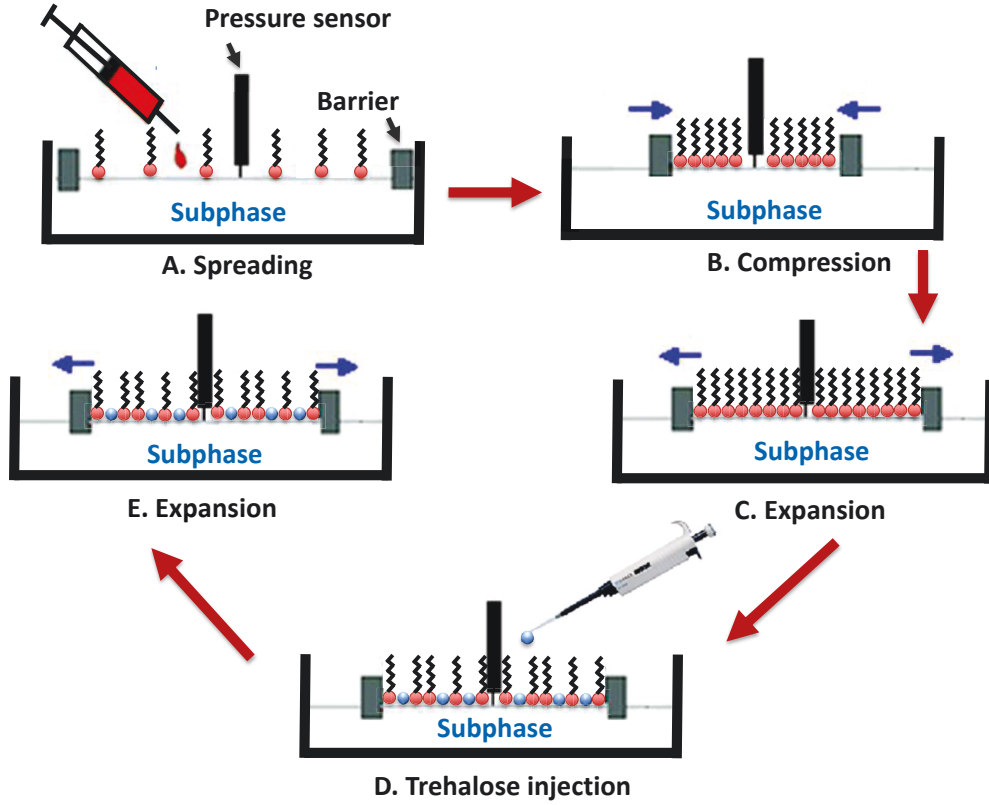


Figure 3.6: Schematic representation of pressure-area isotherm measurement steps using Langmuir-Blodgett technique.

Here, we have run full expansion isotherms without and with trehalose. The relation:

$$\frac{\Delta A_L}{A_L} = K \cdot e^{\frac{-A_t \cdot \pi}{RT}} \quad (3.4)$$

was used to approximate the molecular area (A_t) occupied by trehalose in the PL film. It was obtained from the slope of the $RT \cdot \ln (\Delta A_L / A_L)$ vs. π plot, where A_L is the PL surface area at a given pressure of $25 \text{ mN/m} > \pi > 19 \text{ mN/m}$ in the absence of trehalose and ΔA_L is the area increase in the presence of trehalose at the same π .¹¹⁶ K is the partitioning constant of trehalose between the aqueous and the lipidic phase.¹¹⁷ The free enthalpy of trehalose was derived from the y-axis interception of the linear regression line through the $RT \cdot \ln (\Delta A_L / A_L)$ vs. π plot. The purity of trehalose used in all experiments was verified by FTIR spectroscopy using the IR spectrum of amorphous

trehalose as a reference.¹¹⁸

Thermo-tropic Measurements by Fluorescence

3.8 Spectroscopy

Vesicles Preparation: Appropriate amounts of PL organic solution were mixed with LAURDAN in chloroform, and then dried under nitrogen gas followed by vacuum-drying for at least 2 h. The dried LAURDAN-lipid film was then rehydrated in either phosphate buffer solution (pH 7.4) or trehalose solution, which heated above the transition temperature of the particular lipid, to a final total lipid: trehalose ratio of 1:20. The final total lipid and fluorescent probe concentrations were 0.3 mM and 0.3 μ M, respectively. LUVs were prepared of each lipid for Fluorescence measurements similar to the vesicles preparation protocol mentioned in chapter 3.5.

Experimental Procedures: Steady-state LAURDAN fluorescence excitation and emission were monitored with a LS55 Fluorescence Spectrometer, (PerkinElmer, Rodgau-Jügesheim, Germany) equipped with a thermostatic 130 μ L cuvette at different temperatures. The temperature was regulated by a circulating water bath connected to the cuvette holder. The emission spectra were then recorded between 400 and 530 nm at $\lambda_{ex} = 340$ nm, and the excitation spectra between 310 and 420 nm at $\lambda_{em} = 440$ nm (slit width 5 nm). All measurements were performed from the average of 10th accumulated scans at 2 °C. Temperature was then raised to 25 °C, the sample re-equilibrated (generally about 1h) until temperature was stable, and fluorescence data again acquired. The procedure was repeated at 65 °C.

From the spectroscopic data, the LAURDAN “generalized polarization” GP was calculated from the emission spectra using the following equation adapted from the work of Parasassi et al.⁹¹

$$GP = \frac{[F_{440} - F_{490}]}{[F_{440} + F_{490}]} \quad (3.5)$$

F_{440} and F_{490} are the LAURDAN fluorescence intensities at the blue and red edges of the emission spectrum, respectively.

Differential Scanning Calorimetry (DSC)

3.9 Studies

3.9.1 DSC Measurements

Vesicles preparation: Model PLs used in the Calorimetry experiments were dried from chloroform-methanol as described above in chapter 3.5. The dried lipid was rehydrated in either water or trehalose solution heated above the transition temperature of the particular lipid at a concentration of 1 mg/ml. For samples containing trehalose, an aqueous solution of lipid: trehalose 1:20 ratio by dry weight was used.

Experimental Procedures: The LUVs suspension was sealed in small aluminum Calorimetry pans and scanned. A volume of 0.6 ml of 1mg/ml vesicles was injected into the sample cell, and the same volume of water was placed into the reference cell. Scans were carried out at heating and cooling rates (2–80 °C) of 0.5 °C min⁻¹. The reference was always water. For each sample a series of 20 consecutive heating-cooling scans were performed to prove the reproducibility. All presented curves originate from the second heating scan. The measurements were performed on a VP-DSC calorimeter (MicroCal, Inc., Northampton, USA). All samples were degassed before each run. In all the experiments the pressure in the calorimeter was approximately 3 atm (above atmospheric pressure). The heat capacity profiles of only model lipids (DMPA, DMPC, DMPE & DMPG) in the absence and presence of trehalose were recorded. Unfortunately, the material quantities did not allow the NPLs / PPLs experiments.

DYNAMICS OF HEADGROUP HYDRATION & ACYL CHAIN DISORDER IN *C. elegans* PLs

Contents

4.1	Hydration-Induced Lyotropic Structural Transitions in <i>C. elegans</i> Derived PLs	58
4.2	Desiccation Stress Depletes Phosphatidylcholine in Cell Membranes & Enhances their Interaction with Trehalose	65
4.3	Interaction of Trehalose with PLs & Residual Water in Response to Membrane Hydration	70
4.4	Hydration-Induced Volume Changes & Lipid Expansion Coefficient in <i>C. elegans</i> PL Films (Swelling Behavior)	73
4.5	Discussion	75
4.6	Conclusions	81

In the following chapter, we present the results of a newly established technique, i.e., hydration pulse-induced time-resolved ATR-FTIR spectroscopy, which was performed on a hydrated native lipid membrane extracted from differently pre-treated *C. elegans* larval states. FTIR spectroscopy was chosen as a label-free method to observe the physical state of all chemical constituents of the samples based on their intrinsic vibrational absorption. In order to understand whether preconditioning alters the physiochemical properties of membranes of *C. elegans* dauer larvae, we used time-resolved FTIR difference spectroscopy. Rapid scan FTIR was used here to monitor specifically fast hydration-induced structural changes in PL films prepared from two populations of larvae (preconditioned and non-preconditioned). Thereby, we attempt to correlate lipid properties with the observed phenotypes of desiccation tolerance vs. cell membrane damage, respectively.

In contrast to previous studies, we have studied these structural transition changes at constant ambient temperature, where the transition is only water-driven. By using FTIR difference spectroscopy with the hydration perturbation method, it is possible to observe only the few added water molecules due to the hydration pulse (incremental hydration and not total water content), and their effect on changing the hydration shell structure and eventually their role in evoking PL conformational transitions.

Hydration-Induced Lyotropic Structural Tran-

4.1 sitions in *C. elegans* Derived PLs

One of the major questions in the physiological context is how the lipid headgroup hydration is linked to acyl chain packing? While the former is the primary process in lipid water interactions, the latter corresponds to the response of the lipidic phase as a whole, thereby, it determines macroscopic properties such as membrane swelling, rigidity and, consequently, mechanical sensitivity to hydration-induced strain. What are the dynamics of water mediated structural transitions in PL extracts from *C. elegans* dauer larvae? To address these questions, the hydration of a PL film, which is equilibrated at 75% RH, was transiently increased in an automated fashion (see chapter 3.5) to monitor the transient absorption changes of the lyotropic phase transitions within seconds.

The chemically and topologically different regions of the PL architecture contribute to specific IR absorptions originating in stretching vibrations of asymmetric phosphate $\nu_{as}(\text{PO}_2^-)$ at $\sim 1260\text{ cm}^{-1}$, symmetric phosphate $\nu_s(\text{PO}_2^-)$ at $\sim 1085\text{ cm}^{-1}$, ester carbonyl $\nu(\text{C}=\text{O})$ at $\sim 1740\text{ cm}^{-1}$, and acyl methylene $\nu(\text{CH}_2)$ modes between 3000 and 2800 cm^{-1} . Whereas the $\nu(\text{PO}_2^-)$, and $\nu(\text{C}=\text{O})$ frequencies are affected directly by H-bonding through corresponding changes in force constants, the $\nu(\text{CH}_2)$ respond to changes in acyl chain free volume (alternatively expressed as area per lipid). Thus, the IR signature of transient lipid hydration provides a view on the extent of H-bonding at different sites in the PL headgroups and on the acyl chain order.¹¹⁹

Data were obtained as a time-dependent sequence of difference spectra (Fig. 4.1A) with positive hydration-induced absorption bands from which the spectrum of the initial 75% RH state shown in the Figure 4.1(ii) was subtracted (negative peaks). Thereby, water uptake is represented by the increase of the water $\nu(\text{OH})$ band between 4000 cm^{-1} and 2700 cm^{-1} range, whereas frequency shifts of the PL film cause negative (absorption of the initial state) as well as positive bands (absorption of the hydration-induced state). After a rapid increase of hydration (within 4 s), the PL film reverts to its initial hydration state as can be seen from the successive reduction of the absorption difference spectra over time. This re-equilibration was followed by rapid scan FTIR difference spectroscopy to determine in addition to the general hydration-induced spectral changes also the kinetics of H-bonding and structural rearrangements at the chemically and topologically different sites of the PLs according to their IR group frequencies. Figure 4.1(i) shows the representative hydration-induced IR absorption difference spectra at $t=0$.

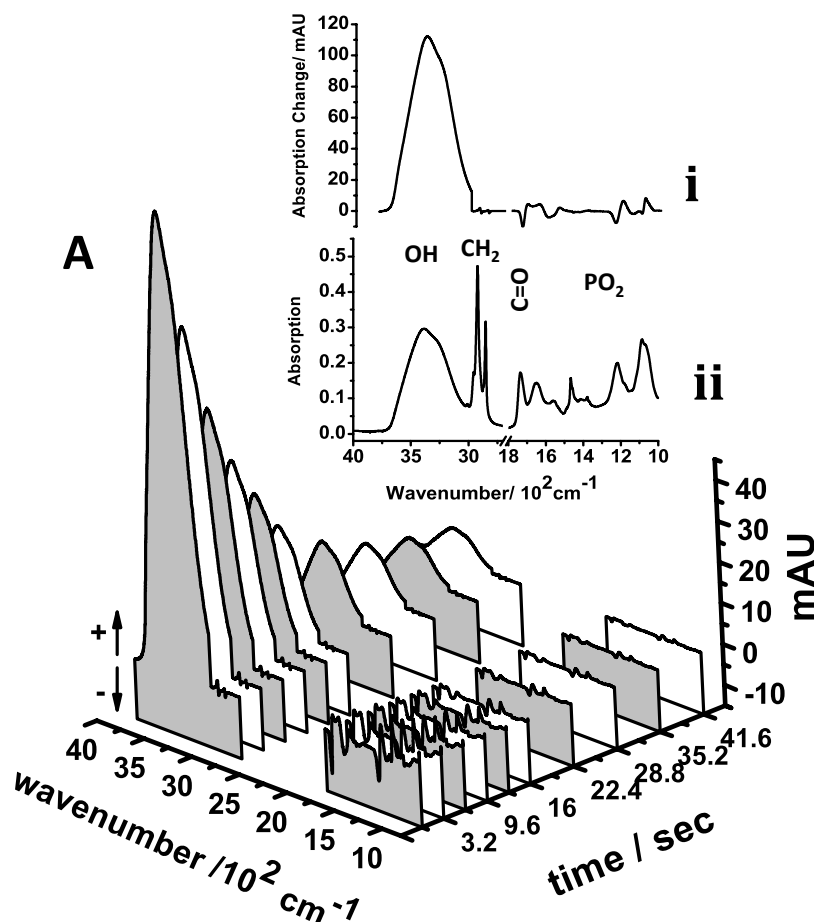


Figure 4.1: Hydration pulse-induced rapid scan FTIR-difference spectra of a PL films. By rapid scan FTIR spectroscopy, the relaxation of the PL film to its initial hydration is monitored. A) Overview of the time-dependent evolution of difference spectra in response to a single hydration pulse. In an automated fashion, 10 hydration pulses were applied and difference spectra co-added for each time slice to improve the signal to noise ratio. Inset: i) The first difference spectrum at $t=0$ calculated from the first data acquisition interval and the reference spectrum. The increased absorption between 4000 and 3000 cm^{-1} is caused by water uptake by the PL film. Absorption changes of the PL acyl chains (3000 - 2800 cm^{-1} , water background subtracted for clarity) and headgroups (1800 - 1000 cm^{-1}) are smaller and exhibit negative and positive lobes due to hydration-induced shifts of their vibrational frequencies. ii) initial PL absorption (reference spectrum).

In the physiological context, the comparison of the amplitudes of the $\nu(\text{CH}_2)$ absorption changes (2800 - 3000 cm^{-1} range) with the amplitude of the H-bond-dependent absorption change of the $\nu_{as}(\text{PO}_2^-)$ (1200 - 1250 cm^{-1} range) and the $\text{C}=\text{O}$ stretching mode (1700 - 1750 cm^{-1} range) immediately after the hydration pulse is of particular interest. The corresponding difference spectra are shown for non-preconditioned phospholipids (NPLs) and preconditioned phospholipids (PPLs) in Fig. 4.2A and B, respectively. The $\nu(\text{CH}_2)/\nu(\text{C}=\text{O})$ amplitude ratios reflect the physiologically relevant

relation between the gain of acyl chain free volume (up-shift of the $\nu(\text{CH}_2)$) and sub-headgroup hydration (down-shift of the $\nu(\text{C=O})$). Upon hydration of the sub-headgroup region of NPLs, the $\nu(\text{C=O})$ shifts down in response to increased H-bonding which gives rise to a difference band with a negative lobe at 1741 cm^{-1} caused by the depletion of the initially less H-bonded C=O state. Correspondingly, the positive lobe at 1713 cm^{-1} is caused by the newly formed $\nu(\text{C=O})$ stretching modes of the more strongly H-bonded ester carbonyl groups after water uptake. The symmetric $\nu_s(\text{CH}_2)$ and asymmetric $\nu_{as}(\text{CH}_2)$ give rise to difference bands at $2849/2859\text{ cm}^{-1}$ and $2917/2949\text{ cm}^{-1}$, respectively. Their frequency up-shift evidences the expected increase of area per lipid upon PL headgroup hydration, typical of a lyotropic phase transition.¹⁰⁸ The decrease of these perturbations over time is exemplified for the first, fifth and tenth difference spectra after the hydration pulse at the indicated times. Similar to the down-shift of the $\nu(\text{C=O})$, also the $\nu_{as}(\text{PO}_2^-)$ of the phosphodiester becomes down-shifted upon hydration and evidences that, at a basal humidity of 75% RH, H-bonding to the PO_2^- groups is not saturated and can thus further increase by the hydration pulse.

From the water $\nu(\text{OH})$ and the $\nu_{as}(\text{PO}_2^-)$ band in the reference spectrum before the hydration pulse (Fig. 4.1(ii)) a basal hydration of Γ of 15 and 13 is obtained²⁴ for NPLs and PPLs, respectively at 75% RH. Applying the same spectroscopic determination of the water/phosphate ratio,¹⁰⁷ the hydration-induced increase of the $\nu(\text{OH})$ in the first difference spectrum (exemplified in Fig. 4.1(i)) corresponds to a water uptake of $\Delta\Gamma$ 4-5 mol H_2O / mol P within 4 s hydration pulse in both NPLs and PPLs. Comparison with PL films measured at different RH, the equivalent water content would require 80-82% RH if it was to be produced by basal equilibrium hydration. Therefore, in terms of total water content, the described spectral changes are induced by the transient increase of the RH by 5-7%.

Figure 4.2B shows the equivalent data set for PPLs. As expected, the overall spectral appearance of hydration-induced frequency shifts is almost identical to the NPLs as it is caused by the general properties of PLs. The salient difference, however, is the increased amplitude of the $\nu(\text{CH}_2)$ difference bands in PPLs as compared to NPLs, when normalized to the amplitude of the $\nu(\text{C=O})$ absorption change. Hence, the spectra reveal a much larger increase of free acyl chain volume in PPLs at the same increase of

sub-headgroup hydration.

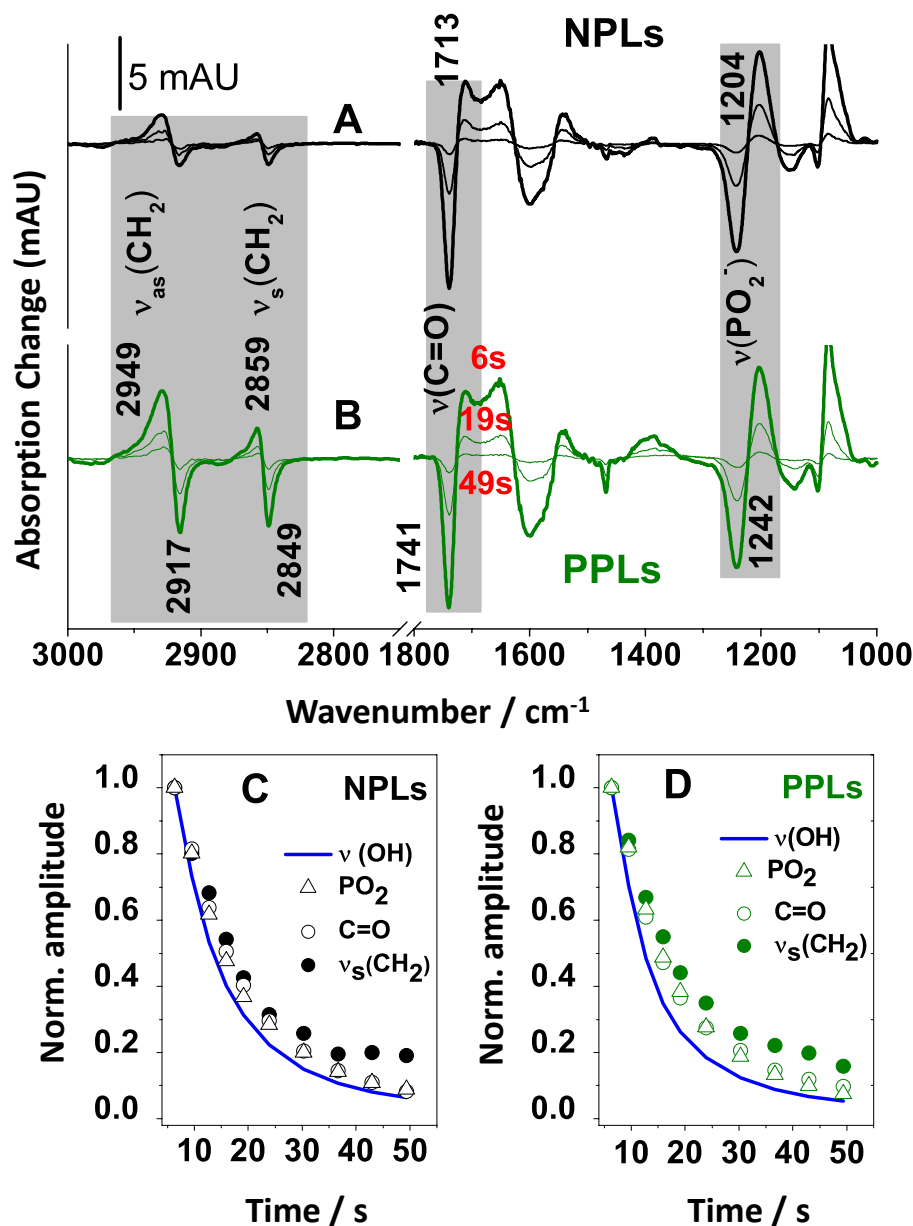


Figure 4.2: Time-resolved hydration-pulse-induced IR absorption changes of PL extracts in the absence of trehalose. A) Representative selection of hydration-induced difference spectra of NPLs recorded at the indicated times after the hydration pulse. The hydration-induced down shift of the $\nu(\text{C=O})$ and $\nu_{as}(\text{PO}_2^-)$ causes the difference bands at 1741/1713 and 1242 /1204 cm⁻¹ due to increased H-bonding to the ester carbonyl and phosphates, respectively. Increase of acyl chain free volume is monitored by the up-shift of the $\nu_s(\text{CH}_2)$ and $\nu_{as}(\text{CH}_2)$ frequencies from 2849 to 2859 and from 2917 to 2949 cm⁻¹, respectively. Spectra are normalized to the amplitude of the $\nu(\text{C=O})$ difference band. B) As in (A) obtained with PPLs. C) Relaxation of absorption changes in A. IR frequencies are assigned to chemical groups as indicated. The loss of water to the gas phase (reduction of $\nu(\text{OH})$ amplitude) is shown for comparison (blue). D) As (C) obtained with PPLs. Spectral noise is < 0.1 mAU (see Fig. 3.5) Color code: NPLs black, PPLs green, water: blue.

Table 4.1 summarizes the measured amplitudes of headgroup and acyl chain difference bands normalized to the difference band of the C=O stretching mode and thus to the same transient hydration-induced increase of H-bonding at the sub-headgroup region. On this basis the response of the different samples to hydration can be compared quantitatively. For the $\nu_s(\text{CH}_2)$ at 2849/ \sim 2859 cm^{-1} the normalized amplitudes are 0.16 and 0.46 for NPLs and PPLs, respectively, evidencing an approximately three-fold larger gain of acyl chain free volume upon hydration of the sub-headgroup region. Regarding the H-bond changes at the PO_2^- groups, NPLs and PPLs exhibit very similar values of their $\nu_{as}(\text{PO}_2^-) / \nu(\text{C=O})$ ratios of 0.97 and 0.93, respectively. Evidently, the PO_2^- -hydration in relation to ester-carbonyl hydration is barely affected by preconditioning. Thus, the much larger increase in hydration-induced acyl chain disorder in PPLs can't be explained by a relocation of hydration water from the PO_2^- to the C=O groups in the sub-headgroup region. Instead, it must originate predominantly in a structurally different coupling of the sub-headgroup H-bond network to acyl chain packing.

Relaxation Kinetics Induced by Hydration of *C. elegans* PLs in the Absence of

Trehalose: The kinetics of $\nu(\text{OH})$, $\nu(\text{C=O})$, $\nu_{as}(\text{PO}_2^-)$ and $\nu_s(\text{CH}_2)$ absorption bands are shown in Figs. 4.2C and D for NPLs and PPLs, respectively. The maximal hydration of the PL corresponds to an increase of the RH by 5-7% and occurred within 10 second in both PL extracts. From then on, the hydration decreases and the lipid relaxes back toward the equilibrium state. Clearly, the re-equilibration of water with the gas phase (blue traces) during the reversal from 80-82% RH back to 75% RH precedes the absorption changes of the phosphodiester (PO_2^-), the carbonyl (C=O) and acyl chains (CH_2). The order of relaxation rates exhibits a close relation to the topology of these chemical groups. In NPLs (Fig. 4.2C), the slower rate of the $\nu_{as}(\text{PO}_2^-)$ as compared to the $\nu(\text{C=O})$ is consistent with the diffusion of water from the "deeper" ester-carbonyl region to the more surface-exposed PO_2^- -region. Thereby, water lost from the phosphate hydration shell to the gas phase is partially replenished by water diffusing from the ester-carbonyl layer to the headgroups, leading to a faster water loss at the carbonyls than at the PO_2^- -groups.

Sample	$\nu_{\text{as}}(\text{CH}_2)$ 2910-2950 cm^{-1}	$\nu_{\text{s}}(\text{CH}_2)$ 2850-2860 cm^{-1}	$\nu_{\text{as}}(\text{PO}_2^-)$ 1240-1200 cm^{-1}	rel. molar expansion $\Delta V/(V \Delta \Gamma)$	TRH mol. area $\Delta G/\text{mol}$
NPLs	25	16	97	0.89	n.a.
PPLs	66	46	93	0.86	n.a.
PPLs + Bovine PC	32	23	143	3.1	n.a.
Bovine PC	35	29	161	2.9	n.a.
NPLs + TRE	37	16	36	0.95	60 \AA^2 -9.5 kJ
PPLs + TRE	78	29	47	1.1	77 \AA^2 -12.8 kJ

Table 4.1: Normalized amplitudes of absorption changes of selected group frequencies of PLs. The tabulated values are the peak to peak intensities of the absorption differences in the first difference spectrum after the hydration pulse in per cent of the intensity of the negative depletion signal at 1740 cm^{-1} (ester carbonyl $\nu(\text{C}=\text{O})$ of the initial state). The wavenumber ranges of the spectral changes are given for each mode. The second to last column shows the relative expansion of the PL films (volume change per water added per phosphate). The last column shows the area of trehalose occupied in the respective PL monolayer and the free energy of trehalose binding to the monolayer. See Materials and Data Acquisition for details. TRE: trehalose.

In PPLs, however, the H-bond network between $\text{C}=\text{O}$ and PO_2^- groups is more strongly coupled, resulting in indistinguishable equilibration rates at these sites (Fig. 4.2D). Despite this stronger H-bond linkage between the $\text{C}=\text{O}$ and PO_2^- sites in PPLs, the delayed response of the acyl $\nu(\text{CH}_2)$ changes demonstrates that sub-headgroup hydration is not cooperatively coupled to acyl chain order on the time scale of seconds in either PL sample.

In summary, hydration transients of NPLs and PPLs induce similar responses, which reflect the expected increased H-bonding to PO_2^- and $\text{C}=\text{O}$ groups. However, in PPLs these H-bond networks evoke a much larger increase in acyl chain disorder at the same incremental hydration of the carbonyl region. This is the case despite lower water content in PPLs (Γ of 13 versus 15 in NPLs).

Desiccation Stress Depletes Phosphatidylcholine in Cell Membranes & Enhances their

4.2 Interaction with Trehalose

The different physical properties of NPLs and PPLs revealed by the IR-difference spectra imply that during the four days of preconditioning, chemical differences are generated among the PLs that cause the different kinetics of sub-headgroup H-bond changes and hydration-induced acyl chain disorder. Therefore, the headgroup composition of the total PL content of dauer larvae was analyzed after incorporation of ^{14}C into *de novo* synthesized lipids by supplementing the food source of growing worms with 10 μCi ^{14}C -labeled acetate (see chapter 3.3). Extracted PLs were separated by two-dimensional thin layer chromatography (2D-TLC) according to their hydrophobicity (Fig. 4.3A). Comparing the abundance of PL classes in non-preconditioned and preconditioned larvae shows that preconditioning dramatically decreases the phosphatidylcholine (PC) levels, whereas other PL classes such as phosphatidylethanolamine (PE), phosphatidylserine (PS), phosphatidylinositol (PI), and phosphatidic acid (PA) are not much affected. These results suggest that the PC content may be specifically reduced to enhance desiccation tolerance after preconditioning. In fact, it is well known from previous FTIR work that PC binds water in a "phosphocholine water pattern"¹²⁰ more strongly than PE, which instead forms direct headgroup phosphate interactions upon drying.^{121,122} Our data suggest that this different headgroup hydration patterns are of direct physiological relevance to adapt the lyotropic phase behavior of the cell membranes to the conditions of anhydrobiosis. Can PC depletion explain the different lyotropic behavior of PPLs? We addressed this question by supplementing PPLs from *C. elegans* dauer larvae with bovine PC (PPLs: PC= 2:1), followed by vesicles preparation and performing again hydration-induced time-resolved ATR-FTIR difference spectroscopy. Figure 4.3B shows that the increase of acyl chain disorder in relation to sub-headgroup hydration as measured by the amplitude ratio of the $\nu_s(\text{CH}_2)$ and $\nu(\text{C=O})$ difference bands, is indeed reduced to the value found with NPLs as also clearly shown in Table 4.1 and Figure

4.4. This result confirms the critical role of PC in regulating the lyotropic properties of the cell membranes in the anhydrous state.

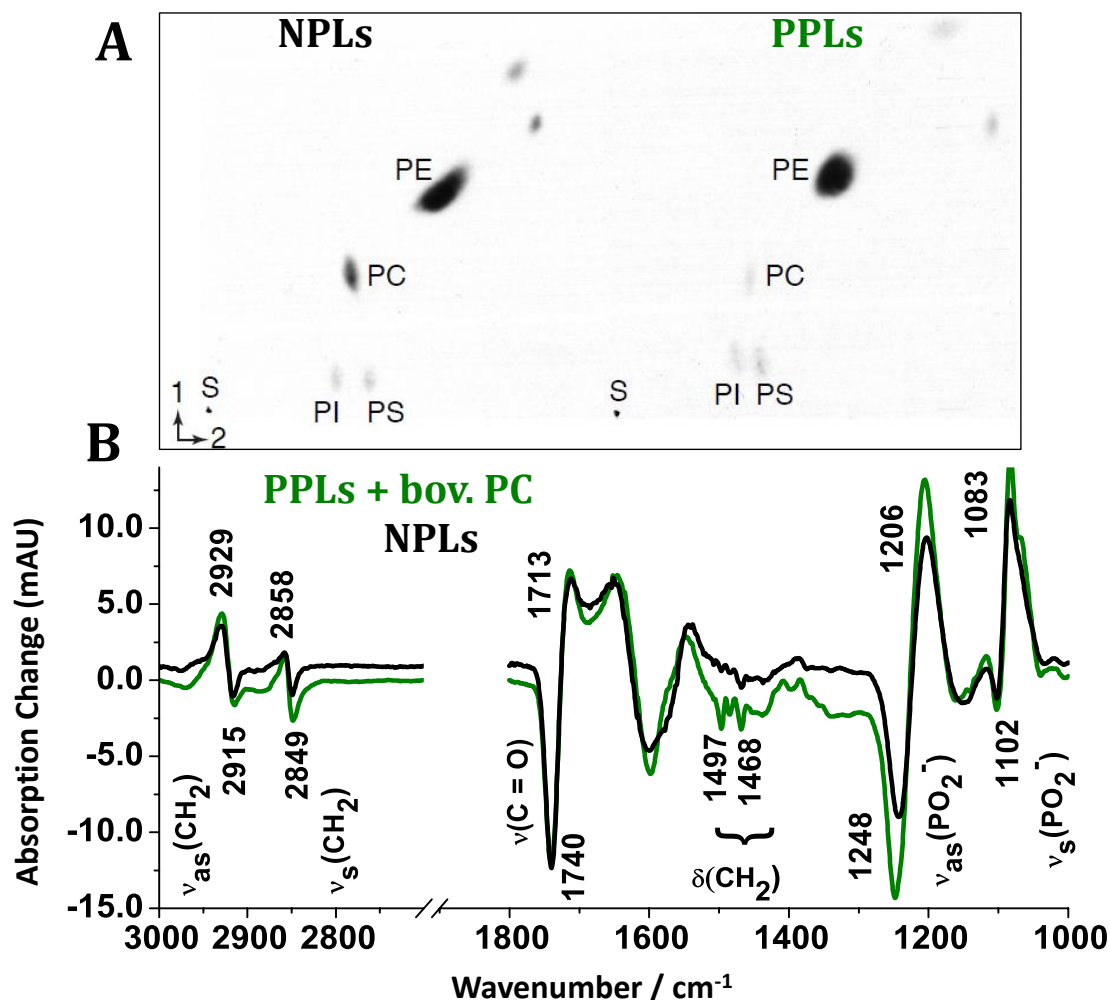


Figure 4.3: Correlation of PL headgroup composition and hydration responses. A) TLC radiogram of ^{14}C -labeled PLs. Among the major PL classes, only PC displays a dramatic decrease in the preconditioned sample. PE: Phosphatidylethanolamine, PC: Phosphatidylcholine, PI: Phosphatidylinositol, PS: Phosphatidylserine, S: Starting point. Dimensions are indicated with arrows. Solvent 1: $\text{CHCl}_3:\text{CH}_3\text{OH}:32\% \text{NH}_3$ (65:35:5, v:v:v); solvent 2: $\text{CHCl}_3:\text{CH}_3\text{OH}:(\text{CH}_3)_2\text{CO}:\text{CH}_3\text{COOH}:\text{H}_2\text{O}$ (50:10:20:12.5:5, v:v:v:v:v)). B) Time-resolved hydration-pulse-induced IR absorption changes of an NPLs film (black) and a PPLs film (green) which was supplemented with bovine PC (PPLs:PC= 2:1), thereby PC addition to the PPLs film restores the $\nu(\text{CH}_2) / \nu(\text{C}=\text{O})$ amplitude ratio of NPLs.

Our results so far demonstrated the intrinsic behavior of preconditioned and non-preconditioned *C. elegans* PLs during a rehydration pulse and revealed a predominant role of PC-containing lipids in regulating the rate and extent of lyotropic transitions. The PLs were devoid of trehalose because the organic extraction separates hydrophobic lipids and hydrophilic sugars into different phases. However, previous work clearly

showed that *C. elegans* dauer larvae synthesize and accumulate large amounts of trehalose during preconditioning.¹² Furthermore, the presence of this disaccharide is essential for desiccation tolerance.

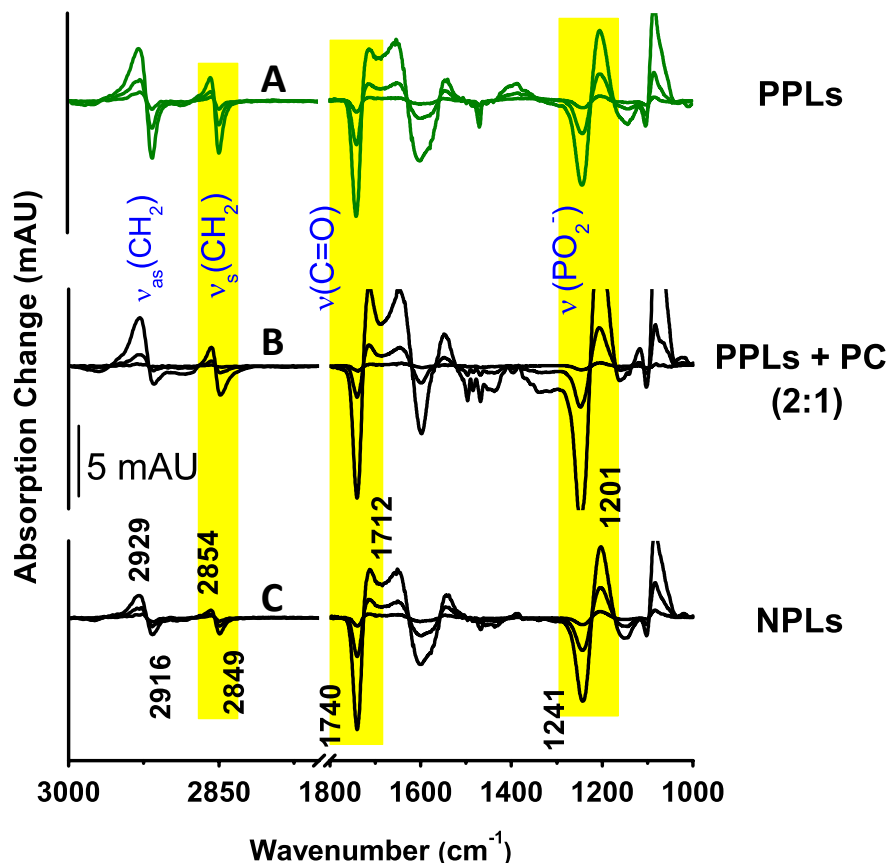


Figure 4.4: Time-resolved hydration-pulse-induced IR absorption changes. Representative selection of hydration-induced difference spectra recorded at the indicated times (Fig. 4.2 (A-B)) after the hydration pulse of (A) PPLs, (B) PPLs which was supplemented with bovine PC (PPLs:PC= 2:1) and (C) NPLs.

In addition to bilayer experiments, we also performed experiments with monolayers at the air-water interface. Based on the former finding, we asked whether the reduced PC-content of PPLs might additionally affect their interaction with trehalose. Therefore, the energetic properties of trehalose-PL interactions were studied by Langmuir-Blodgett monolayers, which are a suitable model for the interactions of the sugar with bilayers.¹²³ Figure 4.5A shows the expansion isotherm of a PPLs monolayer followed by the injection of trehalose into the subphase at a pressure of ~ 20 mN/m. Adsorption of the sugar to the monolayer caused a pressure increase to ~ 23.5 mN/m over one hour. The subsequent film expansion reduced the pressure again. From the area differences between the two

branches, we have obtained the fractional area increase $\Delta A_L/A_L$ induced by trehalose at constant pressure for the pressure values covered by both expansion isotherms. The ability of trehalose to increase the monolayer area of *C. elegans* PLs agrees with our studies on model lipids DMPA (Fig. 4.6) and with previous studies on the interaction of carbohydrates with model lipids.^{124,125}

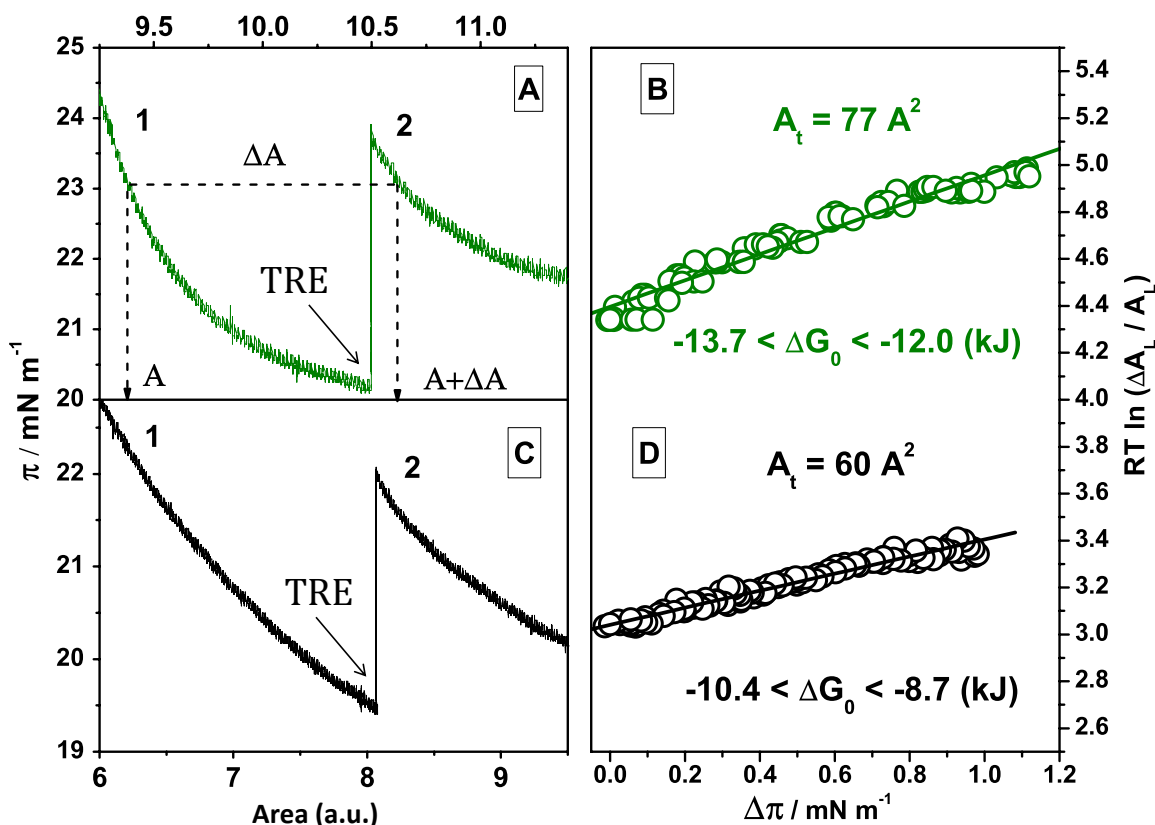


Figure 4.5: Interaction of trehalose with PL monolayers. Expansion of a monolayer of PPLs (A) and NPLs (B) before (1) and after (2) injection of trehalose (TRE) to the subphase at a final concentration of 125 mM. Broken arrows exemplify the area increase induced by trehalose at constant pressure. C) The molecular area A_t occupied by TRE in the monolayers is derived from the slope of the linear regressions of the $RT \ln(\Delta A_L/A_L)$ plots over a range of pressures. The free enthalpy difference of binding of TRE to PPLs vs. NPLs is reduced by $1.6 \text{ kJ} < \Delta \Delta G_0 < 5 \text{ kJ}$ (determined from the offsets of the linear regressions and allowing an uncertainty of the minimal area per lipid of $45\text{--}65 \text{ \AA}^2$).

The slope of the plot $RT \ln(\Delta A_L/A_L)$ vs. π gives the molar area occupied by trehalose in the monolayer, which corresponds to $A_t = 77 \text{ \AA}^2$ (Fig. 4.5B) of PPLs. A smaller $A_t = 60 \text{ \AA}^2$ is obtained for NPLs (Fig. 4.5C and D). These areas are in good agreement with the predicted projection surface of trehalose shown in Fig. 4.7, which has a long and short axis of 10.9 and 6.5 \AA , respectively.

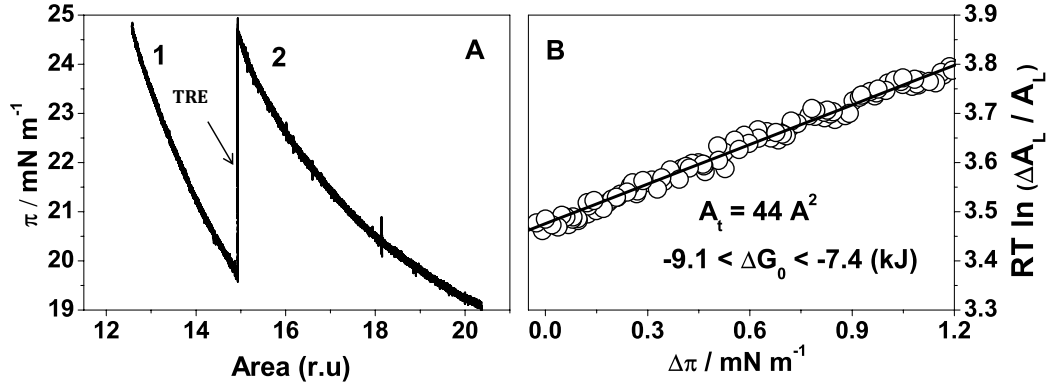


Figure 4.6: The expansion isotherms of DMPA monolayer on phosphate buffer 10 mM (pH 7.4) as subphase (A). Left branch (1): subphase without trehalose. Right branch(2): after addition of 125 mM trehalose which increases surface pressure (π). B) The molecular area A_t occupied by TRE in the lipidic film is derived from the slope of the linear regressions of the RT and is equal to 44 \AA^2 . $\ln(\Delta A_L / A_L)$ plots over a range of pressures. The free enthalpy of binding of TRE to DMPA lipid film is $-9.1 \text{ kJ} < \Delta G_0 < -7.4 \text{ kJ}$.

This corresponds to an area of $\sim 70 \text{ \AA}^2$ (without VDW radius).¹²⁶ Also the free enthalpy of the binding of the disaccharide (trehalose) to PLs increased from $-12.8 \text{ kJ mol}^{-1}$ in PPLs to -9.5 kJ mol^{-1} in NPLs as determined from the zero pressure extrapolation of the two regression lines in Fig. 4.5B and D (see chapter 3.7 for calculations). These results demonstrate that preconditioning enhances the affinity of the PLs to the disaccharide. Additionally, its larger molar area in PPL monolayers suggests that it also covers a larger surface in a single leaflet of cell membranes in preconditioned worms.

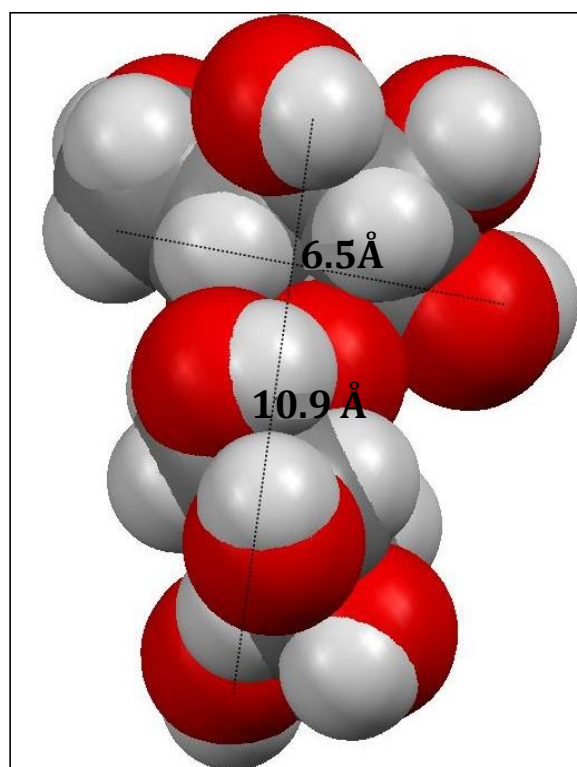


Figure 4.7: Molecular modeling of α,α -trehalose single molecule. The predicted projection surface of trehalose has a long and short axis of 10.9 and 6.5 Å.¹²⁶

Interaction of Trehalose with PLs & Residual

4.3 Water in Response to Membrane Hydration

As shown above, the reduction of the PC-content during preconditioning increases the coupling of acyl chain disorder to sub-headgroup hydration on the time scale of seconds, already in the absence of trehalose. Physiologically, this situation is not sufficient to maintain membrane organization upon water loss, because preconditioned but trehalose-deficient worms do not survive desiccation. Motivated also by our finding that trehalose had higher affinity for PPLs, we have also studied the influence of trehalose on the structural transitions of NPLs and PPLs by time-resolved hydration-induced ATR-FTIR-difference spectroscopy. Figure 4.8 shows an equivalent data set as Figure 4.2, recorded from PLs supplemented with trehalose at a ratio of 1:20 (trehalose: lipid). In the presence of trehalose, the coupling of acyl chain disordering to sub-headgroup hydration as reflected by the ratio between the $\nu(\text{CH}_2)$ and $\nu(\text{C=O})$ difference bands,

is again larger in PPLs as compared to NPLs (Table 4.1). Remarkably, for both PLs, the $\nu_{as}(\text{PO}_2^-)$ amplitude relative to the $\nu(\text{C=O})$ is reduced to about one third of that measured without the disaccharide (Fig. 4.2). This demonstrates that already at 75% RH, trehalose almost completely saturates the majority of H-bond interactions at the PO_2^- groups, which agrees with the water replacement mechanism.^{26,127} Since hydration increases acyl chain disorder without increasing H-bonding at the PO_2^- groups the observed acyl chain disordering must be induced predominantly by transient hydration of the ester carbonyl region. Indeed, a much more pronounced down shift of the $\nu(\text{C=O})$ in Fig. 4.8A and B as compared to trehalose-free PLs (Fig. 4.2A and B) is observed for both PL extracts and evidences stronger H-bonding at the ester-carbonyls: the negative lobe at 1741 cm^{-1} is unaffected by the sugar but the positive lobe is down-shifted to $\sim 1700\text{ cm}^{-1}$ as compared to 1713 cm^{-1} in the absence of trehalose. The unaffected initial $\nu(\text{C=O})$ at 1741 cm^{-1} shows that stronger carbonyl H-bonds are not established by trehalose per se but form transiently upon hydration beyond the 75% RH level. Trehalose thus saturates the PO_2^- H-bonds and directs further H-bond formation efficiently to the sub-headgroup region in a dynamic hydration-induced process. Likewise, the $\nu(\text{CH}_2)$ frequencies at 75% RH at 2849 and 2917 cm^{-1} (negative bands) are unaffected by trehalose, which indicates an unchanged static acyl chain free volume. In the hydrated state however, the band broadening (particularly at $\sim 2949\text{ cm}^{-1}$) evidences a higher heterogeneity of acyl chain conformations as in the absence of the sugar.

In summary, hydration in the presence of trehalose is directed preferentially to the ester carbonyl region and increases the heterogeneity of acyl chain structures in the more disordered hydrated state. These features become obvious only during a hydration transient and are not present in the equilibrated state of the PLs. Since they are dynamically induced in NPLs as well as PPLs, they are independent of the PC content but reflect a general water-dependent dynamics of trehalose lipid interactions.

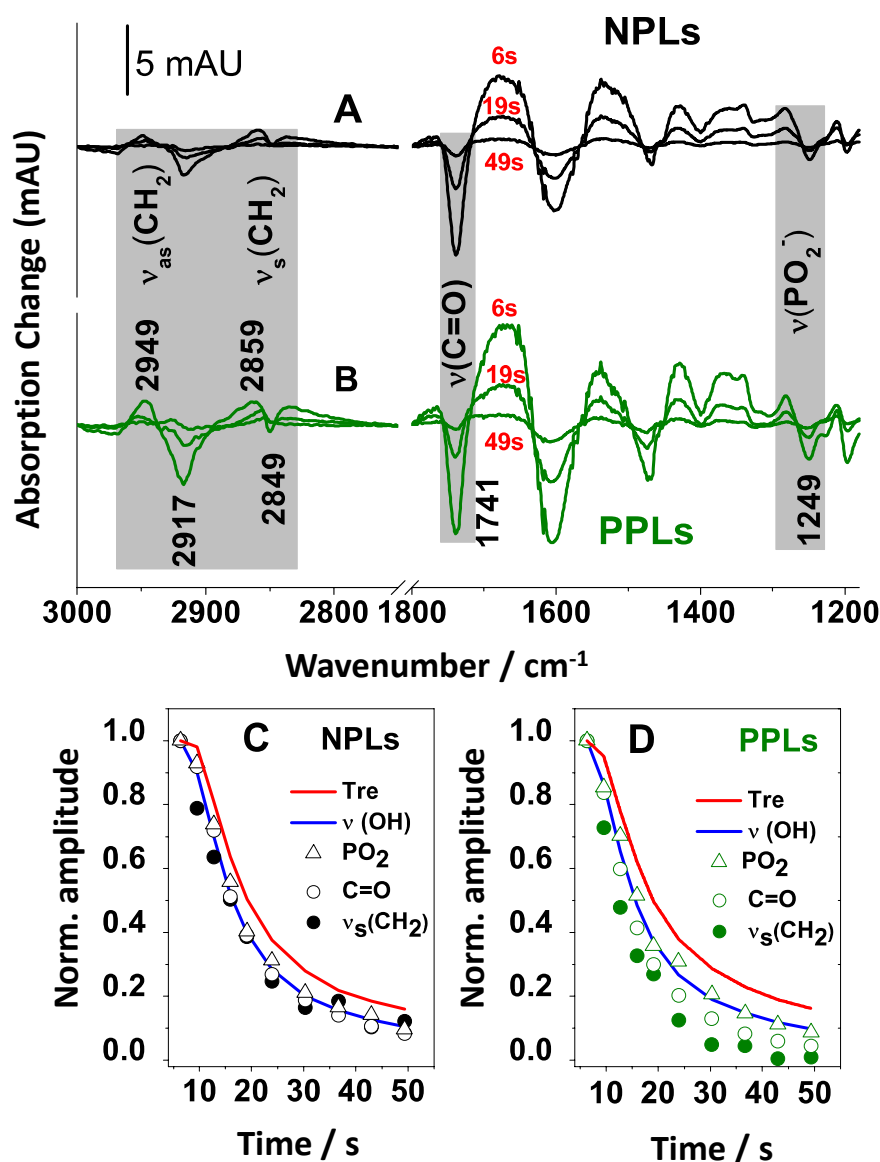


Figure 4.8: Time-resolved hydration-pulse-induced IR absorption changes of PL extracts in the presence of trehalose. A) Representative selection of hydration-induced difference spectra of NPLs recorded at the indicated times after the hydration pulse. The hydration-induced down shift of the $\nu(\text{C=O})$ and $\nu_{as}(\text{PO}_2^-)$ causes the difference bands at 1741/1700 cm^{-1} due to increased H-bonding to the ester carbonyl. Little changes are observed for the phosphates at 1249-1200 cm^{-1} . The increase of acyl chain free volume is monitored by the up-shift of the $\nu_s(\text{CH}_2)$ and $\nu_{as}(\text{CH}_2)$ frequencies (2849/2859 and 2917/2949 cm^{-1} , respectively). B) As in (A) but obtained with PPLs. C) Relaxation of absorption changes of NPLs. D) as in (C) but for PPLs. Infrared frequencies are assigned to chemical groups as indicated. The loss of water to the gas phase (reduction of $\nu(\text{OH})$ amplitude) is shown for comparison (blue) as well as the change in H-bonding to trehalose.

Relaxation Kinetics Induced by Hydration of *C. elegans* PLS in the Presence of

Trehalose: The described trehalose PL interactions are exhibited by both PL extracts.

A remarkable influence of preconditioning, however, is seen on the relaxation kinetics. The absorption changes of the water $\nu(\text{OH})$ as well as $\nu(\text{C}=\text{O})$ and $\nu_{as}(\text{PO}_2^-)$ are slowed down by the sugar (Figure 4.8C and D) in accordance with earlier FTIR studies.¹²⁸ Furthermore, they become essentially synchronized with the acyl chain relaxation in NPLs as shown in Fig. 4.8C. This is surprisingly not the case for PPLs (Fig. 4.8D). Despite the very similar spectral properties of NPLs and PPLs, the relaxation rates of the different PL chemical groups is clearly more heterogeneous and indicate larger flexibility in PPLs. Particularly the acyl chain re-ordering occurs faster than the re-equilibration of water with the gas phase. PPLs are thus unique in allowing trehalose to slow down headgroup hydration changes without rigidifying but actually softening the hydrophobic core of the PPLs. We think that the accelerated acyl chain relaxation under conditions of a decelerated water exchange with the gas phase is the crucial physical basis of maintaining membrane integrity during hydration transients.

In summary, the demonstrated change in lipid composition during preconditioning leads to an increased gain of acyl chain free volume, to accelerated acyl chain dynamics during hydration transients and to a more efficient trehalose insertion into PPLs. These physical parameters correlate with the previously observed occurrence of membrane ruptures in *C. elegans* dauer larvae after desiccation and are probably of key importance for trehalose-dependent desiccation tolerance.

Hydration-Induced Volume Changes & Lipid Expansion Coefficient in *C. elegans* PL Films

4.4 (Swelling Behavior)

Previous electron microscopy showed desiccation-dependent damage by mechanical strain.²⁰ Therefore, we have also addressed the macroscopic PL volume changes (i.e. 3D expansion as compared to 2D lateral expansion studied above). The absolute absorption of the PL films in ATR geometry depends on film thickness.¹⁰⁵ Hence, the ATR geometry allows deducing changes in sample thickness from changes in the absolute absorption of the PL films. This information is obtained with the collection of the raw data. Such that at each of the ten sampled time points after the hydration pulse that

indicated by arrows (Fig. 4.9A and B), the change of sample volume relative to that in the initial state can be derived. The relative volume changes per water molecule and lipid (relative molar expansion coefficient) $\alpha = \Delta V \cdot V^{-1} \cdot \Delta \Gamma^{-1}$ were determined from the corresponding absorption decrease upon hydration (see chapter 3.5 calculations). Although NPLs take up more water ($\Gamma = 15$) than PPLs ($\Gamma = 13$) at the same RH, their 3D expansion coefficient α is almost identical in the absence of trehalose (Fig. 4.9A). In the presence of trehalose, the degree of basal hydration is increased as previously observed.¹²⁸ Figure 4.9B shows a basal hydration Γ of 33 and 27 as compared to 15 and 13 without trehalose for NPLs and PPLs, respectively. Also the amount of water taken up under the identical pulse conditions is about twice as large, evidencing the strong hygroscopic effect of the sugar. The volume changes (swelling) of the lipidic films are larger for PPLs than for NPLs, indicating a larger degree of hydration-induced structural transitions. Since this difference between NPLs and PPLs is observed only in the presence of trehalose. The kinetically more heterogeneous H-bond network established in the sub-headgroup region in PPLs in the presence of trehalose and the faster acyl chain structural transitions are very likely the cause for a larger expansion coefficient of the PL on the time scale of seconds.

Finally, water taken up in the presence of trehalose forms a population with similar H-bond strength as in pure PL films and an additional one with stronger H-bonding, indicated by the distinct $\nu(\text{OH})$ shoulder at lower frequency (Fig. 4.9C). The direct participation of trehalose in remodeling of the H-bond network is evident from its hydration-induced difference bands shown in Figure 4.9D.

The different dynamic and mechanical responses of PLs to hydration and trehalose insertion correlate strictly with the occurrence of membrane ruptures and with the survival of *C. elegans* dauer larvae. Therefore, the chemical, structural and physical PL parameters revealed here are probably of key importance for desiccation tolerance. The regulation of both intrinsic and trehalose-dependent properties through the PC-content is a salient adaptation of the molecular physiology in anhydrobiosis.

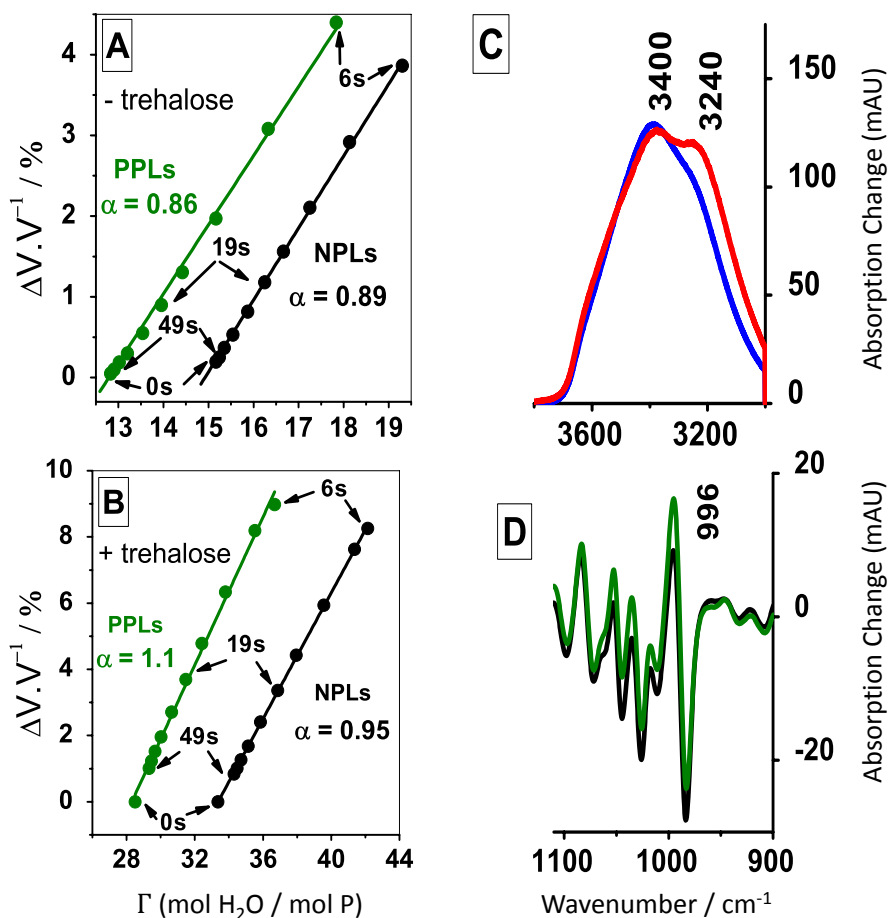


Figure 4.9: Time-resolved volume and H-bond changes. Relative expansion of PL films in the absence (A) and presence (B) of trehalose. The evaluation is based on the time-dependent data shown in Figs. 2 and 8, respectively. The sequence of swelling / shrinking is indicated by the selected time points, the slopes α are relative expansion coefficients ($\alpha = \Delta(\Delta V/V) \cdot \Delta\Gamma^{-1}$, standard error $< 10^{-2} \%$). C) $\nu(\text{OH})$ contour of water adsorbed during the hydration pulse in the absence (blue) and presence (red) of trehalose. D) Hydration-induced absorption changes of trehalose in PLs. Color code: black, NPLs; green, PPLs.

4.5 Discussion

The dauer larvae of the nematode *C. elegans* are capable of adopting an anhydrobiotic state in which they survive desiccation over months.²⁰ Desiccation tolerance depends on a limited number of strategies that are employed during preconditioning.¹²⁹ One of them is the biosynthesis of trehalose (α, α -1,1-glucoside) during a preconditioning phase, when they are exposed to 98% RH, before experiencing harsher desiccation. It has been previously shown that non-preconditioned worms are not desiccation tolerant. Furthermore, trehalose-deficient worms are desiccation sensitive even after

preconditioning and exhibit irreversible damage to cell membranes upon rehydration. Motivated by these findings, we have studied fast non-equilibrium structural transitions induced by hydration in PLs extracted from dauer larvae of the *C.elegans* strain *daf-2*. The salient physical feature revealed here by time-resolved rapid scan FTIR difference spectroscopy is the more efficient almost three-fold increase in acyl chain free volume upon fast hydration of PPLs already in the absence of trehalose as shown in Table 4.1. This corresponding methylene stretching absorption changes occurred in response to transient hydration from 75% to $\sim 82\%$ RH. These amplitudes are proportional to the size of the underlying frequency shifts. The $\nu_s(\text{CH}_2)$ frequency shift scales with the area per lipid¹⁰⁸ evidencing that it is increased by hydration of PLs from preconditioned larvae more than twice as much as in PLs from non-preconditioned larvae. This behavior is independent of trehalose and originates in a different coupling of the sub-headgroup H-bond network to acyl chain packing. We have shown that the chemical basis for remodeled H-bond network is the reduction of the PC-content during preconditioning. Previous FTIR work on model lipids at extremely low hydration (Γ of 3-5) demonstrated that the tri-methyl hydrogens of PC can form strong water contact,¹²⁰ whereas PE exhibits weaker water binding upon drying.^{121,122} Our data suggest that the different intrinsic headgroup hydration patterns of PC and PE contribute to the unexpected differences in coupling headgroup hydration to acyl chain disorder. In concert with possible other acyl chain packing preferences, e.g., a tilted acyl chain packing in PC over PE,¹³⁰ the regulation of the PC:PE ratio in vivo could be an essential factor in rendering cell membranes desiccation-resistant.

Next, we have asked whether the different physiochemical properties of the *C. elegans* PL extracts are important for the protective function of trehalose. The general effects of the disaccharide on PL hydration are a higher basal hydration, a slower water exchange rate with the gas phase, and the saturation of H-bonds to the PO_2^- groups already at reduced humidity. All these features are independent of preconditioning. Saturation of H-bonds to the PO_2^- groups is consistent with water replacement hypothesis.¹³ In contrast to both water replacement and water entrapment hypotheses, however, trehalose does not affect the H-bond strength at the ester carbonyls at 75% RH, because the $\nu(\text{C=O})$ difference band stays at 1741 cm^{-1} , irrespective of the presence of sugar.

This indicates that trehalose neither substitutes for H-bonds, nor entraps water in the sub-headgroup region at reduced humidity. Instead, trehalose mediates the transient hydration-driven formation of an H-bond network in the sub-headgroup region. This is in clear contrast to the action of trehalose on model lipids in aqueous suspension, where the $\nu(\text{C=O})$ gradually decreases with the amount of trehalose.¹³¹ In agreement with these studies, the hydration-induced newly formed H-bonds are then indeed much stronger than in pure PL extracts, leading to a larger frequency downshift (positive lobes of the $\nu(\text{C=O})$ difference bands at 1713 cm^{-1} and $\sim 1700\text{ cm}^{-1}$ in NPLs and PPLs, respectively). The potential of trehalose to organize an unusually large dynamical hydration shell¹³² may be crucial in linking lipid surface hydration to an increase transient sub-headgroup H-bonding shown here. It was surprising that at 75% RH trehalose has no effect at all on the carbonyl H-bond showing that trehalose does not increase sub-headgroup hydration per se. The interaction of the *C. elegans* PLs with trehalose is strongly hydration-driven and the topology of trehalose within the PLs may not be static. A dynamic hydration driven trehalose-mediated H-bond network describes the data much better and appears to be the crucial factor in tailoring PL properties for desiccation tolerance.

Since, the dynamic molecular properties of PLs also correlate with their mechanical behavior during hydration-dependent expansion, we have derived estimates of the PL compressibility modulus K_c (Fig. 4.10), based solely on the FTIR data used in Figs. 4.2 and 4.8. K_c relates the area increase per lipid ΔA_L linearly to the change of the free enthalpy of water per lipid, i.e., $\Delta(\Gamma \ln(a_w))$,¹⁰⁹ with a_w the water activity at thermodynamic equilibrium (see chapter 3.5.3). The frequency change of the acyl chain $\Delta\nu(\text{CH}_2)$ (and thus the amplitude ΔA of the difference band) correlates also linearly with ΔA_L .¹⁰⁸ Therefore, under equilibrium conditions, the $\nu_s(\text{CH}_2)$ amplitude ΔA scales with $\Delta(\Gamma \ln(a_w))$. Of course, an equilibrium is not generally expected for fast hydration transients and a non-linear relation is indeed found for both PL samples in the absence of trehalose (Fig. 4.10A). However, an almost linear plot is obtained in the presence of trehalose (Fig. 4.10B), demonstrating that the disaccharide permits a close to equilibrium lyotropic transition even during fast hydration transients. Lateral tension estimates of 2.6 N/m and 1.0 N/m are obtained for NPLs and PPLs, corresponding

to a molar compressibility of 16.0 and 6.4 KJ/A², respectively. These estimates agree with recent molecular dynamics (MD) calculations for trehalose-containing bilayers,²⁷ which show that trehalose may increase the compressibility modulus up to 6 N/m in PC-PLs, in contrast to earlier MD studies suggesting a decrease.¹³³ Remarkably, PPLs with reduced PC content exhibit a lower compressibility modulus and are thus "softer" than NPLs with trehalose.

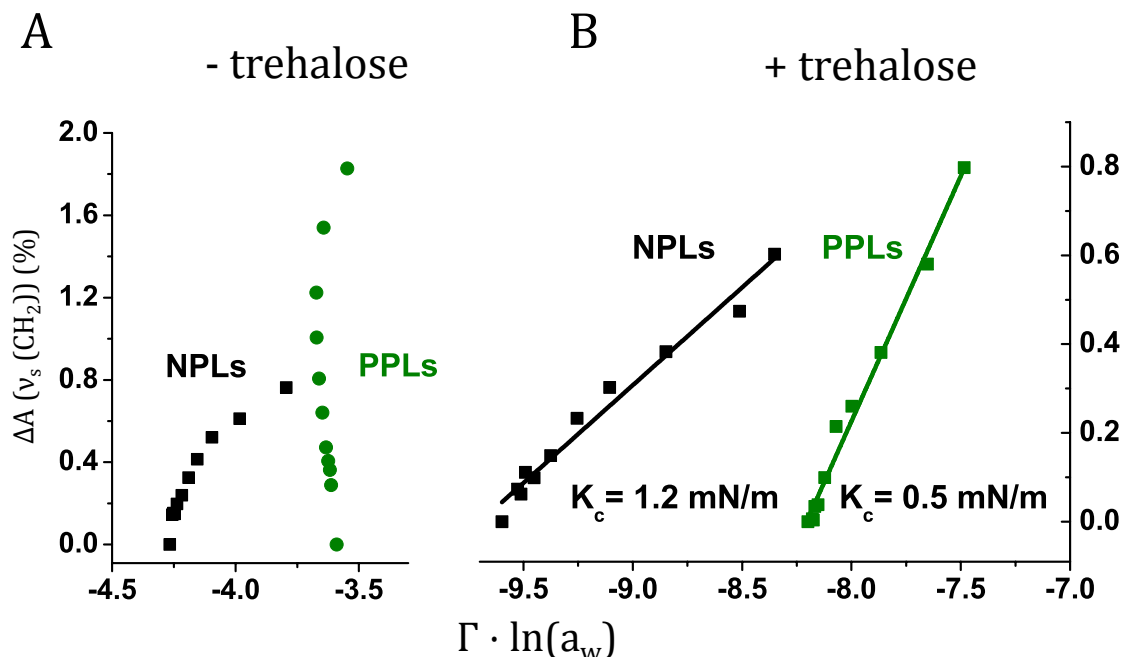


Figure 4.10: Absorption change ΔA of the symmetric CH_2 stretching mode as a function of the chemical potential of water. The time-dependent amplitude of the 2849/2859 cm^{-1} difference bands (in per cent of the total absorption at 2850 cm^{-1}) is plotted versus the chemical potential of water in the absence (A) and presence of trehalose (B). From the slopes, compressibility modules are derived (see chapter 3.5.3).

In addition to the softened two-dimensional lateral expansion in PPLs, the PL extracts differ in their three-dimensional swelling which includes the contributions from inter-membranous water. Trehalose increases the fractional gain in volume per added water molecule more pronouncedly in PPLs (from 0.86% to 1.1%) than in NPLs (from 0.89% to 0.95%), see Figure 4.9A and B, respectively. In both cases trehalose causes the formation of an additional strongly H-bonded water population (Fig. 4.9C) and exhibits extensive hydration-dependent H-bond changes (Fig. 4.9D). Only in the PE rich PPLs, these H-bonds grow into a more voluminous inter-membranous network. This supports again the crucial role of matching the intrinsic headgroup hydration

properties to the trehalose-mediated water structures to produce a favourable lyotropic behavior of the carbohydrate PL composite.

Our data show that the PC-reduction is a factor that enhances the effect of trehalose on the lateral and three-dimensional expansion of the native PL mixture. Furthermore, hydration transiently extends the trehalose-mediated H-bond network to the sub-headgroup. This implies that the sugar may promote a more extensive increase of the lipid lateral area by sliding deeper into the sub-headgroup region upon water uptake (hydration). This will further increase the area per lipid particularly in PPLs, which show higher trehalose affinity and molar area requirement. Therefore, PPLs should resist better to strain generated in a cellular compartment that grows during swelling. A correlation between lipid lateral expansion and the number of trehalose to C=O H-bonding has been seen in MD simulations in the fully hydrated¹²³ and recently also in the dehydrated state.¹³⁴ Here, we propose a hydration-driven trehalose insertion into the ester carbonyl region of PPLs at reduced humidity (Fig. 4.11). This relocation probably presents an extreme but physiologically relevant case of the trehalose repulsion/attraction mechanism as previously proposed for high and low trehalose:water ratios in hydrated PLs.¹³⁵ Importantly, the bilayer-stabilizing function of trehalose is clearly not only dependent on its crucial α,α -1,1 glycosidic linkage,⁴⁴ but also on PL headgroup composition. Hence, the mechanical response of cell membranes to fast hydration transients is further regulated in the anhydrobitotic dauer state by the lipid headgroup chemistry. MD calculations have focused only on PC and show headgroup fluctuations between parallel and perpendicular orientations with respect to the fully hydrated membrane.¹³⁶ The parallel arrangement is populated upon dehydration^{137,138} but not influenced by trehalose.¹³⁴ It remains to be elucidated whether such orientational features contribute to PE being the preferred headgroup over PC in the trehalose-dependent desiccation tolerance of the *C. elegans* dauer larvae.

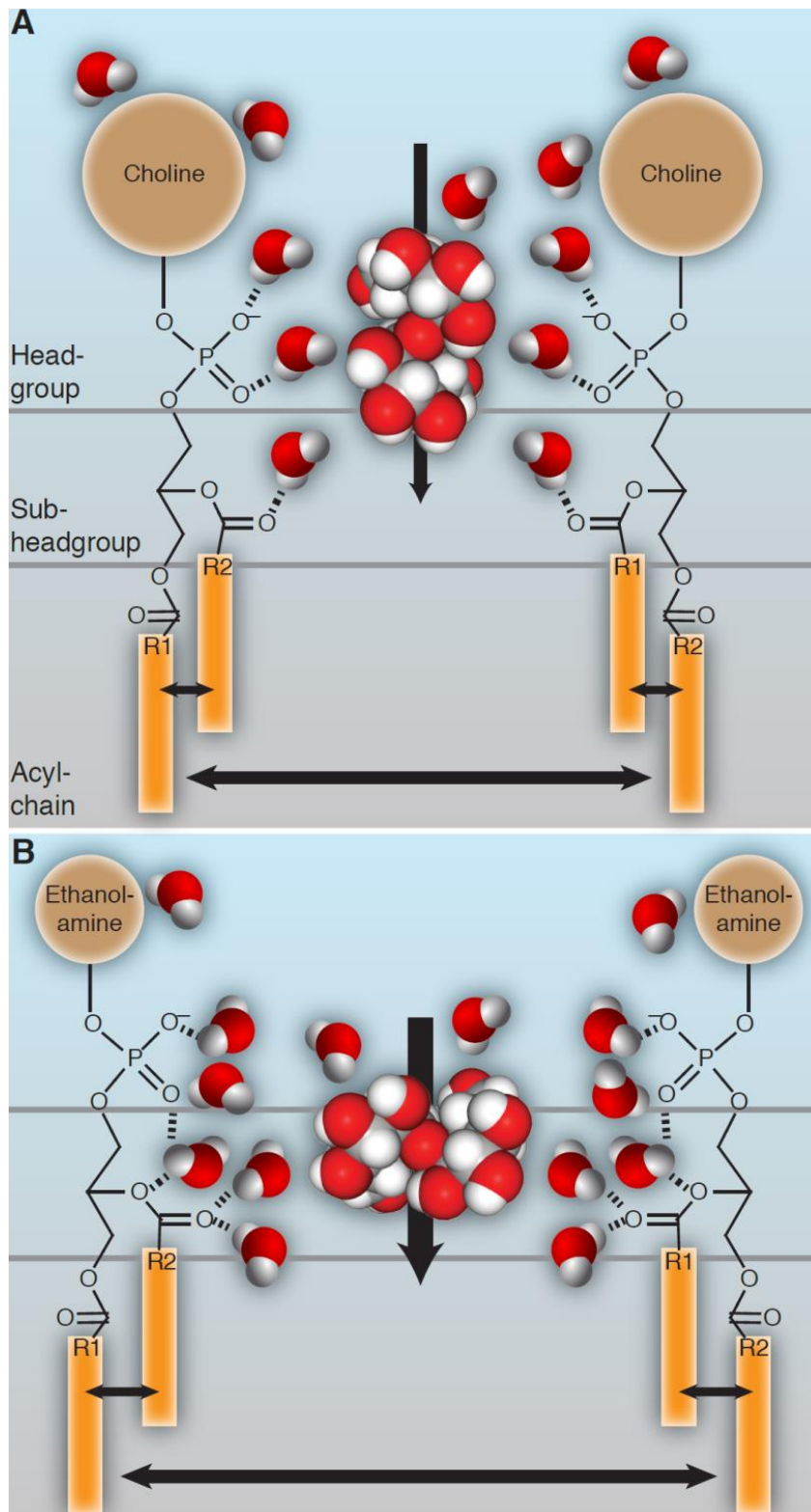


Figure 4.11: Dynamic interaction of trehalose with lipid headgroups during transient hydration at reduced humidity. Hydration of the trehalose-containing PLs leads to the insertion of the disaccharide into the headgroup/sub-headgroup interface (vertical arrows), allowing direct and water-mediated H-bonding to the ester carbonyls. The stronger water headgroup interaction in PC restricts this motion in NPLs (A), whereas efficient intercalation of the sugar occurs in the PE-dominated PPLs (B). The higher water-induced acyl chain disorder in PPLs further allows a larger gain of molecular area (horizontal arrows) upon fast hydration, leading to a “softer” (lower lateral tension) response of PPLs.

4.6 Conclusions

All anhydrobiotes have to preserve their membranes in the dry state and during quick rehydration. Furthermore, at the molecular level, many anhydrobiotic strategies are shared among organisms from different taxa.^{129,139} Trehalose is not the only sugar associated with desiccation tolerance in anhydrobiotes. Plants, for instance, synthesize sucrose as an osmoprotectant.¹⁴⁰ Therefore, accelerating the relaxation of desiccated PLs relative to the change in water content by the help of sugars can be a common mechanism among anhydrobiotes. A better understanding of the physicochemical basis of this behavior can in the future help us in engineering desiccation tolerance for practical applications. We have shown that dauer larvae of the nematode *C. elegans* prepare for anhydrobiosis by reducing the PC headgroup content of their PL composition. We think that this is a systemic response to mildly reduced humidity during preconditioning. It results in a higher affinity of trehalose to the PLs, a larger surface coverage of the disaccharide in the desiccation-resistant membranes and a larger and accelerated gain of acyl chain free volume upon fast hydration. Importantly, lyotropic transitions can then progress close to thermodynamic equilibrium within seconds and is accompanied by a larger gain in acyl chain free volume as shown schematically in Fig. 4.11 than in the normal PL headgroup composition. Hence, trehalose synthesis and PC-reduction act synergistically in promoting desiccation tolerance of cell membranes. Given the wide-spread synthesis of sugars in anhydrobiotes, the systemic response demonstrated here may represent an evolutionarily conserved chemical adaptation for anhydrobiosis.

THERMO-TROPIC PHASE BEHAVIOR & HEADGROUP INTERACTIONS OF *C.elegans* PLS IN THE DEHYDRATED STATE

Contents

5.1	Temperature-Induced Phase Transitions in PLs from Dauer Larvae in the Absence of Trehalose	85
5.2	Temperature-Induced Phase Transitions in PLs from Dauer Larvae in the Presence of Trehalose	88
5.3	Thermally Induced Changes of H-Bonding in the Sub- Headgroup Region of <i>C. elegans</i> PLs in the Absence of Tre- halose	90
5.4	Thermally Induced Changes of H-Bonding in the Sub- Headgroup Region of <i>C. elegans</i> PLs in the Presence of Tre- halose	95
5.5	Discussion	99
5.6	Conclusions	99

Temperature-induced absorption FTIR spectroscopy has been widely used to study lipid phase transitions in model and natural membranes. It has been shown that spectroscopic markers emanating from infrared-active groups present in the hydrophobic, interfacial, and headgroup regions of the lipid bilayer show different sensitivity to the thermo-tropic phase transition observed by calorimetry.¹⁴¹ However, no studies have specially focused on *C. elegans* lipid membranes in the dehydrated state. Particularly, the thermo-tropic phase behavior of lipids from preconditioned and non-preconditioned dauer larvae and its dependence on trehalose has not been addressed. For this purpose, we evaluated the temperature-induced changes of the methylene and carbonyl stretching modes of NPLs and PPLs to investigate how the sub-headgroup hydration (monitored by the C=O vibration) and the acyl chain disorder (reported by the CH₂ frequency) depend on temperature at constant 75% RH. In addition, emphasis is put on the influence of trehalose on the lipid phase transition under biologically relevant conditions by a detailed analysis of the lipid C=O H-bond environment. These data were recorded in the 2-80 °C range to complement the time-resolved FTIR investigations of the influence of preconditioning and of trehalose on the PLs membrane phases. This proved to be sufficient model system to study the phase transitions and the thermo-tropic responses to the preconditioning and trehalose binding because the phase transition temperatures (T_m) are well separated.

Physiologically, the data address the possible consequences of temperature variations on *C. elegans* membranes at reduced humidity. Physically, the experiments will provide further evidence for the adaptation of lipid headgroup composition during preconditioning to allow specific hydration-dependent interactions with trehalose that are not realized in the lipid composition of non-preconditioned dauer larvae.

Temperature-Induced Phase Transitions in PLs from Dauer Larvae in the Absence of

5.1 Trehalose

Thermodynamic parameters of desiccation tolerant *C. elegans* PLS can be deduced from temperature dependent shifts in characteristic IR group frequencies. IR absorption spectra as a function of temperature that were dehydrated at moderate relative humidity 75% of NPLs (Fig. 5.1A-C) and PPLs (Fig. 5.1D-F) show shifts of bands, associated with melting of the PLS. The Characteristic absorbance bands arising from water and PLS are indicated. It is evident that both the OH stretching and H₂O scissoring vibrational modes of water decrease in intensity during drying, which is the result of evaporation of water from the PLS film. Additionally, the lipid CH₂, C=O and PO₂⁻ stretching bands increase in intensity during drying, which is due to the increase in lipid concentration of the PLS film. Furthermore, the $\nu(\text{OH})$ presents a broad peak in the FTIR spectra from about 3800 cm⁻¹ to 3000 cm⁻¹ indicating a wide variety of H-bond strengths. In NPLs and PPLs, the OH stretching band shifts to higher wavenumber with increasing temperature (Fig. 5.1A & D, respectively), which indicates a decrease in H-bonding between water and PL. The CH₂ symmetric stretching band $\nu_s(\text{CH}_2)$ near 2850 cm⁻¹ is of special significance because of its sensitivity to changes in the conformational disorder of the hydrocarbon acyl chains.¹⁴² In Figure 5.2A, the wavenumbers at the absorbance maximum of the symmetric CH₂ stretching vibration band $\nu_s(\text{CH}_2)$ of NPLs and PPLs are presented as a function of temperature. For NPLs and PPLs in the gel phase, the absorption maximum of the CH₂ stretching band is observed near 2851.2 and 2850.8 cm⁻¹. Upon transition to the liquid-crystalline phase, the maximum increases to frequencies near 2853.4 cm⁻¹. This frequency increase is accompanied by a broadening of the CH₂ band (Fig. 5.1B; for NPLs & Fig. 5.1E; for PPLs) and it is coinciding with the loss of water (decrease in intensity of the OH band), as shown in NPLs Fig. 5.1A and PPLs Fig. 5.1D. These changes are a diagnostic signature of the induced phase transitions from a highly ordered gel phase to the fluid phase of the lipid bilayers.¹⁴² Interestingly, preconditioning produces a larger frequency

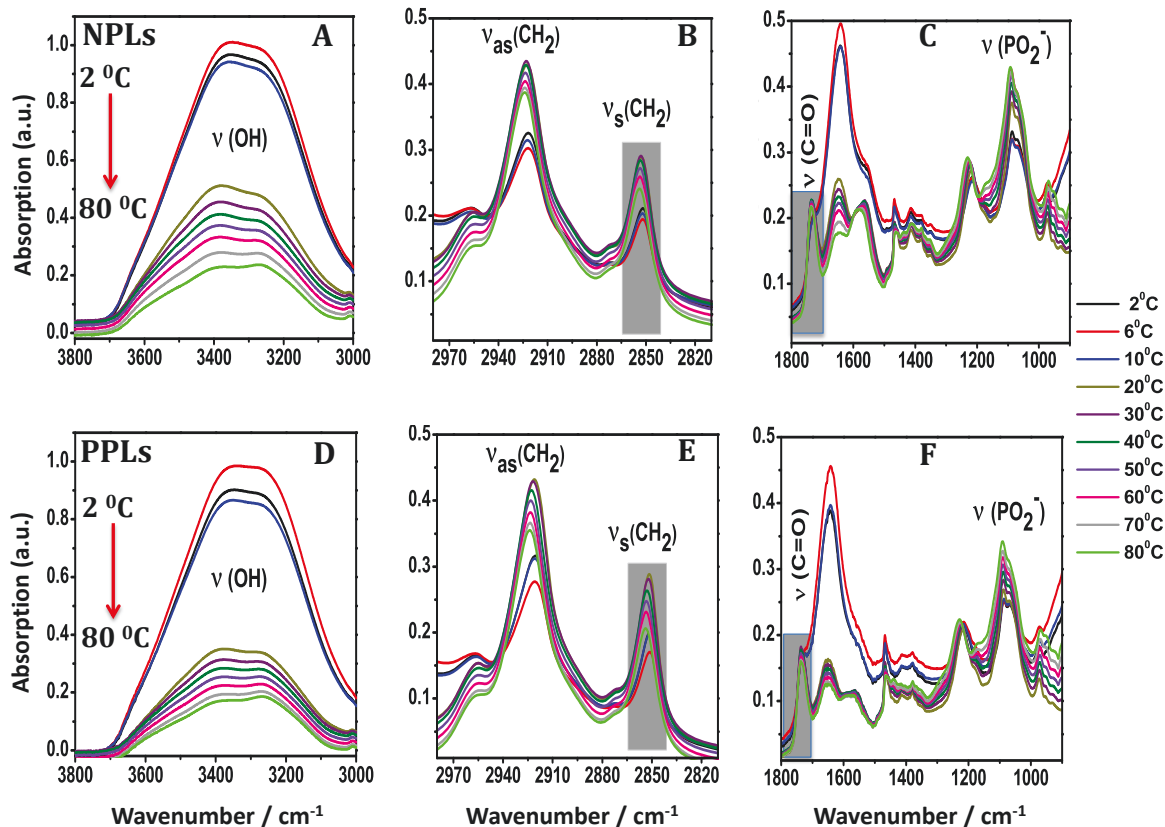


Figure 5.1: Temperature-dependent ATR-FTIR spectral changes. The main characteristic stretching absorption bands are: OH ($3800\text{--}3000\text{ cm}^{-1}$), CH_2 ($2970\text{--}2820\text{ cm}^{-1}$), C=O ($1800\text{--}1660\text{ cm}^{-1}$) and PO_2^- ($1250\text{--}1050\text{ cm}^{-1}$). Panels A-C: NPLs; panels D-F: PPLs. Spectra were acquired at the indicated temperatures at 75% relative humidity.

shift of the CH_2 band ($\Delta\nu = 2.6\text{ cm}^{-1}$) as compared with NPLs. This result indicates that during the transition from gel to the liquid crystalline states there is a larger increase in the conformational disorder in the PPLs hydrocarbon chains¹⁴³ resulting from an increase in the gauche isomers, decrease in the van der Waals attractions, and thus an increase in membrane PLs fluidity.¹⁴¹

Additional information can be deduced from the first derivative analysis of the FTIR absorption spectra of the $\nu_s(\text{CH}_2)$, which identifies the transition temperature (T_m) as the midpoint temperature of the phase transition (steepest slope of the frequency shift). As shown in Figure 5.2B, three phase transitions can be seen in NPLs at 10, 22 and 30 °C. The first transition is similar to that reported previously.¹⁴⁴ This result indicates that a high proportion of chain melting has already occurred at lower temperature at about 10 °C. On the other hand, PPLs shows three transitions at 6, 22 and 36 °C with a higher total change in CH_2 vibrational frequency. Clearly, the PPLs exhibit the more

homogenous thermal response with one predominant cooperative transition at 36 °C. The obvious heterogeneity of melting temperatures seen in the NPLs is not unexpected, because many lipid species are present, which cannot be assigned to individual transition temperatures, though.

The main feature that distinguishes PPLs from NPLs is thus the large amplitude of the phase transition at 36 °C at the expense of the lower temperature components that are resolved in the NPLs. This behaviour shows that after preconditioning the coexistence of different PLs species can nevertheless form a rather homogenous mixture with a common transition temperature.

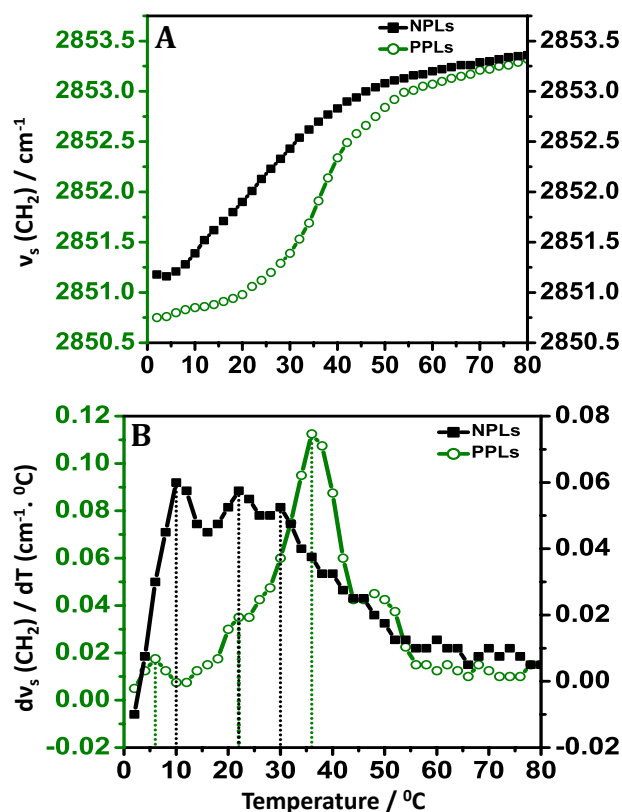


Figure 5.2: Lipid melting curves. The increase in the $\nu_s(\text{CH}_2)$ peak vibrational frequency of PPLs (green circles) and NPLs (black squares) is plotted as a function of temperature (2-80 $^{\circ}\text{C}$) (A). For comparison the left and the right scale is the same in panel A. The first derivatives of the presented curves on (B). The peak maxima (vertical dotted lines) indicate the phase transition temperatures of both NPLs and PPLs. The first derivative plot shows the phase transitions as the regions of greatest slope.

Temperature-Induced Phase Transitions in PLs from Dauer Larvae in the Presence of

5.2 Trehalose

The Thermo-tropic phase behavior of the mildly dehydrated *C. elegans* membrane PLs was further investigated in the presence of trehalose. Figure 5.3 shows an example of temperature-dependent FTIR spectra of NPLs (A-C) and PPLs (D-F) in the presence of trehalose. A remarkable difference in the effect of trehalose on the water H-bond network is revealed: in PPLs, the $\nu(\text{OH})$ is shifted to lower wavenumbers to around 3266 cm^{-1} (see Fig. 5.3D), indicating the strong H-bond interaction between water and the trehalose-containing PLs.

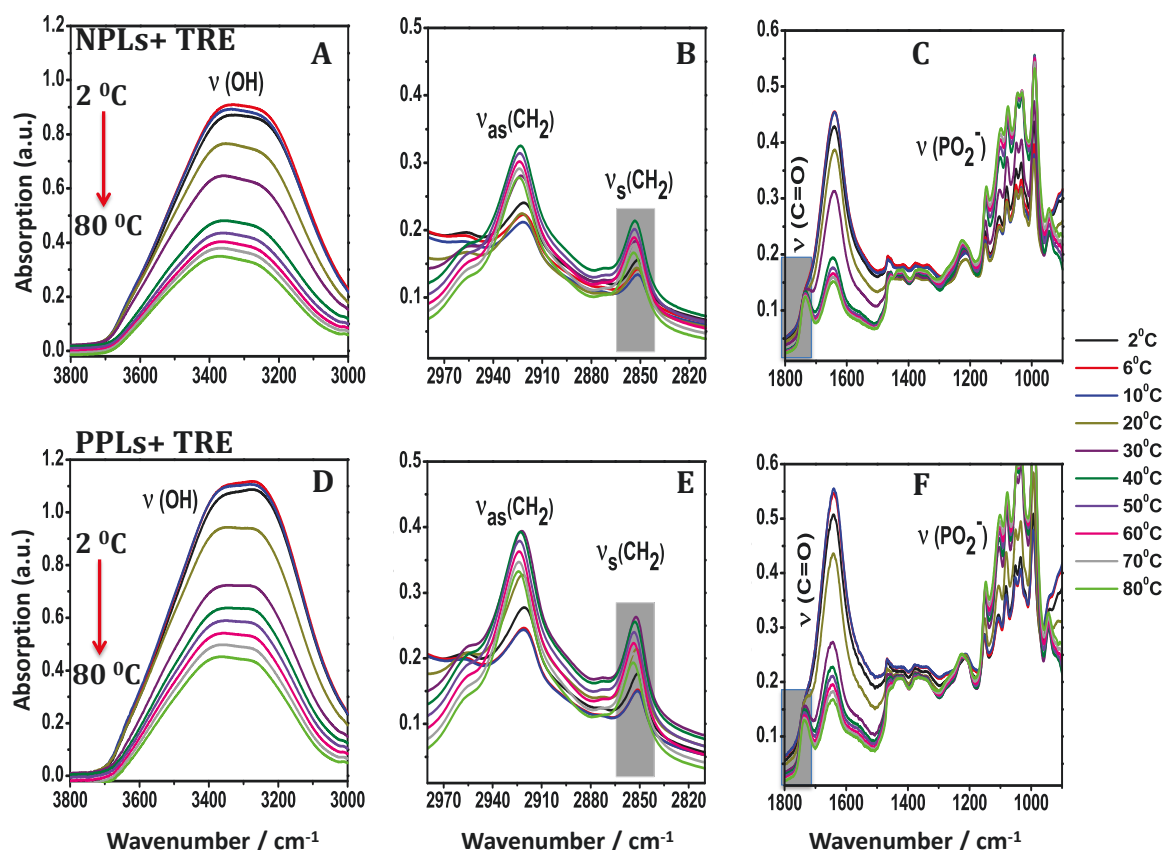


Figure 5.3: Temperature-dependent ATR-FTIR spectral changes induced by trehalose. The main characteristic stretching absorption bands: OH ($3800\text{--}3000\text{ cm}^{-1}$), CH_2 ($2970\text{--}2820\text{ cm}^{-1}$), C=O ($1800\text{--}1660\text{ cm}^{-1}$) and PO_2^- ($1250\text{--}1050\text{ cm}^{-1}$). Panels A-C: NPLs; panels D-F: PPLs. Spectra were acquired at the indicated temperatures at 75% relative humidity.

In contrast, NPLs containing trehalose exhibit a higher $\nu(\text{OH})$ (Fig. 5.3A), indicating a weaker H-bond network despite the presence of the sugar. Only at elevated temperatures, the stronger H-bond network of trehalose-containing PPLs is broken and the $\nu(\text{OH})$ band contour becomes more similar to that of NPLs. The corresponding melting curves of NPLs and PPLs derived from the data in Fig. 5.3B and E are presented in Fig. 5.4A. The transition from gel to liquid crystalline phase is clearly visible from the frequency shift by $\Delta\nu = 2.7 \text{ cm}^{-1}$ in both lipid extracts, whereas it was smaller for NPLs than PPLs in the absence of trehalose. The more similar behavior of both lipid extracts in the presence of the sugar is due to two factors: 1) the lowering of initial CH_2 frequency in NPLs to the same frequency as that in PPLs 2) the formation of a more prominent T_m (at 32°C) for the majority of the PLs. The data reveal that trehalose induces an increase of acyl chain order in NPLs, whereas it has little effect on acyl chain packing.

The derivatives of the wavenumber-temperature curves (Figure 5.4B) reveal the more distinct phase transitions of the NPLs and show that trehalose increases the transition temperatures in both NPLs and PPLs with T_m at 20, 26 and 32°C for NPLs; and at 16, 22 and 40°C for PPLs. The general rise in main transition temperature indicates a stabilization of the gel phase in the presence of trehalose. Despite the general trehalose-induced stabilization of the gel phases at 75% RH, the NPLs still exhibit the stronger temperature-dependence of their acyl chain order than the PPLs.

The interesting question related to our results is whether the phase transitions correlate with the physiology of the intact organism. It has been shown by electron spin resonance (ESR) data and the Arrhenius plot of respiration in a previously reported study¹⁴⁴ that *C. elegans* does not survive temperatures below about 10°C and typically live in the $10\text{--}25^\circ\text{C}$ range. Our data show that in this temperature range and at reduced humidity, preconditioning has the following salient effects: 1. The thermal response of the PLs is minimized by rigidification of the membranes (slope of the melting curves is always smaller for PPLs than for NPLs, Figs. 5.2B & 5.4B) 2. Trehalose induces a stronger water H-bond network on PPLs than on NPLs $\nu(\text{OH})$ band contours Fig. 5.3A & D).

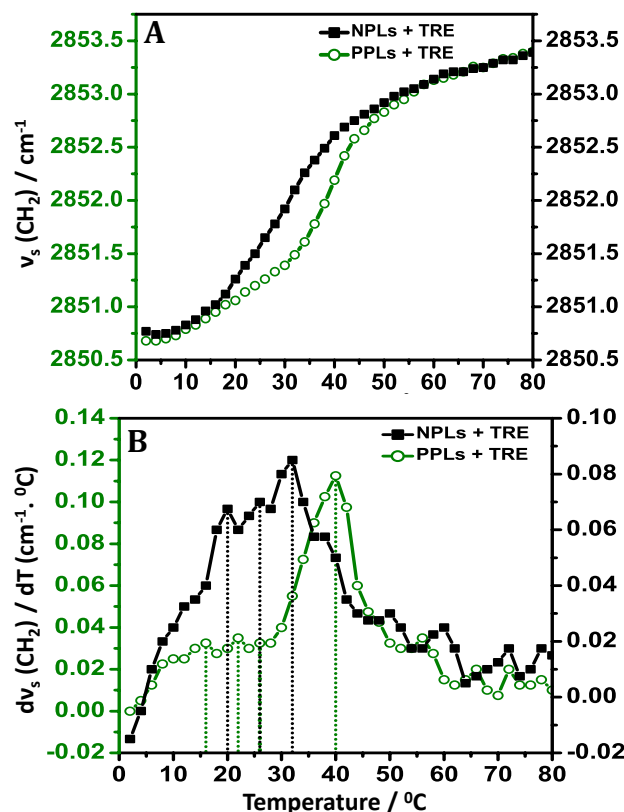


Figure 5.4: Lipid melting curves in the presence of trehalose. The increase in the $\nu_s(\text{CH}_2)$ peak vibrational frequency of PPLs (green circles) and NPLs (black squares) is plotted as a function of temperature (2-80 $^{\circ}\text{C}$) (A). For comparison the left and the right scale is the same in panel A. The first derivatives of the presented curves on (B). The peak maxima (vertical dotted lines) indicate the phase transition temperatures of both NPLs and PPLs. The first derivative plot shows the phase transitions as the regions of greatest slope.

Thermally Induced Changes of H-Bonding in the Sub-Headgroup Region of *C. elegans* PLS

5.3 in the Absence of Trehalose

The carbonyl ester ($\text{C}=\text{O}$) groups, which reside at the interface between the hydrophobic hydrocarbon chains and the more hydrophilic headgroup region, are potential partners for H-bonding interactions with water or sugars.^{131, 145–152} The $\text{C}=\text{O}$ groups give rise to a major peak in the infrared spectra of PLS at around 1738 cm^{-1} , which is sensitive to the polarity of and interactions with the local environment. In the presence of water, the $\nu(\text{C}=\text{O})$ peak is shifted to lower wavenumbers and broadened compared to the less hydrated membranes,^{148, 149, 152} which is due to water-dependent $\text{C}=\text{O} \cdots \text{HO}$ H-bonding interactions.

The preconditioning of *C. elegans* dauer larvae produces striking changes in the C=O region of the infrared spectra. The contour of the ester carbonyl band, is shown at various temperatures in Fig. 5.1C and Fig. 5.1F of NPLs and PPLs, respectively. The $\nu(\text{C=O})$ peak (located at $\sim 1738 \text{ cm}^{-1}$) can be resolved into two sub-components. The higher wavenumber band component ($1740\text{--}1742 \text{ cm}^{-1}$) arises from free C=O groups (C=O_{Free}), while the lower wavenumber component ($\sim 1728 \text{ cm}^{-1}$) originates from C=O groups involved in H-bonding ($\nu\text{C=O}_{\text{H-bonded}}$).^{145,153} In order to improve the visualization of the highly overlapped spectral features, these two components can be quantified by deconvolution of the main $\nu(\text{C=O})$ band.¹¹⁴ Fig. 5.5 and Fig. 5.6 shows the analysis of C=O peaks for NPLs and PPLs, respectively, which was performed at 6, 10 and 70 °C. At 6 °C, where the dehydrated NPLs are in the gel phase (Fig. 5.5A), the absorbance of the C=O vibration resolved into two well-defined band components C=O_{Free} at 1740 cm^{-1} and $\nu\text{C=O}_{\text{H-bonded}}$ at 1728 cm^{-1} . The two band components $\nu\text{C=O}_{\text{Free}}$ and $\nu\text{C=O}_{\text{H-bonded}}$ show temperature-dependent changes of their relative area (A; the area under the fitted peak). It has been found that the relative area (A) of the two band components is proportional to the number of free and H-bonded C=O groups.^{114,154} The fitted peak areas $\text{AC=O}_{\text{H-bonded}}$ and $\text{AC=O}_{\text{Free}}$, are 39.8% and 60.2% for NPLs (Fig. 5.5A). This shows that the dehydrated (free) C=O groups population is larger than the population of C=O groups involved in H-bonding interactions with water.

There was a dramatic increase in $\text{AC=O}_{\text{H-bonded}}$ with increasing the temperature to 10 °C and to the 70 °C in both NPLs (Fig. 5.5B-C) and PPLs (Fig. 5.6B-C). This result suggests an increase in the spacing of the lipids which allows more access of water to the sub-headgroup region. However, it must be emphasized that only in NPLs this sub-headgroup hydration is accompanied by a phase transition of a sub-population of PLs (Fig. 5.2B large and small values of the derivatives of the melting curves for NPLs and PPLs, respectively). This differentiation exemplifies the specificity of FTIR spectroscopy in resolving local structural transitions within PLs and clarifying their linkage to or independence from acyl chain phase transition. In summary, the data show that already at the onset of the physiological temperature range of $T > 10 \text{ }^{\circ}\text{C}$ the sub-headgroup regions of NPLs and PPLs are predominantly hydrated when trehalose

is absent. In the following the influence of trehalose on these hydration properties will be investigated, as PPLs will always coexist with trehalose which is produced during preconditioning.

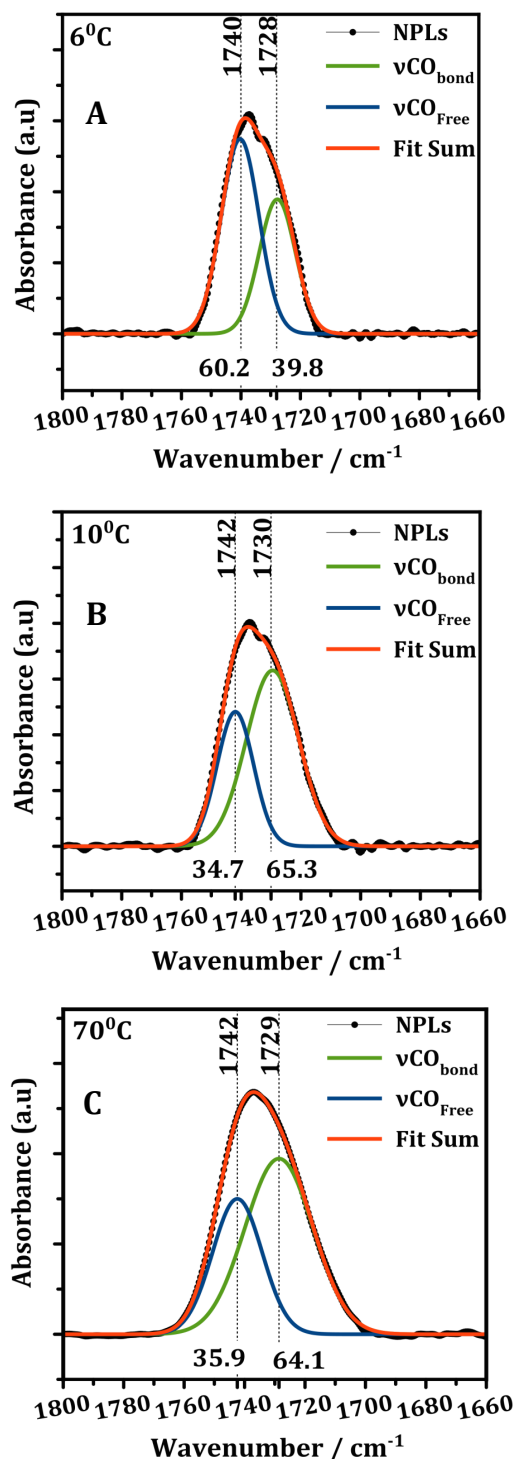


Figure 5.5: Infrared absorption spectra of carbonyl (C=O) stretching modes of NPLs. Panel A: 6 °C (gel phase); Panel B: 10 °C (at the T_m); Panel C: 70 °C (fluid phase). The original bands (black circles) are fitted with 2 Gaussians (blue line, green line), representing two distinct states of hydration: $\nu\text{C}=\text{O}_{\text{Free}}$ (higher wavenumber, dehydrated) and $\nu\text{C}=\text{O}_{\text{H-bonded}}$ (lower wavenumber, hydrated), respectively. The summation of the fit components is shown in red. The relative area (area under the fitted peak) of the C=O band components are given as percentages underneath the respective fitting curve. The correlation coefficients (R^2) for the fitted curves were always 0.999. The vertical dotted lines indicate the positions of the fit components of pure NPLs. All analyzed bands originate from the heating scan.

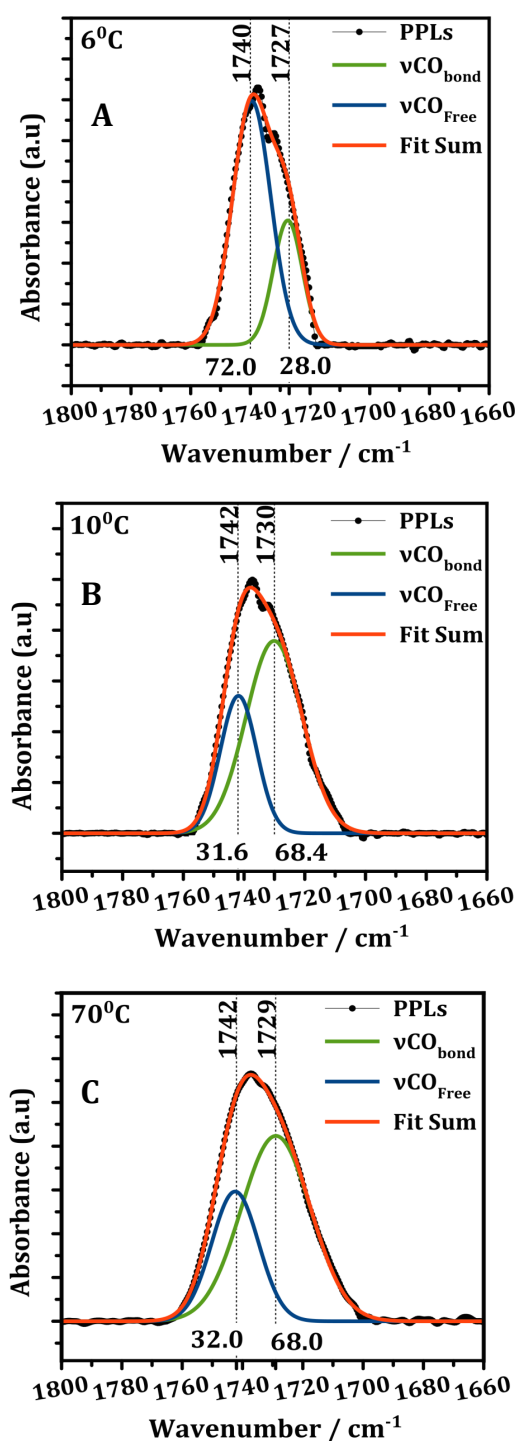


Figure 5.6: Infrared absorption spectra of carbonyl (C=O) stretching modes of PPLs. Panel A: 6 °C (gel phase); Panel B: 10 °C (at the T_m); Panel C: 70 °C (fluid phase). The original bands (black circles) are fitted with 2 Gaussians (blue line, green line), representing two distinct states of hydration: $\nu\text{C}=\text{O}_{\text{Free}}$ (higher wavenumber, dehydrated) and $\nu\text{C}=\text{O}_{\text{H-bonded}}$ (lower wavenumber, hydrated), respectively. The summation of the fit components is shown in red. The relative area (area under the fitted peak) of the C=O band components are given as percentages underneath the respective fitting curve. The correlation coefficients (R^2) for the fitted curves were always 0.999. The vertical dotted lines indicate the positions of the fit components of pure PPLs. All analyzed bands originate from the heating scan.

Thermally Induced Changes of H-Bonding in the Sub-Headgroup Region of *C. elegans* PLS

5.4 in the Presence of Trehalose

In addition to the data concerning the influence of trehalose on the hydration-dependent (Chapter 4.3) and the temperature-dependent behavior of PL acyl chain order (Chapter 5.2), the current section addresses temperature-dependent interactions of trehalose in the lipid interfacial region in the dehydration state. Such interactions were again investigated at the level of the carbonyl groups using the above introduced band deconvolution. Comparing Fig. 5.7 and Fig. 5.8 for NPLs and PPLs, respectively, it is obvious that the two band components $\nu\text{C}=\text{O}_{\text{Free}}$ and $\nu\text{C}=\text{O}_{\text{H-bonded}}$ differ in wavenumber, relative area (A) and temperature sensitivity. Whereas in the trehalose-containing NPLs exhibit a higher fraction of H-bonded over free C=O groups at all temperatures, the sub-headgroup region sampled by the ester carbonyls in PPLs provides clearly less H-bonds to the C=O groups as evident from the smaller integral intensity of the low-wavenumber component (green) in relation to the high frequency component (blue). In fact, the ratio $\nu\text{C}=\text{O}_{\text{H-bonded}} : \nu\text{C}=\text{O}_{\text{Free}}$ in NPLs (63%: 37%) is inverted in PPLs (36%: 64%). Only at 70 °C the same equilibrium ~6:4 between $\nu\text{C}=\text{O}_{\text{H-bonded}}$ and $\nu\text{C}=\text{O}_{\text{Free}}$ is reached (table 5.1). Of course it cannot be stated whether the H-bonded C=O groups are linked to water, trehalose or other headgroups. However, it is clear that trehalose acts quite differently on PPLs and NPLs. In PPLs, the ester carbonyls appear still dehydrated at 10 °C (Fig. 5.8B versus Fig. 5.7B) whereas NPLs have already reached an equilibrium between $\text{C}=\text{O}_{\text{H-bonded}}$ and $\text{C}=\text{O}_{\text{Free}}$ that does not further increase upon heating to 70 °C (Fig. 5.7B and C). Although, trehalose appears to dehydrate the sub-headgroup specifically in PPLs but not in NPLs, the remaining H-bonds are stronger as is evident from a comparison of the peak frequencies of the $\nu\text{C}=\text{O}_{\text{H-bonded}}$. PPLs show the H-bonded C=O stretch at 1729 cm⁻¹ which is 5 cm⁻¹ lower than in NPLS (Figs. 5.8B & 5.7B). This indicates that different H-bond geometries are established in the two PLs extracts.

In summary, the altered headgroup composition in PC-rich NPLs and PC-poor PPLs

leads to strikingly opposing patterns of trehalose carbonyl interactions particularly in the physiological range of 10-20 °C exemplified here with the spectra taken at 10 °C.

	6 °C		10 °C		70 °C	
Samples	ACO _{Bond}	ACO _{Free}	ACO _{Bond}	ACO _{Free}	ACO _{Bond}	ACO _{Free}
NPLs	39.8	60.2	65.3	34.7	64.1	35.9
PPLs	28.0	72.0	68.4	31.6	68.0	32.0
NPLs+TRE	63.4	36.6	63.5	36.5	58.1	41.9
PPLs+TRE	36.0	64.0	33.4	66.6	59.4	40.6

Table 5.1: The relative areas ($AC=O_{Free}$ and $AC=O_{H-bonded}$) of H-bonded and free C=O groups of the the two component fitted peaks of the carbonyl (C=O) stretching band shown in NPLs and PPLs in the absence and in the presence of trehalose (TRE). The data are acquired at 6 °C (gel phase), 10 °C (T_m) and 70 °C (fluid phase). The relative area (A) is significance indicator proportional to the number of free and H-bonded C=O groups.

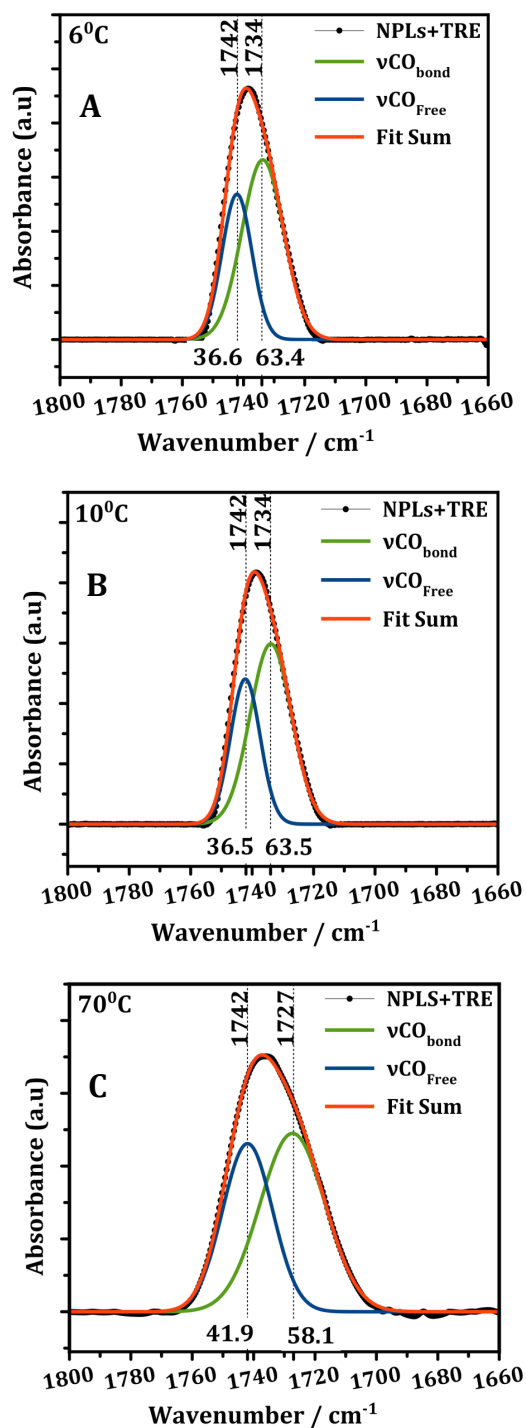


Figure 5.7: Infrared absorption spectra of Carbonyl (C=O) stretching vibrational bands of NPLs in the presence of trehalose (TRE). Panel A: 6 °C (gel phase); Panel B: 10 °C (at the T_m); Panel C: 70 °C (fluid phase). The original bands (black circles) are fitted with 2 Gaussians (blue line, green line), representing two distinct states of hydration: $\nu\text{C}=\text{O}_{\text{Free}}$ (higher wavenumber, dehydrated) and $\nu\text{C}=\text{O}_{\text{H-bonded}}$ (lower wavenumber, hydrated), respectively. The summation of the fit components is shown in red. The relative area (area under the fitted peak) of the C=O band components are given as percentages underneath the respective fitting curve. The correlation coefficients (R^2) for the fitted curves were always 0.999. The vertical dotted lines indicate the positions of the fit components of NPLs containing trehalose. All analyzed bands originate from the heating scan.

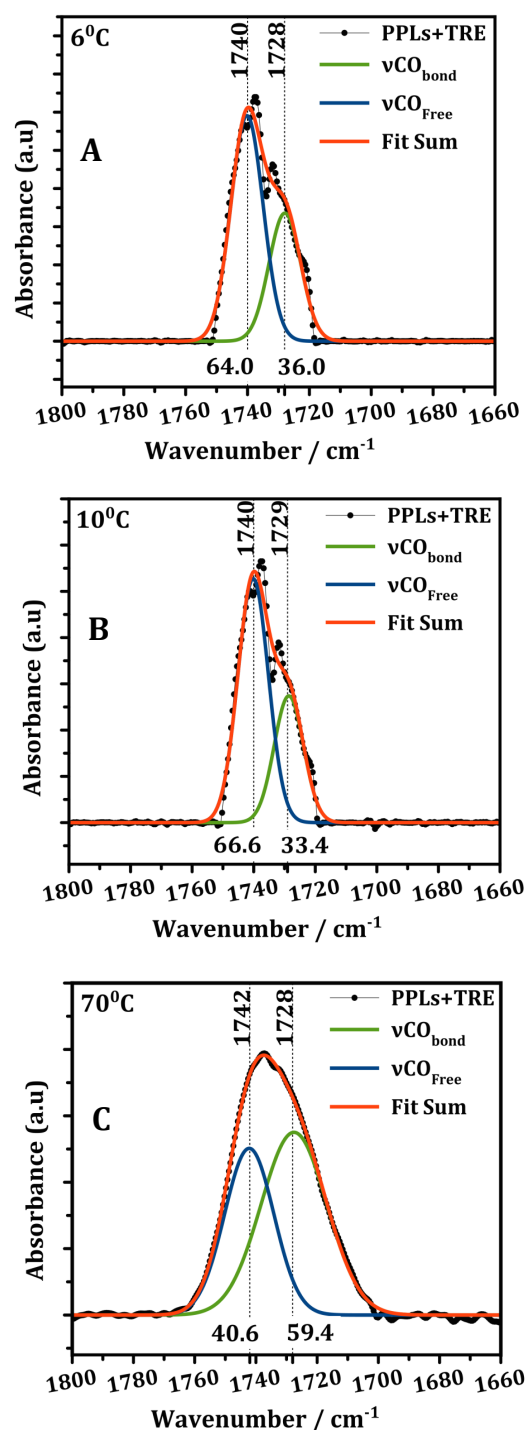


Figure 5.8: Infrared absorption spectra of Carbonyl (C=O) stretching vibrational bands of PPLs in the presence of trehalose (TRE). Panel A: 6 °C (gel phase); Panel B: 10 °C (at the T_m); Panel C: 70 °C (fluid phase). The original bands (black circles) are fitted with 2 Gaussians (blue line, green line), representing two distinct states of hydration: $\nu\text{C=O}_{\text{Free}}$ (higher wavenumber, dehydrated) and $\nu\text{C=O}_{\text{H-bonded}}$ (lower wavenumber, hydrated), respectively. The summation of the fit components is shown in red. The relative area (area under the fitted peak) of the C=O band components are given as percentages underneath the respective fitting curve. The correlation coefficients (R^2) for the fitted curves were always 0.999. The vertical dotted lines indicate the positions of the fit components of PPLs containing trehalose. All analyzed bands originate from the heating scan.

5.5 Discussion

In this chapter, temperature-dependent ATR-FTIR spectroscopy was used to determine the thermo-tropic phase behavior and the molecular interactions of *C. elegans* dehydrated PLs and trehalose based on the analysis of acyl chain and sub-headgroup vibrations provided by the CH₂ and C=O stretching modes, respectively.¹⁴² The temperature-induced transition from gel to liquid crystalline phase is clearly visible by the increase in frequency of $\nu_s(\text{CH}_2)$ of both NPLs and PPLs. But, the latter show a more cooperative behavior with a T_m at 36 °C, whereas NPLs exhibit multiple transitions at lower temperatures. These differences have to be attributed to the different headgroup composition particularly the reduced PC content in PPLs (see TLC radiogram of ¹⁴C-labeled PLs shown in Fig. 4.3A).

The salient result of this set of experiments is the entirely different H-bonding pattern of the trehalose-containing PL extracts. PPLs show stronger water H-bond networks than NPLs but exhibit less H-bonding in the sub-headgroup region. This suggests that, at a reduced humidity of 75% RH, trehalose organizes surface bound H-bond networks that dehydrate the sub-headgroup region of PPLs. In contrast, trehalose has little influence on the sub-headgroup hydration of NPLs. In addition to these different H-bonding properties, PPLs exhibit weaker thermally induced structural transitions in their acyl chains than NPLs in the physiologically relevant temperature range.

5.6 Conclusions

The preservation of cell membrane structure by the synthesis of trehalose and the reduction of the PC content in membrane lipids of preconditioned *C. elegans* dauer larvae correlates with the H-bond networks that are formed in the presence of trehalose in the lipid headgroup and sub-headgroup regions. The trehalose-induced relocation of water from the sub-headgroup region to the lipid surface in PPLs appears to be a crucial mechanism. It supports our suggestion that trehalose does not permanently reside in the sub-headgroup region of PPLs, but inserts there only under the influence of an increase of hydration water. This water-driven insertion would contribute to the

fast gain of lateral extension during quick rehydration of the larvae. In physical terms, the result of preconditioning can be expressed in the following: at reduced humidity PPLs show minimal structural responses to temperature changes but react maximally to hydration changes. The adaptation to drought, which is accomplished to a significant part by the reduction of the PC content, thus relies on reducing thermo-tropic and enhancing lyotropic phase transitions.

Temperature-dependent FTIR analysis has proven to be a very useful method to study conformation and stability of lipid molecules in the dry cellular environment of anhydrobiotic organisms. A comprehensive characterization of dehydrated dauer larvae membrane PLs have been provided, which will help to evaluate the molecular mechanisms of trehalose and the conformational changes of PLs upon preconditioning that may be involved in the cellular desiccation tolerance of *C.elegans*. Particularly, the detailed temperature-dependent FTIR analysis of the interfacial and headgroup regions of *C. elegans* membrane PLs will enable a detailed understanding of the key role of such protective trehalose molecules that may play crucial roles in anhydrobiosis²⁰ that still consider one of the most mysterious phenomena in biology.

FLUORESCENCE SPECTROSCOPY STUDIES OF THE GEL-TO LIQUID TRANSITION IN PLS FROM *C. elegans* DAUER LARVAE

Contents

6.1	Use of LAURDAN Fluorescence Intensity to Monitor the Effect of Preconditioning on Membrane Fluidity & PLs Order	102
6.2	LAURDAN reveals Different Fluidity & Hydration in the Presence of Trehalose in the Gel & Liquid Phase of PLs Bilayer	106
6.3	Temperature Dependence of the Generalized Polarization Measured by LAURDAN-loaded PL Vesicles in Response to Preconditioning & Trehalose Binding	109
6.4	Discussion	111
6.5	Conclusions	112

The penetration of water into the hydrophobic interior leads to polarity and hydration profiles across lipid membranes, which are two fundamental physiochemical characteristics in the maintenance of membrane architecture. This study is an attempt to evaluate the hydration and the polarity properties of dauer larvae derived PL bilayers by using LAURDAN as a polarity-sensitive fluorescent probe. Importantly, it has been reported that LAURDAN presents a large excited state dipole moment. This results in its ability to report the extent of water penetration into the bilayer surface due to the dipolar relaxation effect.¹⁵⁵ Moreover, LAURDAN fluorescence properties provide a unique possibility to study lipid phase behavior because of the different excitation and emission spectra of this fluorescent probe in the gel and in the liquid-crystalline phase in biological membranes.^{156,157} Hence, LAURDAN has been extensively used in membrane studies, because the water penetration has been correlated with the lipid packing and membrane fluidity.¹⁵⁶ In addition, as the polarity and hydration control many process in the membrane, the study of these properties is of peculiar importance for understanding the mechanisms of bio-membrane structure and can thus help to identify molecular mechanisms underlying desiccation tolerance of *C. elegans* dauer larvae. Using steady-state excitation and emission spectral properties to determine the generalized polarization (GP) value(see chapter 3.8 for definition), an estimate of the effect of preconditioning and trehalose binding on the bilayer hydration at the hydrophobic-hydrophilic interface can be obtained.

Use of LAURDAN Fluorescence Intensity to Monitor the Effect of Preconditioning on Me-

6.1 mbbrane Fluidity & PLs Order

In this study, we have performed experiments on NPLs and PPLs vesicles in suspension at different temperatures in the presence of the amphiphilic fluorescence probe LAURDAN reaching from below to above the expected phase transition temperature, where gel and liquid-crystalline phases are likely to be maximal. Here, we attempted to detect differences in PL order and membrane fluidity between NPLs and PPLs by examining the

temperature dependence of LAURDAN excitation and emission spectra. Fluorescence excitation and emission spectra are shown in Figure 6.1 for LAURDAN in NPLs (black) and PPLs (green) at 2 °C (gel phase; panel A & B), 25 °C (during phase coexistence; panel C & D) and 65 °C (liquid-crystalline phase; panel E & F). The LAURDAN excitation spectrum in both NPLs and PPLs in the gel phase (Fig. 6.1A), shows two maxima at 359 nm and 382 nm.¹⁵⁸ However, the excitation spectrum of PPLs exhibits a higher intensity in the excitation band at longer wavelength compared with NPLs. It has been attributed to the stabilization of the probe ground-state L_α conformation, due to polar molecules (water, glycerol OH groups) being oriented around the LAURDAN dipole, i.e., already relaxed.⁹¹ Evidently, the increase of the red excitation band in PPLs suggests an increase of the water dipole alignment around the naphthalene moiety in NPLs, whereas the dipolar relaxation phenomenon in the excited state is negligible.⁹¹ In other words, preconditioning allows water penetrating into sub-headgroup region in the gel phase but shows little mobility (no solvent relaxation in the excited state of LAURDAN). Therefore, little differences are observed in the LAURDAN emission between NPLs and PPLs vesicles as shown in Figure 6.1B because NPLs do not show solvent relaxation.

During the phase transition, we can observe major changes in the excitation (Fig. 6.1C) and to a lesser extent in the emission (Fig. 6.1D) band shape in both NPLs and PPLs. The excitation spectra of both PLs extracts exhibit a blue shift of the short wavelength excitation peak to 351 nm and a strong decrease of the excitation at 382 nm. Furthermore, a broad shoulder is observed at about 390 nm. Indeed, these results are in agreement with what was reported previously,⁹¹ that a decrease in polarity induces a blue shift of excitation spectra and a clear disappearance of the longer wavelength excitation band. The much stronger effect on the excitation spectra as compared to the emission confirms the expected larger heterogeneity of water alignments around the ground state fluorophores at the phase transition temperature. However, the mobility of these disordered waters is nevertheless still very low on the time scale of the excited state lifetime (ns). This follows from the lack of a solvent relaxation-related red shift in the emission. Only a marginal increase at 480 nm is visible.

In the liquid-crystalline phase at 65 °C, the longer wavelength excitation band of

both PLs is blue-shifted to 378 nm (Fig. 6.1E). Interestingly, the LAURDAN emission (Fig. 6.1F) is red-shifted to 436 nm and 438 nm in NPLs and PPLs as compared to the emission spectra observed in the gel phase. This broadening of the LAURDAN emission at longer wavelengths is more pronounced in PPLs than in NPLs. These results show that preconditioning renders the interfacial region of the PL bilayers, which is probed by LAURDAN, more mobile for the reorientation of water molecules ,i.e., preconditioning increases the fluidity in the PL bilayers.

In summary, our observations can help to clarify, at a molecular level, the importance of preconditioning in regulating the desiccation state by providing more freedom to the water molecules to access the interfacial region of PLs bilayer during the desiccation of *C. elegans* dauer larva. Remarkably, these observations confirm our former findings on the critical role of preconditioning on the organization and dynamics of lipid bilayers (see chapter 4 & chapter 5).

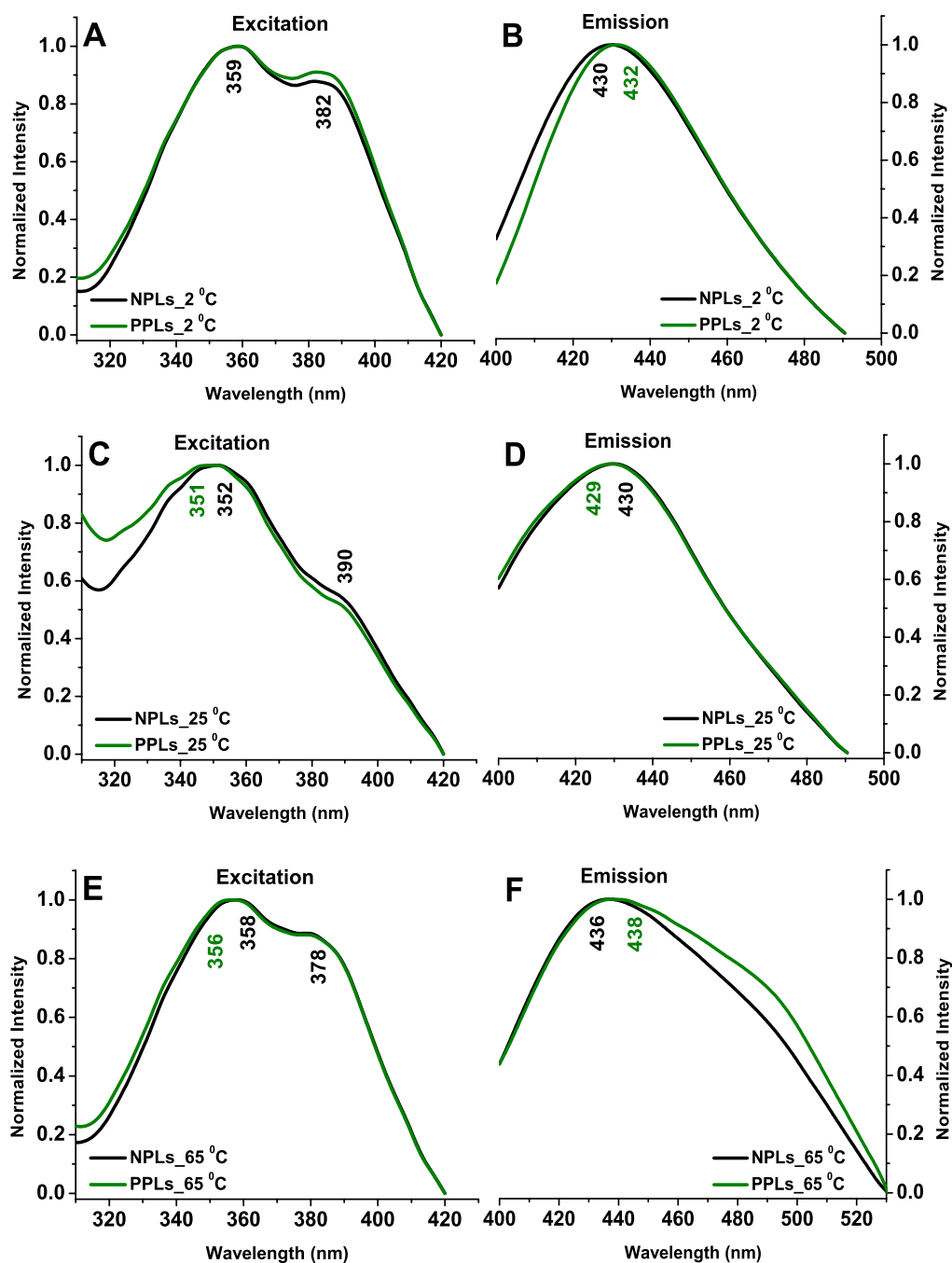


Figure 6.1: Temperature effect on the fluorescence excitation and emission spectra of LAURDAN in LUVs composed of NPLs (black) and PPLs (green) prepared in phosphate buffer (10 mM, pH 7.4). The measurements were performed at 2 °C (panel A & B), 25 °C (panel C & D) and 65 °C (panel E & F). The total lipid concentration was 0.3 mM with the ratio of LAURDAN probe to lipid (1:1000). Fluorescence spectra were normalized to their maximum. The excitation spectra were measured at an emission wavelength of 440 nm, and the emission spectra were measured with an excitation wavelength of 340 nm.

LAURDAN reveals Different Fluidity & Hy- dration in the Presence of Trehalose in the

6.2 Gel & Liquid Phase of PLs Bilayer

The addition of trehalose to PLs produces modifications of both the excitation and emission spectra of LAURDAN probe. The type and amount of these changes depend on the temperature and accordingly depend on the PL phase state. The experiments shown in Figure 6.1 were repeated with vesicles in the presence of 6 mM trehalose. In the gel phase of PPL vesicles at 2 °C, the addition of trehalose causes a small decrease of the 382 nm excitation band, and a slight blue shift of both the excitation (Fig. 6.2A) and emission spectrum (Fig. 6.2B) and a broadening of the emission band in comparison with pure PPLs (Fig. 6.1A & Fig. 6.1B, respectively). Virtually no effect of trehalose is seen with NPLs. Thus, PPLs exhibit a unique role in responding to trehalose already in the gel phase, probably by allowing trehalose to replace some of the water molecules surrounding the LAURDAN naphthalene moiety. This agrees with the larger affinity of trehalose for PPLs than NPLs as detected by monolayer studies; see chapter 4.2. It probably originates in a more efficient trehalose insertion into the PPL bilayers which may be of key importance for trehalose-dependent desiccation tolerance. This is in full agreement with the previous findings (see chapter 4.4).

The ensemble of the data shows that trehalose modulates the phase behavior of NPLs and PPLs differently. In the gel phase, trehalose reduces the initially higher polarity (382 nm excitation band) of the sub-headgroup region in PPLs to the same degree as in NPLs in line with replacement of water. Trehalose inserts into the gel phase of PPLs but not NPLs as shown here at full hydration at 2 °C. Correspondingly, the gel phase formed at higher temperatures (10-25 °C) by drying may as well be more responsive to trehalose than the corresponding phase of NPLs. Thus, preconditioning would be a mechanism to allow trehalose penetrating into the gel phase of dauer larvae membranes during the gel phase formation upon drying.

Due to the relatively little effects on the emission spectra as compared to the excitation spectra, the LAURDAN fluorescence is not easily interpreted in the expected picture of

solvent relaxation in the excited state. Instead, the ground state properties, as reflected by the excitation spectra, appear to be more sensitive to differentiate the physical properties of NPLs and PPLs. This is again seen at the phase transition (at 25 °C), where the addition of trehalose induces an increase of the shoulder centered at about 390 nm in PPLs. Thereby, it matches the intensity seen with NPLs and trehalose, whereas in the absence of trehalose the 390 nm excitation is less intense in PPLs (compare Fig. 6.1C & 6.2C). Again, little effects are seen in the emission spectra, indicating that there is no effect on water mobility. The only differences in response to trehalose are thus the stronger increase in polarity in the LAURDAN environment in PPLs. We assign this to intermolecular H-bonds formed preferentially in PPLs between trehalose OH and LAURDAN, rather than H-bonds with water molecules in accordance with our previous results (Chapter 4 and chapter 5).

Unexpectedly, a remarkable influence of preconditioning is also seen in the liquid-crystalline phase in the presence of trehalose. In this case it is obvious from the emission spectra and thus interpretable in terms of solvent relaxation, i.e., water mobility. The larger emission from PPLs than NPLs at long wavelengths (Fig. 6.1F) is clearly reduced by trehalose (Fig. 6.2F) and a decrease of the excitation band at 370-380 nm is observed (Fig. 6.2E). These features show that trehalose reduces water mobility and polarity in the sub-headgroup region of PPLs. Again, the effect of trehalose on NPLs is much smaller also in the liquid crystalline phase.

In this part of the study, our findings have provided clear evidence that trehalose interacts differently with hydrophobic-hydrophilic interface of the bilayer in NPLs and PPLs, which are in agreement with what have been demonstrated in the temperature-dependent FTIR measurements shown in Fig. 5.7 and Fig. 5.8. Strikingly, in the presence of trehalose a bimodal distribution of LAURDAN states is suggested by the more distinct separation of two emission bands as compared to the less structured broad emission from LAURDAN in lipid vesicles prepared from non-preconditioned worms. The bimodal distribution parallels the time resolved infrared results showing two distinct water populations in the presence of trehalose.

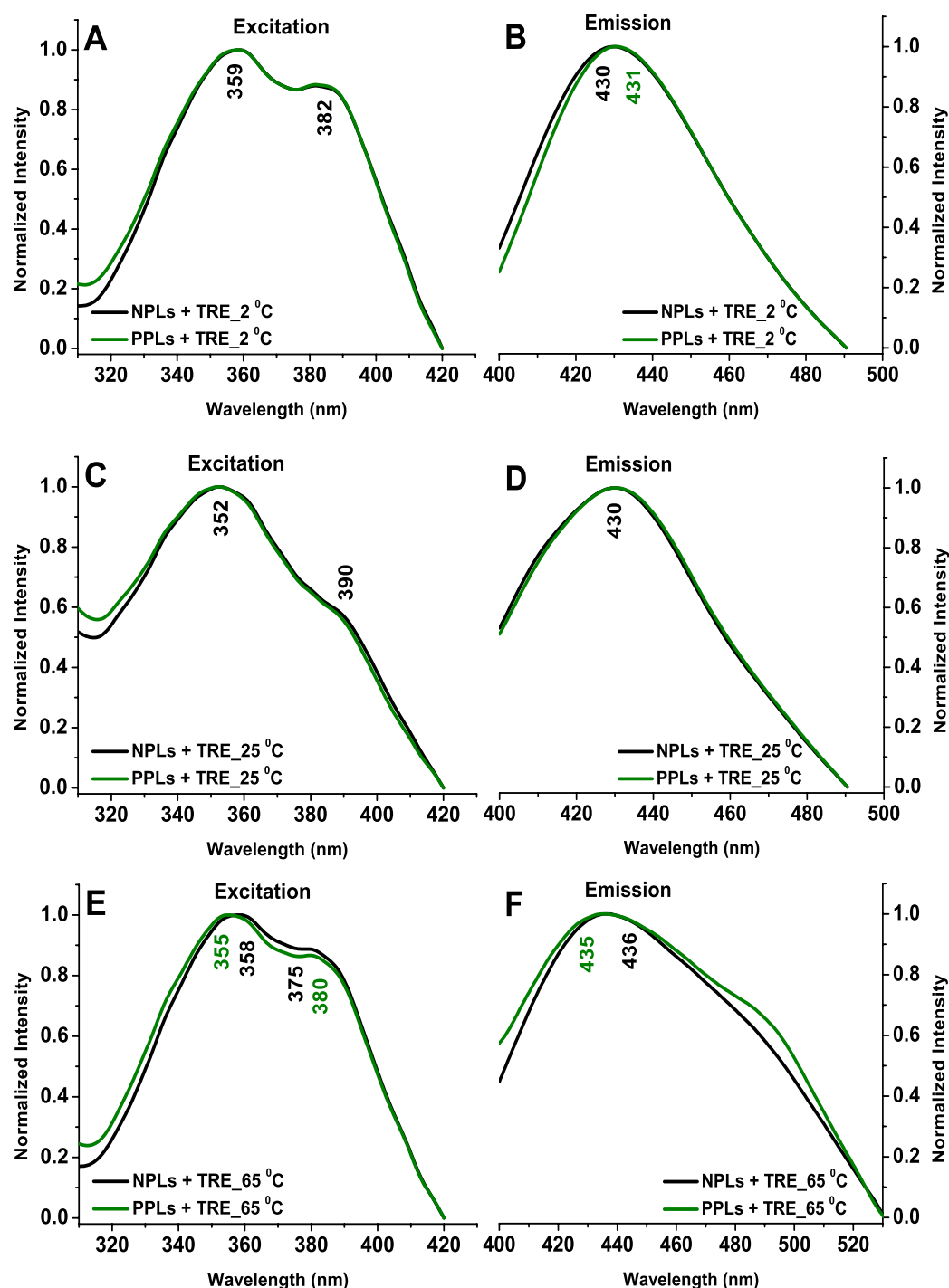


Figure 6.2: Temperature effect on the fluorescence excitation and emission spectra of LAURDAN in LUVs composed of NPLs (black) and PPLs (green) in the presence of trehalose, which was prepared in phosphate buffer (10 mM, pH 7.4). The measurements were performed at 2 °C (panel A & B), 25 °C (panel C & D) and 65 °C (panel E & F). The total lipid concentration was 0.3 mM with the ratio of trehalose to lipid (20:1). Fluorescence spectra were normalized to their maximum. The excitation spectra were measured at an emission wavelength of 440 nm, and the emission spectra were measured with an excitation wavelength of 340 nm.

Temperature Dependence of the Generalized Polarization Measured by LAURDAN-loaded PL Vesicles in Response to Preconditioning &

6.3 Trehalose Binding

The generalized polarization (GP) Function allows assessing polarity in the sub-headgroup region of PLs with high sensitivity.¹⁵⁹ The GP is a numeric value related to the shape of the LAURDAN emission band. It quantitatively relates the emission intensities at 440 and 490 nm (see chapter 3.8).

We calculated the GP values using an excitation wavelength of 340 nm and emission wavelengths of 440 and 490 nm versus temperature. Figure 6.3 displays the temperature dependence of LAURDAN GP values for NPLs and PPLs vesicles. As, expected, the transition of the PL from gel (Fig. 6.1A & B) to liquid-crystalline states (Fig. 6.1E & F) was accompanied by a decrease of GP as the following: (0.40 \rightarrow 0.33 \rightarrow 0.15) for NPLs and (0.42 \rightarrow 0.32 \rightarrow 0.09) for PPLs. Our results are in line with previous studies carried out on model lipids⁹¹ showing that LAURDAN molecules in PL bilayers in the gel phase will be mainly excited in the long wavelength band and will emit with a blue spectrum, i.e., with a high GP value. While, in the case of liquid-crystalline phase, LAURDAN will emit with a red spectrum, i.e., with a low GP value. The lower GP value in PPLs, suggests a higher membrane hydration and less order in the sub-headgroup region in comparison with NPLs. This may be explained by the enhancement of the water penetration upon preconditioning, which increasing accordingly the fluidity in the non-polar core region of the bilayer in order to keep the membrane intact during transition phases.

In contrast to the qualitative description of spectral changes given in chapter 6.2, the GP values clearly show that PPLs exhibit a much larger change in the sub-headgroup polarity with temperature than NPLs. The variations in membrane water content that caused shifts in the LAURDAN emission spectrum are also quantified by calculating the GP in the presence of trehalose.

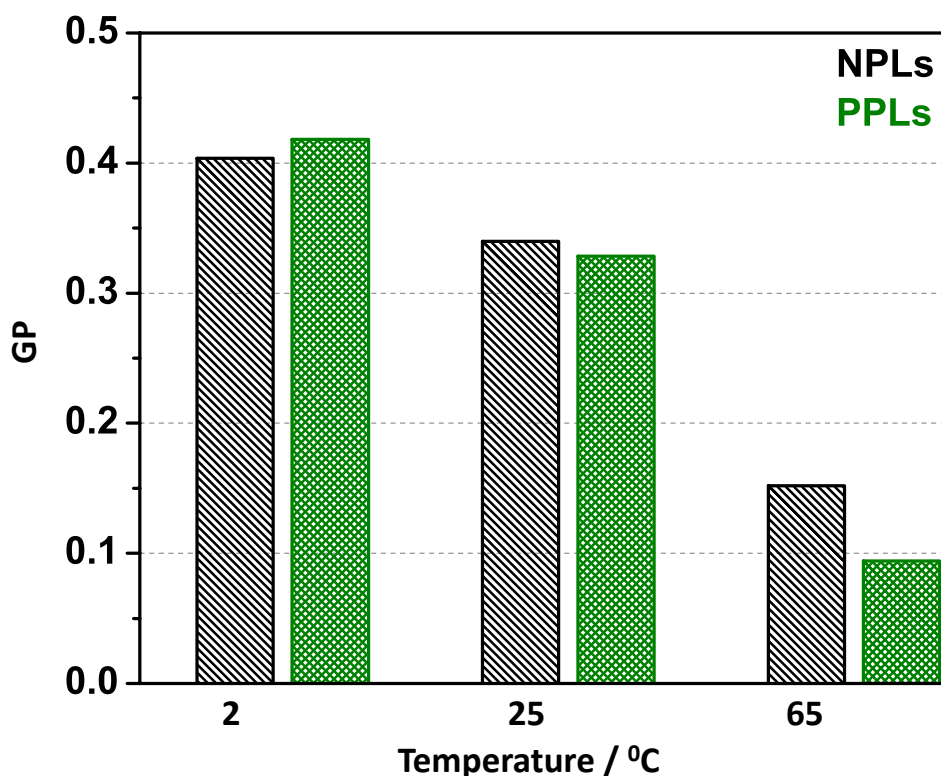


Figure 6.3: Temperature dependence of LAURDAN GP values of NPLs (black) and PPLs (green) in different phases, at the indicated temperatures in Fig. 6.1. The GP values were calculated by $GP = (F_{440} - F_{490}) / (F_{440} + F_{490})$, using emission wavelengths at 440 and 490 nm as explained in chapter 3.8.

Fig. 6.4 illustrates the effect of trehalose on the LAURDAN GP values as a function of temperature. With the above definitions, high GP values are measured in the gel, while low GP values are measured in the liquid- crystalline phase. Only minor effects of trehalose were observed i.e., the differences in GP values between high and low temperatures were the same in the presence of trehalose compared with Pure PLs at the same conditions. The determined GP values decreased as the following: $(0.40 \rightarrow 0.36 \rightarrow 0.16)$ for NPLs and $(0.42 \rightarrow 0.35 \rightarrow 0.1)$ for PPLs, during the transition from gel phase to the liquid-crystalline phases. Again, the polarization in PPLs is more sensitive to temperature than in NPLs. Otherwise, GP value does not resolve further differences between the two PL preparations. The only relevant trehalose effect detected by this analysis is the larger GP value in the phase transition at 25 °C for both, NPLs and PPLs. The more specific response of PPLs to trehalose over NPLs is thus not present in the emission but rather in the excitation spectra as described in the previous chapter.

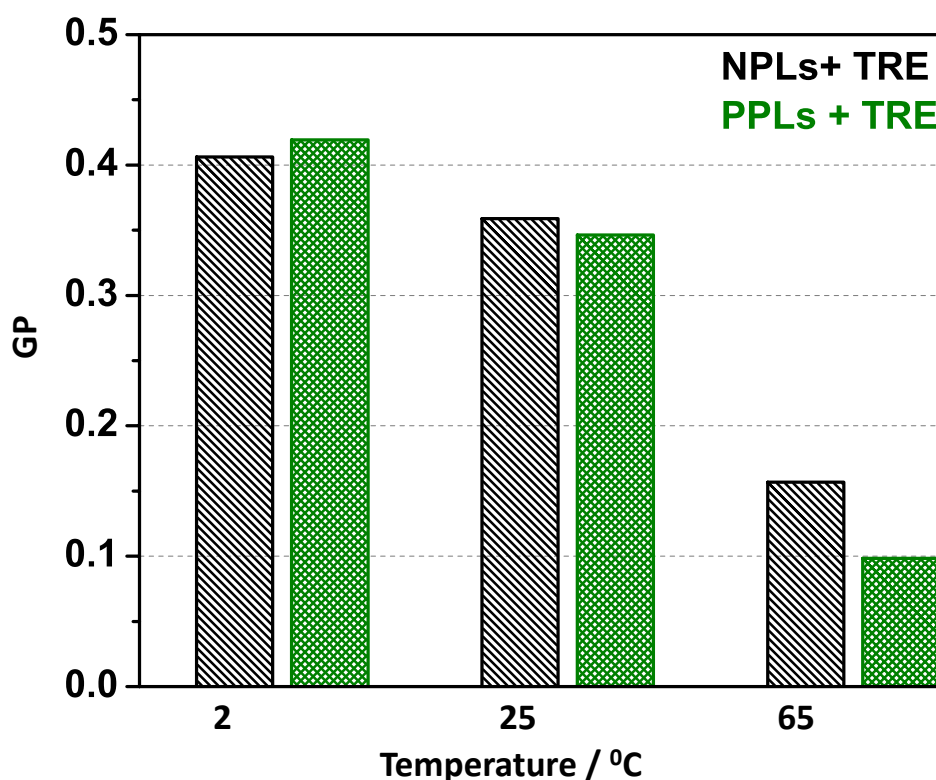


Figure 6.4: Temperature dependence of LAURDAN GP Values in the presence of trehalose of NPLs (black) and PPLs (green) in different phases, at the indicated temperatures in Fig. 6.2. The GP values were calculated by $GP = (F_{440} - F_{490}) / (F_{440} + F_{490})$, using emission wavelengths at 440 and 490 nm as explained in chapter 3.8.

6.4 Discussion

The LAURDAN fluorescence is strongly influenced by the molecular dynamics of water molecules and by the polarity in the vicinity of LAURDAN moiety. The shift of the emission spectrum has been attributed to dipolar relaxation of water molecules surrounding the fluorescent naphthalene moiety at the level of the PL glycerol backbone.^{91, 160} If the rate of relaxation is very small, such as in the PL gel phases, the emission spectral shift is small. In the liquid-crystalline phase, relaxation processes can occur at a much faster rate, and this process gives rise to a large emission red shift.¹⁵⁸

The red spectral shift has been found to be independent of the polar head residue and of its charge. Instead, this shift depends only on the phase state of the bilayer.⁹¹ Thus, the origin of the dipolar relaxation observed in PLs has been attributed to a few water molecules present in the bilayer at the level of the glycerol backbone, where

the fluorescent moiety of LAURDAN resides as schematically shown in Figure 6.5. In the tightly packed gel phase PL bilayers (Fig. 6.5A), red shift of the emission cannot be observed due to the relative low accessibility of water molecules where LAURDAN moiety resides. Instead, the continuous red shift of the emission observed in the liquid-crystalline phase with increasing temperature is due to the increased concentration of water in the bilayer (Fig. 6.5B) and to its increased fluidity.

Our observations revealed that LAURDAN steady-state parameters in NPLs and PPLs do not change much with trehalose in the gel phase because the emission spectra from which the GP values are calculated are little effected. However, the excitation spectra show that trehalose in the gel phase (2 °C) decreases polarity (reduction of the 382 nm band in Fig. 6.2A vs. 6.1A), whereas at the phase transition (25 °C) trehalose increases the polarity in the sub-headgroup region (increase of the 382 nm band in Fig. 6.2C vs. 6.1C), it appears that trehalose dehydrates the gel phase but hydrates the PPLs at 25 °C. We think that this may indicate the dynamic behavior of trehalose: it resides at the headgroup region in the ordered phase, attracting water out of the sub-headgroup region. With loosening of the PL packing at 25 °C, trehalose inserts deeper into the sub-headgroup region and increases polarity. The data show that the nature of the headgroup is crucial for its interaction with trehalose and there is no general mechanism by which the sugar affects lipidic phase transitions. The intercalation into a phosphatidylethanolamine-rich membrane appears to be unique. In this case, neither the phase transition temperature nor its width is affected by the protective sugar, whereas strong effects on these parameters were observed with other model lipids. With respect to membrane preservation, the remodeling of the PL headgroup during preparation for desiccation tolerance indicates that the protective function of trehalose requires specific PL headgroups. Strikingly, the outlook (chapter 7) addresses and supports this notion, because trehalose affects model lipids that differ only in headgroup composition differently.

6.5 Conclusions

The steady-state excitation and emission spectra of LAURDAN in vesicles prepared from NPLs and PPLs have different maxima and shape in dependence of the PL phase.

The latter was defined here by temperature at fully hydration, rather than by humidity as in our FTIR studies.

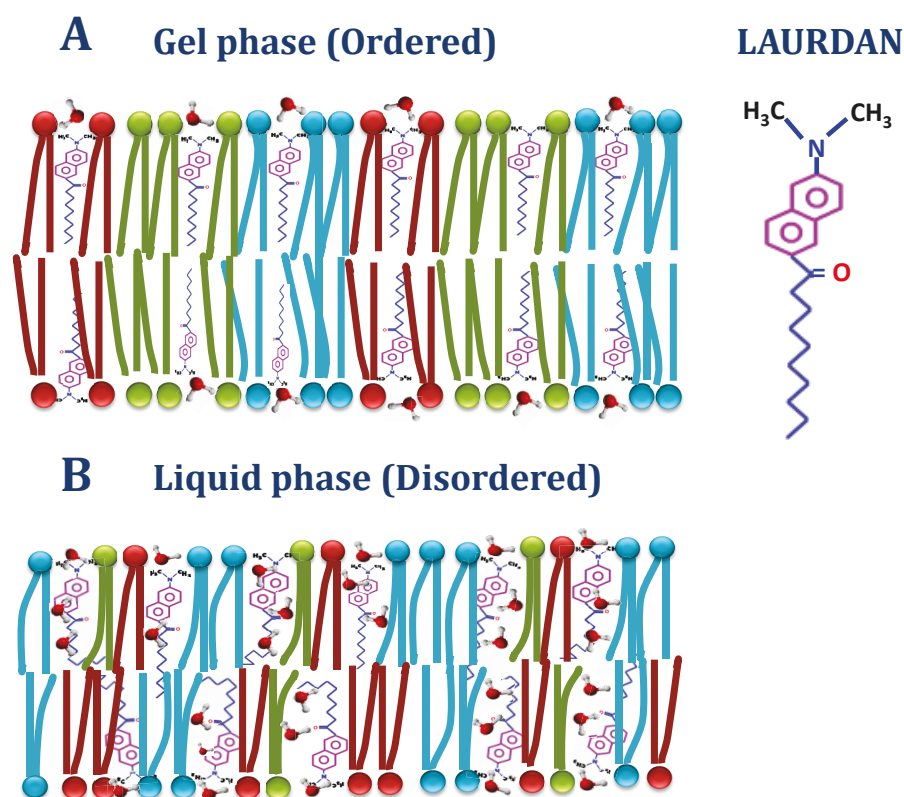


Figure 6.5: Schematic representation of LAURDAN Fluorescent Probe (naphthalene moiety: violet, lauric acid tail: blue) location in the PLs bilayer. LAURDAN detects the polarity of its environment and thus water penetration into the hydrophobic-hydrophilic interfacial region in the bilayer. Its orientation and water content varies in gel phase (ordered, panel A) and liquid phase (disordered, panel B) of PLs bilayer. In the gel phase, lipids have a more restricted motion (so few water molecules sensed by LAURDAN probe). But, in the liquid phase, increased of water accessibility is observed and accordingly increasing of membrane fluidity.

At low humidity the gel phase predominates. Therefore, the data obtained with fully hydrated vesicle suspensions at 2 °C are nevertheless relevant. Despite the unphysiological temperature, they help to elucidate the role of preconditioning for trehalose PL interactions in the gel phase in general. The most striking observation made with LAURDAN excitation spectra is the change from a dehydrating effect of trehalose on PPLs in the gel phase to a hydrating effect at 25 °C. We have suggested that this is due to a change in the topology of trehalose within the PL bilayer. Transferring our results from the fully hydrated vesicle state to the situation at reduced humidity, the model suggests that trehalose inserts preferentially into PPLs during the lyotropic

transition. It resides closely to the headgroups at 75% RH but inserts deeper into the sub-headgroup region when hydration softens the PL packing. Such a model is fully consistent with the the unaltered C=O stretching mode of PLs at 75% RH in the presence of trehalose. Obviously, there is no increased H-bonding to the esters induced by trehalose. Only after hydration beyond 75% RH a strong H-bond was observed. This “sliding in” of trehalose appears to be accompanied by a stronger sub-headgroup hydration in PPLs, than in NPLs.

Based on our results of the native *C. elegans* derived PLs, which have shown that the reduction in PC is probably modulating the effect of trehalose on lyotropic and thermo-tropic transitions. The proposed PC/PE-dependent lipid trehalose interaction should be visible also in other lipids if it is dominated by the nature of the headgroup rather than the nature of the acyl chains. For this purpose, Differential Scanning Calorimetry (DSC) has been used to determine the phase transition temperature (T_m) of different model lipids as a function of headgroup structure and trehalose (more details in chapter 3.9). DSC curves of the fully hydrated DMPA, DMPC, DMPE and DMPG in absence and presence of trehalose are shown in Figure 7.1. Aqueous dispersion of each PL shows endothermic peaks that correspond to an energetic main phase transition from gel to liquid crystalline phase at about T_m DMPA = 52 °C, T_m DMPC = 23 °C, T_m DMPE = 48.6 °C and T_m DMPG = 39 °C.

In this context it is fascinating that the DMPE T_m is not affected by trehalose, whereas it is affected with DMPC, DMPA, DMPG. This would very strongly support our view that the PPLs with trehalose have an increased lyotropic response (shown by FTIR and LAURDAN Fluorescence spectroscopy measurements) but an almost unaltered thermo-tropic response seen in the DSC. It is also evident, that there is no common effect of trehalose on the phase behavior, because the sugar can shift the T_m up or down, depending on the lipid headgroup. Likewise the transition width can be broadened (DMPC, DMPA, DMPG) or stay unaffected (DMPE). It is particularly remarkable that the width of the transition is clearly affected by trehalose in the PC but not in the PE model lipid. The transition width is a measure of the degree of the cooperativity of the phase transition. The data thus indicate that the average number of lipids that undergo a phase transition as a cooperative unit is not affected by trehalose when it interacts with PE. It stays the most narrow transition, evidencing the strongest coupling between the lipid molecules during the phase transition (the largest number of lipids per cooperative unit). These findings from the model lipids would be an interesting

step towards future DSC investigations of the membrane phase transition behavior of dauer larvae PPLs and NPLs in dependence of trehalose. Physically, the experiments will provide further evidence for the adaptation of lipid headgroup composition during preconditioning. We believe that maybe the adaptation to drought means exactly this: change the PLs to allow the membranes expanding laterally very quickly upon uptake of water but have their T_m not affected.

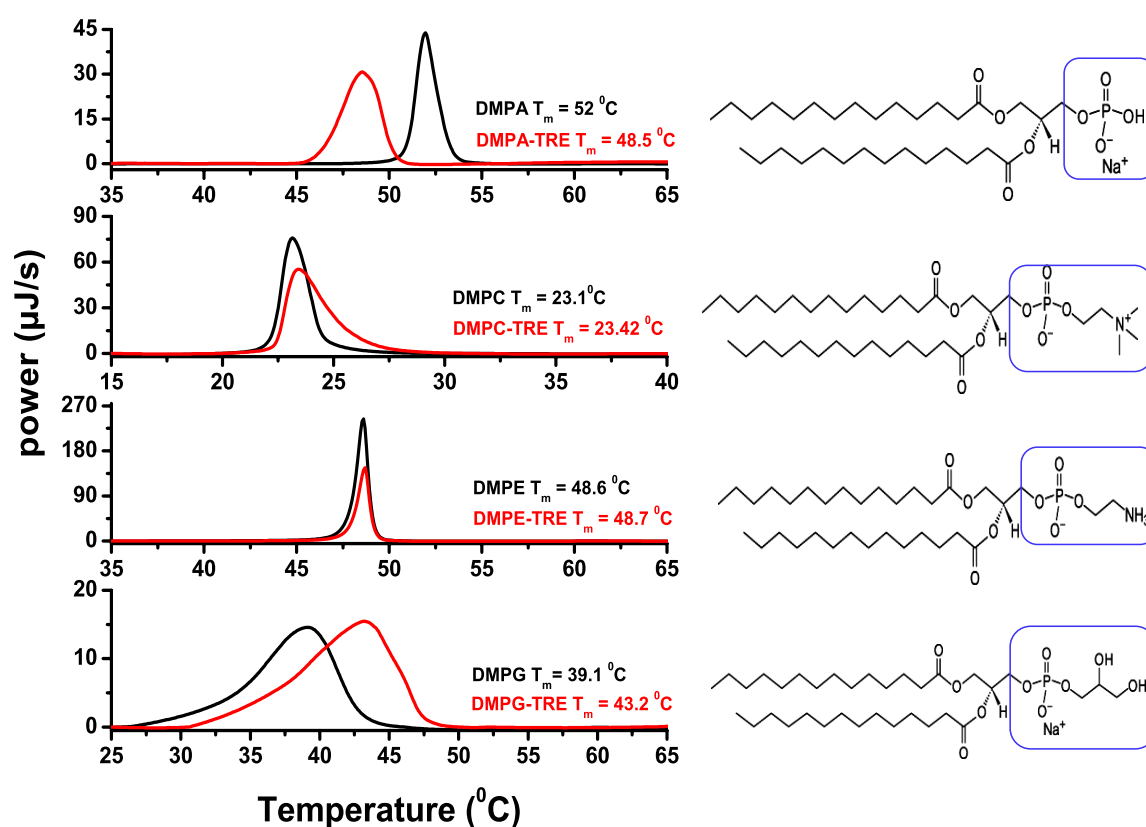


Figure 7.1: (A) DSC heating scans of DMPA, DMPC, DMPE and DMPG vesicles (1mg/ml) in the absence and presence of trehalose (~20 mg/ml) are revealing the main gel to liquid-crystalline phase transition temperature (T_m). The results show that the trehalose lipid interaction is highly dependent on the headgroup. (B) The chemical structure of these model lipids with different headgroups (PA, PC, PE and PG).

BIBLIOGRAPHY

-
- [1] A. H. García. Anhydrobiosis in bacteria: From physiology to applications. *Journal of biosciences*, 36(5):939–950, 2011.
 - [2] A. I. Rapoport, G. M. Khrustaleva, G. I. Chamanis, and M. E. Beker. Yeast anhydrobiosis: permeability of the cytoplasmic membrane. *Microbiology*, 64(2):275–278, 1995.
 - [3] D. Calahan, M. Dunham, C. Desevo, and D. E. Koshland. Genetic analysis of desiccation tolerance in *sachharomyces cerevisiae*. *Genetics*, 189(2):507–519, 2011.
 - [4] W. Welnicz, M. A. Grohme, A. Kaczmarek, R. O. Schill, and M. Frohme. Anhydrobiosis in tardigrades-the last decade. *Journal of insect physiology*, 57(5):577–583, 2011.
 - [5] S. Hengherr, R. O. Schill, and J. S. Clegg. Mechanisms associated with cellular desiccation tolerance of *Artemia* encysted embryos from locations around the world. *Comparative biochemistry and physiology - a molecular and integrative physiology*, 160(2):137–142, 2011.
 - [6] N. Rascio and N. La Rocca. Resurrection plants: the puzzle of surviving extreme vegetative desiccation. *Critical reviews in plant sciences*, 24(3):209–225, 2005.
 - [7] A. Tunnacliffe and J. Lapinski. Resurrecting Van Leeuwenhoek’s rotifers: a reappraisal of the role of disaccharides in anhydrobiosis. *Philosophical transactions of the royal society of london. Series b, biological sciences*, 358(1438):1755–1771, 2003.
 - [8] R. Cornette and T. Kikawada. The induction of anhydrobiosis in the sleeping chironomid: Current status of our knowledge. *International union of biochemistry and molecular biology life*, 63(6):419–429, 2011.
 - [9] P. S. Grewal. Anhydrobiotic potential and long-term storage of entomopathogenic nematodes (Rhabditida: Steinernematidae). *International journal for parasitology*, 30(9):995–1000, 2000.
 - [10] A. J. Shannon, J. A. Browne, J. Boyd, D. A. Fitzpatrick, and A. M. Burnell. The anhydrobiotic potential and molecular phylogenetics of species and strains of *Panagrolaimus* (Nematoda, Panagrolaimidae). *The journal of experimental biology*, 208(12):2433–2445, 2005.
 - [11] D. A. Wharton and O. Aalders. Desiccation stress and recovery in the anhydrobiotic nematode *Ditylenchus dipsaci* (Nematoda: Anguinidae). *European journal of entomology*, 96(2):199–203, 1999.
 - [12] J. H. Crowe and L. M. Crowe. Induction of anhydrobiosis: membrane changes during drying. *Cryobiology*, 328:317–328, 1982.

- [13] J. H. Crowe, L. M. Crowe, and D. Chapman. Preservation of membranes in anhydrobiotic organisms: the role of trehalose. *Science*, 223(4637):701–3, 1984.
- [14] N. Chakraborty, M. A. Menze, H. Elmoazzen, H. Vu, M. L. Yarmush, S. C. Hand, and M. Toner. Trehalose transporter from african chironomid larvae improves desiccation tolerance of chinese hamster ovary cells. *Cryobiology*, 64(2):91 – 96, 2012.
- [15] J. P. Chen, T. Acker, A. Eroglu, S. Cheley, H. Bayley, A. Fowler, and M. Toner. Beneficial effect of intracellular trehalose on the membrane integrity of dried mammalian cells. *Cryobiology*, 43(2):168–181, 2001.
- [16] X.-H. Liu, A. Aksan, M. A. Menze, S. C. Hand, and M. Toner. Trehalose loading through the mitochondrial permeability transition pore enhances desiccation tolerance in rat liver mitochondria. *Biochimica et biophysica acta*, 1717(1):21–26, 2005.
- [17] J. Crowe and K.A.C. Madin. Anhydrobiosis in nematodes : evaporative water loss and survival. *Comparative physiology and biochemistry*, 193(3):323–333, 1975.
- [18] K. A. C. Madin and J. H. Crowe. Anhydrobiosis in nematodes: carbohydrate and lipid metabolism during dehydration. *Journal of experimental zoology*, 193:335–342, 1975.
- [19] M. C. Banton and A. Tunnacliffe. MAPK phosphorylation is implicated in the adaptation to desiccation stress in nematodes. *Journal of experimental biology*, 215:4288–4298, 2012.
- [20] C. Erkut, S. Penkov, H. Khesbak, D. Vorkel, J.-M. Verbavatz, K. Fahmy, and T. V. Kurzchalia. Trehalose renders the dauer larva of *Caenorhabditis elegans* resistant to extreme desiccation. *Current biology*, 21(15):1331–6, 2011.
- [21] C. Erkut, S. Penkov, K. Fahmy, and T. V. Kurzchalia. How worms survive desiccation trehalose pro water. *Lands bioscience*, 1(1):61–65, 2012.
- [22] J. V. Ricker, W. F. Wolkers, N. M. Tsvetkova, C. C. Leidy, K. Gousset, F. Tablin, M. Longo, and J. H. Crowe. Trehalose maintains lipid phase separation in model and biological membranes. *Molecular biology of the cell*, 13:361a, 2002.
- [23] J. V. Ricker, N. M. Tsvetkova, W. F. Wolkers, C. Leidy, F. Tablin, M. Longo, and J. H. Crowe. Trehalose maintains phase separation in an air-dried binary lipid mixture. *Biophysical journal*, 84(5):3045–51, 2003.
- [24] F. Tablin, W. F. Wolkers, N. M. Tsvetkova, and J. H. Crowe. Trehalose maintains membrane lipid domain organization in freeze-dried rehydrated platelets: Implications for long-term storage in the dry state. *Abstracts of papers of the American chemical society*, 229:U641–U641, 2005.

- [25] J. H. Crowe, J. F. Carpenter, and L. M. Crowe. The role of vitrification in anhydrobiosis. *Annual review of physiology*, 60:73–103, 1998.
- [26] L. M. Crowe. Lessons from nature: the role of sugars in anhydrobiosis. *Comparative biochemistry and physiology part A: molecular integrative physiology*, 131(3):505–513, 2002.
- [27] J. Kapla, J. Wohler, B. Stevansson, O. Engström, G. Widmalm, and A. Maliniak. Molecular dynamics simulations of membrane-sugar interactions. *The journal of physical chemistry. B*, 117(22):6667–73, 2013.
- [28] B. A. C. Horta, L. Perić-Hassler, and P. H. Hünenberger. Interaction of the disaccharides trehalose and gentiobiose with lipid bilayers: A comparative molecular dynamics study. *Journal of Molecular Graphics and Modelling*, 29(3):331–346, 2010.
- [29] J. Milhaud. New insights into water-phospholipid model membrane interactions. *Biochimica et biophysica acta*, 1663(1-2):19–51, 2004.
- [30] S. Hoole. *The select works of antony van leeuwenhoek, containing his microscopical discoveries in many of the works of nature*. Volume 2, the philanthropic society, London. translator, 1807.
- [31] D. Keilin. *The problem of anabiosis or latent life: history and current concept*. Number 939. Proceedings of the royal society B: biological sciences, 1959.
- [32] J. S. Clegg. Cryptobiosis - A peculiar state of biological organization. *Comparative biochemistry and physiology b-biochemistry & molecular biology*, 128(4):613–624, 2002.
- [33] W. L. Nicholas and A. C. Stewart. Experiments on anhydrobiosis in *Acrobeloides nanus* de Man, 1880 Anderson, 1986 Nematoda. *Nematologica*, 4:489–491, 1989.
- [34] C. M. Preston and A. F. Bird. Physiological and morphological changes associated with recovery from anabiosis in the dauer larva of the nematode *Anguina agrostis*. *Parasitology*, 95(01):125–133, 1987.
- [35] J. H. Crowe and K. A. Madin. Anhydrobiosis in tardigrades and nematodes. *Transactions of the american microscopical society*, 93(4):513–524, 1974.
- [36] R. N. Perry. Desiccation survival of larval and adult stages of the plant parasitic nematodes, *Ditylenchus dipsaci* and *Ditylenchus myceliophagus*. *Parasitology*, 74(02):139–148, 1977.
- [37] E. Lees. An investigation into the method of dispersal of *Panagrellus silusiae*, with particular reference to its desiccation resistance. *Journal of helminthology*, 27(1-2):95–103, 1953.

-
- [38] G. Steiner and F.E. Albin. Resuscitation of the nematode *Tylenchus polyhypnus*, n. sp., after almost 39 years dormancy. *Journal of the washington academy of sciences*, 36(3):97–99, 1946.
- [39] A. E. Oliver, O. Leprince, W. F. Wolkers, D. K. Hinch, A. G. Heyer, and J. H. Crowe. Non-disaccharide-based mechanisms of protection during drying. *Cryobiology*, 43(2):151–167, 2001.
- [40] J. S. Clegg. Protein stability in *Artemia* embryos during prolonged anoxia. *Biological bulletin*, 212(1):74–81, 2007.
- [41] O. Gusev, R. Cornette, T. Kikawada, and T. Okuda. Expression of heat shock protein-coding genes associated with anhydrobiosis in an African chironomid *Polypedilum vanderplanki*. *Cell stress and chaperones*, 16(1):81–90, 2011.
- [42] S. C. Hand, M. A. Menze, M. Toner, L. Boswell, and D. Moore. LEA proteins during water stress: not just for plants anymore. *Annual review of physiology*, 73(1):115–134, 2011.
- [43] J. S. Clegg. Metabolic studies of crytobiosis in encysted embryos of *Artemia salina*. *Comparative biochemistry and physiology*, 20(3):801–809, 1967.
- [44] F. Albertorio, V. A. Chapa, X. Chen, A. J. Diaz, and P. S. Cremer. The α,α -(1 \rightarrow 1) linkage of trehalose is key to anhydrobiotic preservation. *Journal of the american chemical society*, 129(34):10567–10574, 2007.
- [45] P. S. Belton and A. M. Gil. IR and Raman spectroscopic studies of the interaction of trehalose with hen egg white lysozyme. *Biopolymers*, 34(7):957–961, 1994.
- [46] J. L. Green and C. A. Angell. Phase relations and vitrification in saccharide-water solutions and the trehalose anomaly. *The journal of physical chemistry*, 93(8):2880–2882, 1989.
- [47] R. McSorley. Adaptations of nematodes to environmental extremes. *Florida entomologist*, 86:138–142, 2003.
- [48] D. L. Riddle. *C. elegans II*. Cold spring harbor laboratory press, 1997.
- [49] E. Maupas. *Modes et formes de reproduction des nématodes*. Archives de zoologie experimentale et generale, 8:463–624, 1900.
- [50] C. Kenyon. *The nematode Caenorhabditis elegans*. Cold spring harbor monograph series. Cold spring harbor laboratory, 1988.
- [51] M. Blaxter. Comparative genomics: two worms are better than one. *Nature*, 426(6965):395–396, 2003.

- [52] L. Byerly, R. C. Cassada, and R. L. Russell. The life cycle of the nematode *Caenorhabditis elegans*. I. Wild-type growth and reproduction. *Developmental biology*, 51(1):23–33, 1976.
- [53] Z. F. Altun and D. H. Hall. Introduction to *C. elegans* anatomy. In *worm atlas* (www.wormatlas.org), 2009.
- [54] P. J. Hu. Dauer. *WormBook: the online review of C. elegans biology*, 8:1–19, 2007.
- [55] N. Fielenbach and A. Antebi. *C. elegans* dauer formation and the molecular basis of plasticity. *Genes & development*, 22(16):2149–65, 2008.
- [56] C. Erkut. Molecular mechanisms of Anhydrobiosis in *Caenorhabditis elegans*. *PhD thesis, TU Dresden*, 2012.
- [57] R. C. Cassada and R. L. Russell. The dauer larva, a post-embryonic developmental variant of the nematode *Caenorhabditis elegans*. *Developmental biology*, 46(2):326–342, 1975.
- [58] L. Lin, Y. P. Goldberg, and T. Ganz. Genetic and environmental regulation of dauer larva development. *Blood*, 106:2884–9, 1997.
- [59] J. W. Golden and D. L. Riddle. A pheromone-induced developmental switch in *Caenorhabditis elegans*: Temperature-sensitive mutants reveal a wild-type temperature-dependent process. *Proceedings of the national academy of sciences of the united states of america*, 81(3):819–23, 1984.
- [60] Wikipedia. Cell membrane. http://en.wikipedia.org/wiki/Cell_membrane, 2014.
- [61] S. J. Singer and G. L. Nicolson. The fluid mosaic model of the structure of cell membranes. *Science*, 175(4023):720–731, 2008.
- [62] D. F. Bocian and S. I. Chan. NMR studies of membrane structure and dynamics. *Annual review of physical chemistry*, 29:307–335, 1978.
- [63] L. Stryer. *Biochemistry*. Freeman and Co., New York, 4th ed., 1995.
- [64] M. Eisenberg and S. McLaughlin. Lipid bilayers as models of biological membranes. *BioScience*, 26(7):436–443, 1976.
- [65] R. B. Gennis. *Biomembranes: Molecular structure and function*. Springer advanced texts in chemistry. Springer, 1989.
- [66] S. R. Goodman. *Medical cell biology*. Elsevier science, 3rd ed., 2007.
- [67] K. Satouchi, K. Hirano, M. Sakaguchi, H. Takehara, and F. Matsuura. Phospholipids from the free-living nematode *Caenorhabditis elegans*. *Lipids*, 28(9):837–40, 1993.

- [68] T. Tanaka, K. Ikita, T. Ashida, Y. Motoyama, Y. Yamaguchi, and K. Satouchi. Effects of growth temperature on the fatty acid composition of the free-living nematode *Caenorhabditis elegans*. *Lipids*, 31:1173–1178, 1996.
- [69] D. Chapman. Phase transitions and fluidity characteristics of lipids and cell membranes. *Quarterly reviews of biophysics*, 8(2):185–235, 1975.
- [70] J. R. Hazel and E. E. Williams. The role of alterations in membrane lipid composition in enabling physiological adaptation of organisms to their physical environment. *Progress in lipid research*, 29(3):167–227, 1990.
- [71] O. G. Mouritsen and M. J. Zuckermann. What’s so special about cholesterol? *Lipids*, 39(11):1101–1113, 2004.
- [72] T. Heimburg. A model for the lipid pretransition: coupling of ripple formation with the chain-melting transition. *Biophysical journal*, 78(3):1154–65, 2000.
- [73] D. Freifelder. *Physical biochemistry: Applications to biochemistry and molecular biology*. Life sciences/biochemistry. W. H. Freeman, 1982.
- [74] W.O. George, P.S. McIntyre, D.J. Mowthorpe, and ACOL (Project). *Infrared spectroscopy*. Analytical chemistry by open learning. Published on behalf of ACOL, London, by Wiley, 1987.
- [75] N. B. Colthup, L. H. Daly, and S. E. Wiberley. *Introduction to Infrared and Raman spectroscopy*. Elsevier, New York: academic Press, 1990.
- [76] J. B. Marion and S. T. Thornton. *Classical dynamics of particles & systems*. San Diego: Harcourt Brace Jovanovich, 1988.
- [77] D. L. Pavia, G. M. Lampman, and G. S. Kriz. *Introduction to spectroscopy: A guide for students of organic chemistry*. Saunders golden sunburst series. Harcourt brace college publishers, 2nd ed., 1996.
- [78] B. H. Stuart. *Infrared spectroscopy: Fundamentals and applications*. Analytical techniques in the sciences. Wiley, 2004.
- [79] J. Fahrenfort. Attenuated total reflection: A new principle for the production of useful infrared reflection spectra of organic compounds. *Spectrochimica Acta*, 17(7):698–709, 1961.
- [80] N. J. Harrick. *Internal reflection spectroscopy*. Interscience publishers, New York, 1967.
- [81] C. Kötting and K. Gerwert. Proteins in action monitored by time-resolved FTIR spectroscopy. *ChemPhysChem*, 6(5):881–888, 2005.

- [82] P. R. Griffiths and J. A. De Haseth. *Fourier transform infrared spectrometry*. 2nd ed., Chemical analysis: A series of monographs on analytical chemistry and its applications. Wiley-interscience A John Wiley & Sons. INC., publications, 2007.
- [83] G. G. Roberts. Langmuir-Blodgett films. *Physics today*, 25(2):109–128, 1990.
- [84] B. Mecheri, L. Piras, and G. Caminati. Langmuir-Blodgett films incorporating redox mediators for molecular recognition of NADH. In *bioelectrochemistry*, volume 63, pages 13–18, 2004.
- [85] E. Chifu, M. Tomoaia-Cotisel, I. Albu, M. I. Mocanu, A. Salajan, Cs. Racz, and V. D. Pop. *Experimental methods in chemistry and biophysics of colloids and interfaces*. Life sciences/ biochemistry. University Press, Cluj-Napoca, 2004.
- [86] B. Moghaddam, M. H. Ali, J. Wilkhu, D. J. Kirby, A. R. Mohammed, Q. Zheng, and Y. Perrie. The application of monolayer studies in the understanding of liposomal formulations. *International journal of pharmaceutics*, 417(1-2):235–244, 2011.
- [87] G. F. Lothian. Beer's law and its use in analysis. A review. *Analyst*, 88(1050):678–685, 1963.
- [88] M. Kasha. Characterization of electronic transitions in complex molecules. *Discussions of the Faraday society*, 9(c):14–19, 1950.
- [89] J. R. Lakowicz. *Principles of fluorescence spectroscopy*. Springer, Boston, MA, 2006.
- [90] B. Valeur and M. N. Berberan-Santos. *Molecular Fluorescence: Principles and Applications*. Wiley-VCH, 2013.
- [91] T. Parasassi, G. De Stasio, G. Ravagnan, R. M. Rusch, and E. Gratton. Quantitation of lipid phases in phospholipid vesicles by the generalized polarization of Laurdan fluorescence. *Biophysical journal*, 60(1):179–189, 1991.
- [92] P. Gabbot. *Principles and applications of thermal analysis*. Wiley-Interscience, 2008.
- [93] K. Brandenburg, P. Garidel, J. Howe, J. Andrä, L. Hawkins, M. H. J. Koch, and U. Seydel. What can calorimetry tell us about changes of three-dimensional aggregate structures of phospholipids and glycolipids? *Thermochimica Acta*, 445(2):133–143, 2006.
- [94] S. Bonora, A. Torreggiani, and G. Fini. DSC and Raman study on the interaction between polychlorinated biphenyls (PCB) and phospholipid liposomes. *Thermochimica Acta*, 408(1-2):55–65, 2003.

- [95] T. P. McMullen, R. N. Lewis, and R. N. McElhaney. Differential scanning calorimetric study of the effect of cholesterol on the thermotropic phase behavior of a homologous series of linear saturated phosphatidylcholines. *Biochemistry*, 32(2):516–22, 1993.
- [96] J. P. Elmar, R. N. A. H. Lewis, K. C. Neuman, S. M. Gruner, L. H. Kondejewski, R. S. Hodges, and R. N. McElhaney. Nonlamellar phases induced by the interaction of gramicidin S with lipid bilayers. A possible relationship to membrane-disrupting activity. *Biochemistry*, 36(25):7906–7916, 1997.
- [97] C. Larios, J. Carilla, M. A. Busquets, M. A. Alsina, and I. Haro. Perturbations induced by synthetic peptides belonging to the E2 structural protein of hepatitis G virus (GBV-C/HGV) in lipid membranes: A differential scanning calorimetry study. *Journal de physique IV (proceedings)*, 113:31–34, 2004.
- [98] D. Marsh, A. Watts, and P. F. Knowles. Evidence for phase boundary lipid. Permeability of tempo-choline into dimyristoylphosphatidylcholine vesicles at the phase transition. *Biochemistry*, 15(16):3570–3578, 1976.
- [99] S. Brenner. The genetics of *Caenorhabditis elegans*. *Genetics*, 77(1):71–94, 1974.
- [100] M. Sarov, S. Schneider, A. Pozniakovski, A. Roguev, S. Ernst, Y. Zhang, A. A. Hyman, and A. F. Stewart. A recombineering pipeline for functional genomics applied to *Caenorhabditis elegans*. *Nature methods*, 3(10):839–844, 2006.
- [101] J. E. Sulston and S. Brenner. DNA of *Caenorhabditis elegans*. *Genetics*, 77:95–104, 1974.
- [102] V. Matyash, E. V. Entchev, F. Mende, M. Wilsch-Bräuninger, C. Thiele, A. W. Schmidt, H. J. Knölker, S. Ward, and T. V. Kurzchalia. Sterol-derived hormone(s) controls entry into diapause in *Caenorhabditis elegans* by consecutive activation of DAF-12 and DAF-16. *PLoS biology*, 2(9):e280, 2004.
- [103] R. H. Stokes and R. A. Robinson. Standard solutions for humidity control at 25 °C. *Industrial & engineering chemistry*, 41(9):2013–2013, 1949.
- [104] E. G. Bligh and W. J. Dyer. A rapid method of total lipid extraction and purification. *Canadian journal of biochemistry and physiology*, 37(8):911–917, 1959.
- [105] E. Goormaghtigh, V. Raussens, and J. Ruyschaert. Attenuated total reflection infrared spectroscopy of proteins and lipids in biological membranes. *Biochimica et biophysica acta*, 1422:105–185, 1999.
- [106] H. Khesbak, O. Savchuk, S. Tsushima, and K. Fahmy. The role of water H-bond imbalances in B-DNA substate transitions and peptide recognition revealed by time-resolved FTIR spectroscopy. *Journal of the american chemical society*, 133(15):5834–5842, April 2011.

- [107] D. R. Gauger, C. Selle, M. Hahn, and W. Pohle. Defining the water content in oriented lipid films by Karl-Fischer titration. *Analytical biochemistry*, 299(1):108–110, 2001.
- [108] H. Binder, U. Dietrich, M. Schalke, and H. Pfeiffer. Hydration-induced deformation of lipid aggregates before and after polymerization. *Langmuir*, 15(17):4857–4866, 1999.
- [109] B. W. Koenig, H. H. Strey, and K. Gawrisch. Membrane lateral compressibility determined by NMR and x-ray diffraction: effect of acyl chain polyunsaturation. *Biophysical journal*, 73(4):1954–1966, 1997.
- [110] W. F. Wolkers, L. M. Crowe, N. M. Tsvetkova, F. Tablin, and J. H. Crowe. In situ assessment of erythrocyte membrane properties during cold storage. *Molecular membrane biology*, 19:59–65, 2002.
- [111] W. F. Wolkers and F. Fonseca. Effect of sucrose and maltodextrin on the physical properties and survival of air-dried lactobacillus bulgaricus : an in situ Fourier transform infrared spectroscopy study. *Biotechnol*, 21:885–892, 2005.
- [112] W. F. Wolkers, S. K. Balasubramanian, E. L. Ongstad, H. C. Zec, and J. C. Bischof. Effects of freezing on membranes and proteins in LNCaP prostate tumor cells. *Biochimica et biophysica acta*, 1768(3):728–36, 2007.
- [113] W. F. Wolkers and F. A. Hoekstra. In situ FTIR assessment of desiccation tolerant tissues. *Spectroscopy*, 17(2,3):297–313, 2003.
- [114] C. Cacela and D. K. Hinch. Low amounts of sucrose are sufficient to depress the phase transition temperature of dry phosphatidylcholine, but not for lyoprotection of liposomes. *Biophysical journal*, 90(8):2831–2842, 2006.
- [115] G.G. Roberts. *Langmuir-Blodgett films*. Plenum Press, New York, 1990.
- [116] H. R. Seitz, M. Heck, K. P. Hofmann, T. Alt, J. Pellaud, and A. Seelig. Molecular determinants of the reversible membrane anchorage of the G-protein transducin. *Biochemistry*, 38(25):7950–7960, 1999.
- [117] V. Boguslavsky, M. Rebecchi, A. J. Morris, D. Y. Jhon, S. G. Rhee, and S. McLaughlin. Effect of monolayer surface pressure on the activities of phosphoinositide-specific phospholipase C-beta 1, -gamma 1, and -delta 1. *Biochemistry*, 33(10):3032–3037, 1994.
- [118] A. Ken-ichi, O. Yusei, A. Naoki, I. Yoshio, and S. Minoru. Infrared spectroscopic study on the properties of the anhydrous form (ii) of trehalose. implications for the functional mechanism of trehalose as a biostabilizer. *Carbohydrate research*, 334(3):233 – 241, 2001.

- [119] A. Blume. Properties of lipid vesicles: FT-IR spectroscopy and fluorescence probe studies. *Current opinion in colloid & interface science*, 1(3):431–431, 1996.
- [120] W. Pohle, D. R. Gauger, H. Fritzsche, B. Rattay, C. Selle, H. Binder, and H. Bo. FTIR-spectroscopic characterization of phosphocholine-headgroup model compounds. *Journal of molecular structure*, 563:463–467, 2001.
- [121] H. Binder, A. Anikin, G. Lantzsch, and G. Klose. Lyotropic phase behavior and gel state polymorphism of phospholipids with terminal diene groups : infrared measurements on molecular ordering in lamellar and hexagonal phases. *The journal of physical chemistry B*, 103:461–471, 1999.
- [122] P. B. Hitchcock, R. Mason, K. M. Thomas, and G. Graham. Molecular conformation and intermolecular packing of phospholipids. *Proceedings of the national academy of sciences USA*, 71(8):3036–3040, 1974.
- [123] A. Skibinsky, R. M. Venable, and R. W. Pastor. A molecular dynamics study of the response of lipid bilayers and monolayers to trehalose. *Biophysical journal*, 89(6):4111–4121, 2005.
- [124] J. H. Crowe, M. A. Whittam, D. Chapman, and L. M. Crowe. Interactions of phospholipid monolayers with carbohydrates. *Biochimica et biophysica acta*, 769:151–159, 1984.
- [125] C. Lambruschini, A. Relini, A. Ridi, L. Cordone, and A. Gliozzi. Trehalose interacts with phospholipid polar heads in langmuir monolayers. *Langmuir*, 16(12):5467–5470, 2000.
- [126] Y. Nakahara, M. Watanabe, A. Fujita, Y. Kanamori, D. Tanaka, K.-ichi. Iwata, T. Furuki, M. Sakurai, T. Kikawada, and T. Okuda. Effects of dehydration rate on physiological responses and survival after rehydration in larvae of the anhydrobiotic chironomid. *Journal of insect physiology*, 54(8):1220 – 1225, 2008.
- [127] C. A. López, A. J. Rzepiela, A. H. de Vries, L. Dijkhuizen, P. H. Hünenberger, and S. J. Marrink. Martini coarse-grained force field: Extension to carbohydrates. *Journal of chemical theory and computation*, 5(12):3195–3210, 2009.
- [128] W. F. Wolkers, H. Oldenhof, and B. Glasmacher. Dehydrating phospholipid vesicles measured in real-time using ATR Fourier transform infrared spectroscopy. *Cryobiology*, 61(1):108–114, 2010.
- [129] C. Erkut, A. Vasilj, S. Boland, B. Habermann, A. Shevchenko, and T. V. Kurzchalia. Molecular strategies of the *Caenorhabditis elegans* dauer larva to survive extreme desiccation. *PloS one*, 8(12):e82473, 2013.
- [130] T. J. McIntosh. Differences in hydrocarbon chain tilt between hydrated phosphatidylethanolamine and phosphatidylcholine bilayers. A molecular packing model. *Biophysical journal*, 29(2):237–245, 1980.

- [131] M. C. Luzardo, F. Amalfa, A. M. Nuñez, S. Díaz, A. C. Biondi De Lopez, and E. A. Disalvo. Effect of trehalose and sucrose on the hydration and dipole potential of lipid bilayers. *Biophysical journal*, 78(5):2452–2458, 2000.
- [132] M. Heyden, E. Bründermann, U. Heugen, G. Niehues, D. M. Leitner, and M. Havenith. Long-range influence of carbohydrates on the solvation dynamics of water—answers from terahertz absorption measurements and molecular modeling simulations. *Journal of the american chemical society*, 130(17):5773–5779, 2008.
- [133] R. M. Venable, A. Skibinsky, and R. W. Pastor. Constant surface tension molecular dynamics simulations of lipid bilayers with trehalose. *Molecular simulation*, 32(10-11):849–855, 2006.
- [134] E. A. Golovina, A. Golovin, F. A. Hoekstra, and R. Faller. Water replacement hypothesis in atomic details: effect of trehalose on the structure of single dehydrated POPC bilayers. *Langmuir : the ACS journal of surfaces and colloids*, 26(13):11118–11126, 2010.
- [135] H. D. Andersen, C. Wang, L. Arleth, G. H. Peters, and P. Westh. Reconciliation of opposing views on membrane-sugar interactions. *Proceedings of the national academy of sciences of the united states of america*, 108(5):1874–1878, 2011.
- [136] L. Huynh, N. Perrot, V. Beswick, V. Rosilio, P. A. Curmi, A. Sanson, and N. Jamin. Structural properties of POPC monolayers under lateral compression: computer simulations analysis. *Langmuir : the ACS journal of surfaces and colloids*, 30(2):564–573, 2014.
- [137] B. Bechinger and J. Seelig. Conformational changes of the phosphatidylcholine headgroup due to membrane dehydration. A 2H-NMR study. *Chemistry and physics of lipids*, 58(1-2):1–5, 1991.
- [138] A. S. Ulrich and A. Watts. Molecular response of the lipid headgroup to bilayer hydration monitored by 2H-NMR. *Biophysical journal*, 66(5):1441–1449, 1994.
- [139] R. C. De Carvalho, A. B. Da Silva, R. Soares, A. V. Almeida, A. M. Coelho, J. M. Da Silva, and C. Branquinho. Differential proteomics of dehydration and rehydration in bryophytes: evidence towards a common desiccation tolerance mechanism. *Plant, cell environment*, 37(7):1499–1515, 2014.
- [140] T. Martinelli. In situ localization of glucose and sucrose in dehydrating leaves of *Sporobolus stapfianus*. *Journal of plant physiology*, 165(6):580–587, 2008.
- [141] R. N. Lewis and R. N. McElhaney. Calorimetric and spectroscopic studies of the thermotropic phase behavior of lipid bilayer model membranes composed of a homologous series of linear saturated phosphatidylserines. *Biophysical journal*, 79(4):2043–2055, 2000.

- [142] H. H. Mantsch and R. N. McElhaney. Phospholipid phase transitions in model and biological membranes as studied by infrared spectroscopy. *Chemistry and physics of lipids*, 57(2-3):213–226, 1991.
- [143] J. H. Crowe, F. A. Hoekstra, L. M. Crowe, T. J. Anchordoguy, and E. Drobnis. Lipid phase transitions measured in intact cells with Fourier transform infrared spectroscopy. *Cryobiology*, 26(1):76–84, 1989.
- [144] J. M. Lyons and A. D. Keith. Temperature-induced phase transitions in nematode lipids and their influence on respiration I *Caenorhabditis elegans* storage test. *Journal of nematology*, 7(2):98–104, 1975.
- [145] A. Blume, W. Huebner, and G. Messner. Fourier transform infrared spectroscopy of $^{13}\text{C}=\text{O}$ labeled phospholipids hydrogen bonding to carbonyl groups. *Biochemistry*, 27(21):8239–8249, 1988.
- [146] J. Grdadolnik and D. Hadzi. FT infrared and raman investigation of saccharide “phosphatidylcholine interactions using novel structure probes. *Spectrochimica Acta part A: Molecular and biomolecular spectroscopy*, 54(12):1989 – 2000, 1998.
- [147] J. Grdadolnik, J. Kidriac, and Hadazi D. Hydration of phosphatidylcholine reverse micelles and multilayers: an infrared spectroscopic study. *Chemistry and physics of lipids*, 59(1):57 – 68, 1991.
- [148] A. V. Popova and D. K. Hinch. Intermolecular interactions in dry and rehydrated pure and mixed bilayers of phosphatidylcholine and digalactosyldiacylglycerol: a Fourier transform infrared spectroscopy study. *Biophysical journal*, 85(3):1682–1690, 2003.
- [149] C. Selle and W. Pohle. Fourier transform infrared spectroscopy as a probe for the study of the hydration of lipid self-assemblies. II. Water binding versus phase transitions. *Biospectroscopy*, 4(4):281–294, 1998.
- [150] A. K. Sum, R. Faller, and J. J. de Pablo. Molecular simulation study of phospholipid bilayers and insights of the interactions with disaccharides. *Biophysical journal*, 85(5):2830–2844, 2003.
- [151] M. A. Villarreal, S. B. Díaz, E. A. Disalvo, and G. G. Montich. Molecular dynamics simulation study of the interaction of trehalose with lipid membranes. *Langmuir : the ACS journal of surfaces and colloids*, 20(18):7844–7851, 2004.
- [152] P. T. T. Wong and H. H. Mantsch. High-pressure infrared spectroscopic evidence of water binding sites in 1,2-diacyl phospholipids. *Chemistry and physics of lipids*, 46(3):213 – 224, 1988.
- [153] J. L. R. Arrondo and M. Gon. Infrared studies of protein-induced perturbation of lipids in lipoproteins and membranes. *Chemistry and physics of lipids*, 96:53–68, 1998.

- [154] A. V. Popova and D. K. Hinch. Effects of cholesterol on dry bilayers: interactions between phosphatidylcholine unsaturation and glycolipid or free sugar. *Biophysical journal*, 93:1204–1214, 2007.
- [155] G. Weber and F. J. Farris. Synthesis and spectral properties of a hydrophobic fluorescent probe: 6-propionyl-2-(dimethylamino)naphthalene. *Biochemistry*, 18(14):3075–3078, 1979.
- [156] T. Parasassi and E. Gratton. Membrane lipid domains and dynamics as detected by Laurdan fluorescence. *Journal of fluorescence*, 5(1):59–69, 1995.
- [157] T. Parasassi, E. K. Krasnowska, L. Bagatolli, and E. Gratton. Laurdan and Prodan as polarity-sensitive fluorescent membrane probes. *Journal of fluorescence*, 8(4):365–373, 1998.
- [158] T. Parasassi, G. De Stasio, A. D’Ubaldo, and E. Gratton. Phase fluctuation in phospholipid membranes revealed by Laurdan fluorescence. *Biophysical journal*, 57(6):1179–1186, 1990.
- [159] T. Parasassi, A. M. Giusti, E. Gratton, E. Monaco, M. Raimondi, G. Ravagnan, and O. Sapora. Evidence for an increase in water concentration in bilayers after oxidative damage of phospholipids induced by ionizing radiation. *International journal of radiation biology*, 65(3):329–334, 1994.
- [160] P. L. G. Chong and P. T. T. Wong. Interactions of laurdan with phosphatidylcholine liposomes: a high pressure FTIR study. *Biochimica et biophysica acta (BBA) - Biomembranes*, 1149(2):260 – 266, 1993.

DECLARATION / ERKLÄRUNG

Declaration according to § 5.5 of the doctorate regulations: I herewith declare that I have produced this paper without the prohibited assistance of third parties and without making use of aids other than those specified; notions taken over directly or indirectly from other sources have been identified as such.

This paper has not previously been presented in identical or similar form to any other German or foreign examination board. The thesis work was conducted from January 3, 2011 to June 30, 2014 under the supervision of Prof. Dr. Karim Fahmy at department of Biophysics, HZDR Institute. I declare that I have not undertaken any previous unsuccessful doctorate proceedings. I declare that I recognize the doctorate regulations of the of the Faculty of Science of Dresden University of Technology.

Dresden, December 12, 2014 /Sawsan Abu Sharkh/.....

Erklärung entsprechend § 5.5 der Promotionsordnung: Hiermit versichere ich, dass ich die vorliegende Arbeit ohne unzulässige Hilfe Dritter und ohne Benutzung anderer als der angegebenen Hilfsmittel angefertigt habe; die aus fremden Quellen direkt oder indirekt übernommenen Gedanken sind als solche kenntlich gemacht. Die Arbeit wurde bisher weder im Inland noch im Ausland in gleicher oder ähnlicher Form einer anderen Prüfungsbehörde vorgelegt.

Die Dissertation wurde im Zeitraum vom 3. Januar 2011 bis 30. Juni 2014 verfasst und von Prof. Dr.Karim Fahmy, am Abteilung Biophysik , HZDR institut. Meine Person betreffend erkläre ich hiermit, dass keine früheren erfolglosen Promotionsverfahren stattgefunden haben. Ich erkenne die Promotionsordnung der Fakultät für Mathematik und Naturwissen-Schaften der Technischen Universität Dresden an.

Dresden, den 12. Dezember 2014 /Sawsan Abu Sharkh/

